ELECTROCHEMISTRY RESEARCH LABORATORY

DEPARTMENT OF CHEMISTRY

JOHN SCHOFF MILLIS SCIENCE CENTER

CASE WESTERN RESERVE UNIVERSITY

CLEVELAND, OHIO 44106

Final Technical Report

ELECTROCHEMICAL GENERATION OF OXYGEN

I. The Effects of Anions and Cations on Hydrogen Chemisorption and Anodic Oxide Film Formation on Platinum Electrode

II. The Effects of Anions and Cations on Oxygen Generation on Platinum Electrode

by

Chao-jung Huang, W. E. O'Grady and Ernest Yeager

Principal Investigator: Ernest Yeager

NASA-Ames Grant No. NGR-36-027-052

1 September 1972 to 31 August 1975

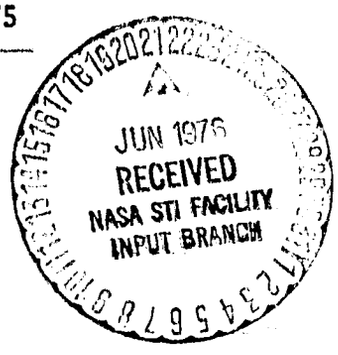

Final Technical Report to NASA
NASA-Ames Grant No. NGR 36-027-052

ELECTROCHEMICAL GENERATION OF OXYGEN

I. The Effects of Anions and Cations on Hydrogen Chemisorption and Anodic Oxide Film Formation on Platinum Electrode

II. The Effects of Anions and Cations on Oxygen Generation on Platinum Electrode

by

Chao-jung Huang, W. E. O'Grady and Ernest Yeager

Principal Investigator: Ernest Yeager

Abstract

The effects of anions and cations have been studied on hydrogen chemisorption and anodic oxide film formation on Pt by linear sweep voltammetry, and on oxygen generation on Pt by potentiostatic overpotential measurement. The effects have provided some insight into these processes.

The hydrogen chemisorption and anodic oxide film formation regions are greatly influenced by anion adsorption. In acids, the strongly bound hydrogen occurs at more cathodic potential when chloride and sulfate are present. Sulfate affects the initial phase of oxide film formation by produced fine structure while chloride retards the oxide film formation. In alkaline solutions, both strongly and weakly bound hydrogen are influenced by iodide, cyanide, and barium and calcium cations. These ions also influence the oxide film formation.

Three factors have been considered to explain these effects; these factors are: (1) displacement of adsorbed anions on different sites, (2) the induced heterogeneity effect, and (3) anion or cation induced changes in the potential distribution across the metal-solution interface.

The Tafel slope for oxygen generation has been found to be independent on the oxide thickness and the presence of cations or anions in the solutions. The catalytic activity indicated by the exchange current density was observed decreasing with increasing oxide layer thickness, only a minor dependence on the addition of certain cations and anions was found. These observations are explained on the basis that oxygen generation involves charge transfer via electron tunnelling through the oxide layer. A mechanism has been proposed with the first step involving the adsorption of OH to form a surface PtOH entity with the OH as an adsorbed radical followed by charge transfer via electron tunnelling.

[This report is adapted from Chao-jung Huang's Ph.D. dissertation.]

TABLE OF CONTENTS

TABLE OF CONTENTS (Cont.)

LIST OF FIGURES

LIST OF FIGURES (Cont.)

LIST OF FIGURES (Cont.)

LIST OF TABLES

CHAPTER I

INTRODUCTION

New ways to conserve energy are becoming a great need. Electrochemistry is one of the technologies which can make contributions toward solving this energy problem. A significant portion of electrical energy is consumed by industrial electrolytic processes, which are performed mostly with relatively low energy efficiency. Improvements in the efficiencies of the processes will result in substantial energy savings.

O_2-generation is an important component in various electrolytic cells. In most of such cells, the overpotential of O_2 anode is the largest voltage loss and increases very substantially the energy requirements over what would be expected thermodynamically. A better understanding of the kinetics of O_2-generation and the dependence of the kinetics on electrolyte composition is needed in order to reduce the energy requirements.

Most metals used as anodes dissolve; hence studies of O_2-generation are restricted principally to noble and highly passivated metals. Platinum has been mostly employed because of its high electrocatalytic activity and stability.

Prior to electrochemical O_2 generation, oxide films are formed on all metal electrodes. The understanding of the kinetics of O_2-generation in relation to the catalytic properties of metals requires information concerning the surface properties of the oxide films whose structure and electronic properties change with potential

and time.

The present work was undertaken to achieve a better understanding of oxide film formation and O_2-generation on platinum. Experiments have been designed to study the effects of anions and cations on the formation of oxide films and the kinetics of O_2-generation.

CHAPTER II

BACKGROUND AND PREVIOUS RESULTS

A. The Surface of Platinum Electrodes

For the kinetic study of oxygen formation at the Pt electrode, it is necessary to know the nature of the Pt surface and its dependence on electrode potential. When subject to anodic polarization, a film of oxide or chemisorbed oxygen is formed on the surface of Pt. Many studies have been conducted on this subject (for details, see review articles by Gilman,[1] Hoare,[2] Damjanovic[3]), but full understanding of the nature and properties concerning the anodic oxygen film has not yet been attained.

Constant current charging and linear potential sweep techniques have been most commonly used to study the oxygen film. A constant current charging-discharging curve and a linear potential sweep voltammogram are shown in Figs. II-1,2 to illustrate the electrochemical behavior of the Pt electrode in acid solution. As seen from the curves, the ionization of hydrogen appears in region A. Region B is the so-called double layer region, where the current almost entirely goes into the charging of the double layer. The oxide film is formed in region C. When the potential reaches region D, O_2 generation becomes significant. In the cathodic sweep or discharging, the oxygen film is reduced principally in region C'.

Some of the characteristics found from these curves are as follows:

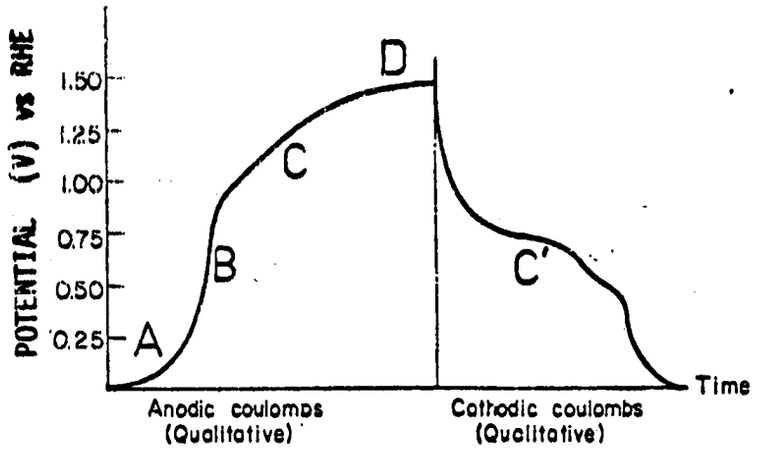

Fig. II-1. A typical constant current charging curve at Pt in acid solution.

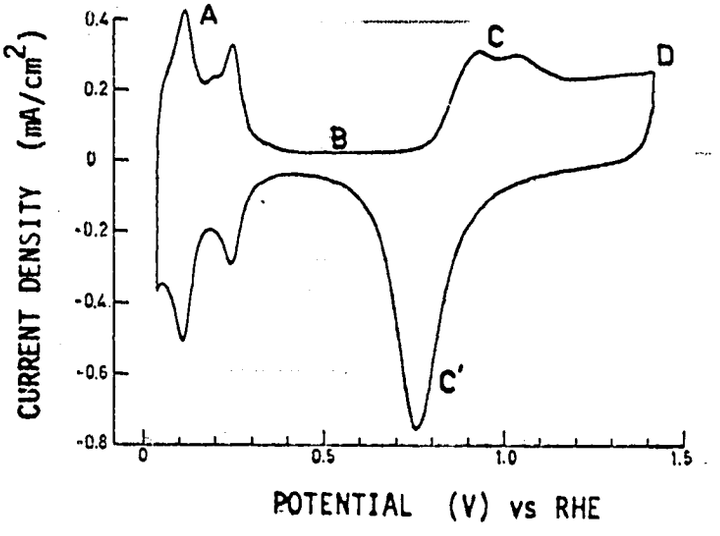

Fig. II-2. A typical linear sweep voltammogram of Pt in acid solution.

(a) The oxidation and reduction of the Pt surface occurs at potentials differing by a large amount. This shows that the oxide film formation and reduction are highly irreversible.

(b) The number of coulombs consumed in forming the oxygen film before O_2 formation becomes appreciable, corresponds to the order of a monolayer of oxygen on the Pt surface and is approximately a linear function of potential.

(c) The number of coulombs consumed to build up the oxygen film (Q_a) was found by most workers (see Refs. 1 and 2) to be larger than the amount of charge (Q_c) required to reduce it. It was observed that the ratio Q_a/Q_c approached unity after repeated potential cycling.[4] Kozlowska, Conway, and Sharp[5] have claimed that $Q_a = Q_c$ only below 1.2 V* in properly purified solutions.

The following are the proposed explanations for $Q_a > Q_c$, some of which may not be valid:

(1) According to Laitinen and Enke,[6] $Q_a > Q_c$ because O_2 is evolved along with the formation of anodic oxygen film during the anodic charging of Pt in $HClO_4$ solution. Actually O_2 generation becomes significant only at potentials > 1.4 V. This explanation also does not explain why $Q_a/Q_c \rightarrow 1$ with repeated potential cycling, as mentioned by Hoare.[2]

(2) Vetter and Berdt[7] observe $Q_a = 2Q_c$ from their constant current charging studies, and postulate that the oxygen species in the anodic oxygen film are only reduced to H_2O_2 instead of H_2O or OH^-. Hoare[2] argues against this view on the basis that Pt is a good peroxide-decomposing catalyst, which decomposes H_2O_2 to form oxygen. This is not always the situation. Under some conditions, O_2 reduction on Pt results in relatively large amounts of H_2O_2.[10]

---

*All potentials are relative to NHE.

Frumkin, Khrushcheva, Tarasevich, and Shumilova[8] and Johnson, Napp, and Bruckenstein[9] using the rotating ring-disc electrode technique, however, did not find any H_2O_2 during the reduction of oxygen film.

(3) Dietz and Goehr[11] explain $Q_a > Q_c$ by proposing that the oxygen film is partly reduced when the potential reaches the region where chemisorption of hydrogen sets in. Feldberg, Enke, and Bricker[4] suggest a two-step reduction to show the difference between Q_a and Q_c:

$$Pt(O)_x^* + xH^+ + xe^- \longrightarrow Pt(OH)_x \qquad \text{(II-1)}$$

$$Pt(OH)_x^* + xH^+ + xe^- \longrightarrow Pt + xH_2O \qquad \text{(II-2)}$$

At the potentials accessible before the hydrogen adsorption region is reached, the reduction partially stops at the $Pt(OH)_x$ stage and the film is not completely reduced to Pt. However, in an electrode potential scanning ellipsometric study of Pt anodic oxide formation by Horkans, Cahan, and Yeager,[12] loop closures of ellipsometric parameters with electrode potentials have been shown. This indicates that the electrode surface has recovered back to its initial state near the hydrogen region (region A in Fig. II-2).

(4) Schuldiner and Warner[13] have attempted to show that oxygen is dissolved in the surface layers of Pt metal when the oxygen film is electrochemically formed in 1 $\underline{M}$ H_2SO_4. The term "demasorbed

---

*The symbols $Pt(O)_x$ and $Pt(OH)_x$ represent the substances O and OH chemisorbed on the Pt surface. The subscript x is not necessarily an integer, but rather represents the ratios of chemisorbed O or OH to surface platinum atoms.

oxygen" is used by these authors. Thacker and Hoare[14] also claim the presence of oxygen in the Pt metal lattice from their constant current discharging studies in 2 N H_2SO_4. The diffusion of oxygen into the lattice of Pt can explain the difference between Q_a and Q_c because the dissolved oxygen is difficult to remove. Norton[15] has shown that oxygen does not diffuse distances of $\sim 10^{-4}$ cm in Pt at significant rates even at 1425°C. However, the distances involved in the dermasorbed oxygen would be of the order of Angstroms.

(5) It is reported by Rand and Woods[16] that the difference between Q_a and Q_c can be explained by the dissolution of Pt into the electrolyte during the anodic charging. They detect the dissolution of Pt in H_2SO_4 after repeated cycling of more than 1000 cycles between 0.41 and 1.46 V. Kozlowska et al.[5] believe that the contribution of anodic charge from the Pt dissolution is negligible below 1.2 V, and that significant dissolution occurs only at more anodic potentials.

(6) Breiter[17] finds that the oxidation of a layer of organic impurities occurs during anodic film formation on Pt in the range 0.6 - 1.5V in 1 N H_2SO_4. Kozlowska et al.[5] indicate that the organic impurities block surface oxide formation between 0.75 and 1.05 V in impure solutions, then become oxidized with the result that the anodic charge is spuriously large and the cathodic charge for oxide reduction is anomalously small. In practice, after several potential cycles, the organic impurities can be oxidized and desorbed off. The contribution of an excess anodic charge from the oxidation of organic impurities is expected to become insignificant unless

large concentrations of dissolved impurities are present in solution. It is very difficult to have a Pt surface free from impurities to start with, even using ultrapure electrolytes. Carbon is a common impurity in Pt and diffuses to the surface in high temperature treatment. Carbon on the surface is oxidized off in the first few potential cycles.

While much effort has been directed to unravelling the nature of the anodic oxygen film on Pt, no unambiguous conclusion about the film has been reached. On the basis of rather circumstantial evidence, two main models have been proposed for the anodic film formed on Pt in the range ~0.8-1.4V. A monolayer of oxygen is formed progressively on the Pt surface. One view is that this anodic layer is a thin film of an oxide such as PtO or PtO_2 grown on the Pt surface, whereas the other view is that the film is composed of oxygen adsorbed on Pt such as Pt-O.

The distinction between the oxide model and the adsorption model is not a clear one at the monolayer level. The strength of the interaction of the oxygen-containing species with the Pt of the electrode surface may range from the relatively low values characteristic of physical adsorption to the much higher values usually characteristic of the chemical interactions. In using the term oxide to denote the layer, the Pt with which the oxygen interacts is viewed as similar in its orbital properties and charge to that in a bulk oxide of a particular valence type. In describing the oxygen as chemisorbed, the Pt with which the oxygen interacts is usually considered to retain some of its metallic character with delocalized

orbital properties and the Pt-O interaction not to be similar to that in an oxide. It is possible, however, to have the Pt and oxygen interaction of an intermediate value between these two extremes.

El Wakkard and Emara,[18] proponents of the oxide model, observed two arrests, one at 0.8V and the other at 1.07V, in low current-density anodic charging curves of Pt in H_2SO_4. On the basis of equilibrium potentials, Pt/PtO (0.88V), reported by Grube[19] and $Pt(OH)_2/PtO_2$ (1.12V), reported by Latimer,[20] they concluded that PtO is first formed over the surface of Pt electrode, followed by PtO_2 before O_2 formation occurs at an appreciable rate. Their charging curves are criticized by Gilman[1] and Hoare[2] on the basis that a long time is required to complete these curves, allowing impurities to diffuse to and adsorb onto the electrode surface. Evidence for such impurity effects is the ill-defined hydrogen region in these curves and the fact that the second arrest at 1.07V does not appear on the freshly anodically pretreated Pt electrode or in the fast charging curves (high current density).

A single arrest is usually observed in constant current charging of Pt electrodes by most workers (e.g. refs. 7, 21-4). With a computed stoichiometry ratio Pt/O = 1 based on charge density at this potential, Hickling[21] considered the observed arrest to be due to the formation of a unimolecular layer of platinous oxide, PtO, while Butler and Armstrong[22] attributed it to the formation of a layer of adsorbed oxygen.

To confirm the existence of anodically formed oxide on Pt,

Anson and Lingane[25] stripped the film from anodized Pt, which had been polarized at +1.5V in H_2SO_4, with 0.2 M HCl + 0.1 M NaCl. From spectrophotometric analysis of $PtCl_4^=$ and $PtCl_6^=$, they concluded that both PtO and PtO_2 are present on the anodized Pt surface. It has been mentioned by Laitinen and Enke[6] that this technique is feasible only under the conditions that the state of the anodized Pt surface has to be unchanged during chemical stripping. Breiter and Weininger,[26] using open-circuit decay in conjunction with cathodic discharging technique on anodized Pt electrodes (pretreated at 1.4V or 1.6V in H_2SO_4) in solutions of 0.2 M HCl + 0.1 M NaCl, concluded that Anson and Lingane's results could be interpreted with an adsorbed oxygen model.

Boeld and Breiter[27] tried to show that the surface oxidation of Pt (in $HClO_4$ and H_2SO_4) in the range 0.8-1.5V, first forms a chemisorbed Pt-OH layer; this in turn oxidizes to form a chemisorbed layer of Pt-O. Gilman,[28] using fast potential-step techniques, modified the model of Boeld and Breiter and concluded that PtOH oxidizes to PtO only below 1.0V. Above 1.2V, PtO further oxidizes to PtO_2. The stoichiometric ratio of Pt and oxygen was used by Gilman to represent the species formed on the Pt surface, without indicating it as an adsorbed oxygen or an oxide.

Gilroy and Conway[29] observe no plateaus at any potentials which would correspond to any distinct valency states such as PtOH, PtO, or PtO_2 in potential-charge plots between 0.5 and 1.8V, and emphasize the difficulty of assigning valence states to Pt atoms on the electrode surface.

At the monolayer level, a place exchange mechanism was proposed by Reddy, Genshaw, and Bockris[30] to indicate the path of oxide formation. The scheme is

$$Pt + H_2O \rightleftharpoons PtOH + H^+ + e^- \qquad \text{(II-3)}$$

$$PtOH \xrightarrow{\text{place exchange}} HOPt \qquad \text{(II-4)}$$

$$HOPt \rightleftharpoons OPt + H^+ + e^- \qquad \text{(II-5)}$$

In this mechanism, the OH species is first chemisorbed on the Pt surface. Next the OH species and a Pt atom change places, placing the OH species in an inverted position below the surface. The HOPt is then oxidized to OPt. A similar view is reported by Kozlowska et al.[5] Vetter and Schultz[31] also favor the place exchange mechanism. However, they suppose that chemisorbed $O^=$ ions, not the OH species, are involved in oxide formation by place exchange with Pt oxidized to $Pt^=$ ions.

Recently Conway et al.[5,32,33] in a series of papers reinvestigated the oxide film formation on Pt by linear potential sweep technique in highly purified H_2SO_4 solution, and find that

(a) considerable structure is evident in the current-potential curve in the beginning of oxygen adsorption;

(b) the film formation process is more or less reversible in the initial stage (0.85 - 1.1 V);

(c) above 1.1 V, the film formation is very irreversible.

On the basis of their results, a three-stage mechanism of oxide formation on Pt is proposed. The scheme is set up as:

$$Pt_4^* + H_2O \rightleftharpoons Pt_4OH + H^+ + e^- \qquad \text{(II-6)}$$

$$Pt_4OH + H_2O \rightleftharpoons Pt_2OH + H^+ + e^- \qquad \text{(II-7)}$$

$$Pt_2OH + H_2O \rightleftharpoons PtOH + H^+ + e^- \qquad \text{(II-8)}$$

until the potential reaches ∿1.1V. Further oxidation of the Pt surface leads to the formation of PtO via place exchange rearrangement (see details illustrated in Ref. 33). This place exchange rearrangement also accounts for the hysteresis between the anodic- and cathodic-going current-potential profiles and the experimentally observed single cathodic peak can be represented in terms of the kinetics of a two-stage reduction of PtO to Pt via PtOH in rearranged states.

Electrochemical techniques alone lack the specificity to resolve the nature of the anodic oxygen film on an atomic level. Non-electrochemical tools may be able to provide such information, although to date they have not yet afforded sufficient specificity.

By employing electrode potential scanning ellipsometric spectroscopy, Horkans et al.[12] have shown that the optical properties of the film changes substantially at 1.1V. This abrupt change seems to indicate a change in intrinsic properties of the film. The results are compatible with the conclusion of Conway et al.[5,33] that at 1.1V the surface is covered with a monolayer of PtOH and conversion to PtO begins as the potential increases anodically to 1.4V. Further-

---

*The species Pt_4 indicates the sites available for chemisorption of OH species on the (100) crystal planes. The formulae shown do not represent stoichiometric species but simply the surface site occupancy ratio.

more, Horkans et al.[12] have found that the film thickness determined ellipsometrically changes linearly with potential and extrapolates to zero at ∿0.8V, in agreement with the results of electrochemical measurements. The thickness of the film is also found to be nearly linearly dependent on charge and extrapolates to zero thickness at zero charge. This behavior with the constancy of the refractive index of the film between 1.1 and 1.6 V leads to the proposition of patch growth of the anodic oxide formation. Other ellipsometric [34,35] and spectro reflective[36] studies of the anodic film on Pt have been reported.

Kim, Winograd, and Davis[37] and Allen, Tucker, Capon, and Parsons[38] have used X-ray photoelectron spectroscopy to study the oxide film formed on Pt. The results from these two groups are quite different. Kim et al.[37] have indicated that PtO_{ads}, PtO, and PtO_2 are formed upon electrochemically oxidized Pt electrodes at potentials of 0.7V, 1.2V, and 2.2V, and predominantly PtO_2 at 2.2V. The Parsons group[38] suggest from their experimental results that a single species, probably $Pt(OH)_2$, exists up to potentials of 2.4V where coulometry[39] indicates a limiting coverage on Pt. No evidence for PtO_{ads} or PtO was found by these workers. Only under extreme oxidizing conditions (at 4V for 4 hr or more) was PtO_2 detected.

Employing Auger spectroscopy to investigate Pt surfaces, anodized in H_2SO_4 at 500 mA/in^2 for 16 hr, John and Heldt[40] have indicated that the anodized Pt surface contains 50% oxygen and corresponds to a composition of PtO. This stoichimetry also corresponds with the interpretation of Thacker and Hoare's electrochemical data.[14]

John and Heldt also claim that it is possible that oxygen is adsorbed or dermasorbed strongly and that its stoichiometry and stability would be difficult to distinguish from an oxide.

B. Reversible Potential of Oxygen at Pt

The standard reversible potentials of O_2 electrodes are:[41]

Acid solution $O_2 + 4H^+ + 4e^- \rightleftharpoons 2H_2O$ $E_o = 1.229V$ at 25°C (II-9)

Alkaline solution $O_2 + 2H_2O + 4e^- \rightleftharpoons 4OH^-$ $E_o' = 0.401V$ at 25°C (II-10)

The Nernst equation for O_2 electrode potential at 25°C is

$$E = E_o + \frac{RT}{4F} \ln p_{O_2} + \frac{RT}{F} \ln a_{H^+} - \frac{RT}{2F} \ln A_{H_2O}$$

$$= E_o' + \frac{RT}{4F} \ln p_{O_2} - \frac{RT}{F} \ln a_{OH^-} + \frac{RT}{2F} \ln A_{H_2O}$$

From the equation, the reversible potential for O_2 electrode should have a ∿60 mV shift per pH unit and a dependence of ∿15mV per ten-fold change of O_2 pressure. These are criteria for the reversible O_2 electrode to be observed under equilibrium conditions.

The reversible O_2 electrode potential is hard to achieve in practice. This can be attributed to the very low exchange current density, which is of the order of $10^{-9} - 10^{-11}$ A/cm^2. Trace impurities in solution and slow metal dissolution can shift the potential drastically. Usually a value in the range 0.8-1.1 V is observed. Even in the absence of impurity effects, a very long time is required for the electrode to achieve its reversible potential. For a capacitance of ∿10^{-4} f/cm^2 and an exchange current density of 10^{-10} A/cm^2,

the time constant is $\sim 10^4$ sec; therefore many hours could be required for the electrode to drift to near the reversible potential on open circuit.

Several theories[2] were advanced to account for the unattainability of the reversible O_2 electrode potential.

The first attempt was the so-called oxide theory, described by Lorenz and Hauser,[42,43] who were the first to use the term. According to this theory, the electrode is covered with an oxide film and the open-circuit potential is determined by the O_2/oxide couple instead of the O_2/Pt couple. However, this theory had failed to explain the observations made by Bain.[44] He measured the O_2 electrode potentials of Grove cells with bright and oxidized (heat in a flame and cool in air) Pt metals as the O_2 electrode, and observed that the initial potentials were different for those electrodes, but the values approached a common one after 30 minutes. He reasoned that if the potential was determined by the O_2/oxide couple, the rest potential would be different at equilibrium conditions. Unfortunately, this was not observed.

The second explanation was tried by the peroxide theory. Brislee[45] observed that the value of the open-circuit potential of the Grove cell was in the range 1.0-1.1 V in 30 days, and detected peroxide in the solution after measurements. When H_2O_2 was added to the solution the potential fell to 0.98 V, and afterward rose to the usual value. If the primary product of the Grove cell was H_2O_2 instead of H_2O, Lewis[46] suggested that the rest

potential could be determined by the peroxide in the solution. O_2 reduction did produce H_2O_2 in solution.[10]

The reactions involved with H_2O_2 and O_2 and their standard potentials[47] are as follows:

Acid solution $O_2 + 2H^+ + 2e^- \rightleftharpoons H_2O_2$ $E_o = 0.682V$ at 25°C (II-11)

Alkaline solution $O_2 + H_2O + 2e^- \rightleftharpoons OH^- + HO_2^-$ $E_o = -0.048V$ at 25°C (II-12)

Traces of H_2O_2 in the solution can cause the open-circuit potential to be observed in the range 0.8-0.9 V. However, Hoare[2] argues that no H_2O_2 is detected under open-circuit conditions. He attributes the H_2O_2 present in the solution to be produced by impurities involved in a local cell phenomenon.

The third one, mixed potential theory, was first proposed by Hoar .[49] He explained that the deviation of rest potential from the equilibrium potential was due to the presence of an oxide film with pores pervious to the solution. A local cell was then set up between the film surface and the relatively anodic metal base of the pores, causing an irreversible removal of oxygen from the film surface. A lowering of the potential then occurred. Giner[50] has suggested that the mixed potential mechanism is composed of either the O_2/H_2O couple or O_2/H_2O_2 couple and Pt/chemisorbed molecular oxygen couple. With no H_2O_2 detected in the solution under open-circuit conditions and in favor of the Pt-O model, Hoare[2] prefers to show that the mixed potential mechanism involves the O_2/H_2O couple and the Pt/Pt-O couple where Pt-O represents

a layer of adsorbed oxygen atoms on Pt. From the analysis of oxide coverage and O_2 pressure dependence of the rest potential, Wroblowa, Rao, Damjanovic, and Bockris[51] have proposed that oxide-free electrodes acquire a mixed potential due to cathodic O_2 reduction and oxidation of impurities as the anodic component. They attribute the lack of reversibility of the O_2 electrode to the presence of impurities. Though mixed potential mechanisms might account for the rest potential observed in the range 0.8-1.1 V, persuasive evidence has not yet been presented at this stage.

There are some indications that the reversible O_2 electrode potential has been observed. These observations are challenged by various workers, due to the improper experimental conditions employed or failure to reproduce the same result. Bockris and Huq[52] claimed that they observed the reversible O_2 potential at Pt by heating the electrode in O_2 atmosphere at 500°C for 2 hours and prolonged pre-electrolysis of the electrolyte. The unattainability of reversible O_2 potential had been attributed to the impurities present in the solution. Watanabe and Devanathan[53] also claimed to observe the reversible O_2 electrode potential with an anodically oxidized Pt electrode in purified solution. The potential observed by these workers, however, probably was an intermediate value as the electrode potential drifted slowly back to the usual observed value following the prior anodic prepolarization.

According to Hoare,[54] after prolonged contact of Pt with concentrated HNO_3, a film of electronically conducting chemisorbed oxygen is produced on Pt. Such a surface is inert and the O_2/H_2O reaction

can be established on this surface. A steady potential of 1.225 V is obtained by Hoare. The potential observed by Hoare can possibly be attributed to those of the redox couple involving NO_2 and NO. These species are produced on the Pt electrode surface during prolonged oxidation of Pt in concentrated HNO_3 and are adsorbed on the electrode surface, which resist through rinsing procedures. The anodic formed oxygen film, which is thought to be electronically conducting, is considered by Schultze and Vetter[55] to be a barrier for electron transfer. They explain the charge transfer through the film for O_2/H_2O reaction via electron tunnelling mechanism.

C. Kinetics and Mechanism of O_2 Generation at Pt

Since oxygen was first obtained by electrolysis of water by Nicholson and Carlisle[56] in 1800, the kinetics of O_2 generation have been studied by many workers (for details, see review articles by Hoare,[2] Vetter,[57] Breiter,[58] Erdey-Gruz[59]) but progress has been slow and the mechanisms proposed are for the most part conjectural.

The reported experimental facts and proposed mechanisms are briefly summarized in the following section.

(1) Experimental Facts

A Tafel relation $\eta = a + b \log i$ is usually observed, and indicates that O_2 formation is under kinetic control provided mass transfer is not limiting. Some kinetic parameters from prior studied are listed in Table II-1. The reported Tafel slopes, b, scatter with no sense of agreement. Factors attributing to this situation

TABLE II-1 Kinetic Parameters for O_2 Generation at Pt

Solution	Temp. °C	Tafel Slope b V/dec.	Exchange Current Density A/cm²	Current Range A/cm²	Ref.
0.2N H_2SO_4	14	0.115	6×10^{-10}	10^{-8}-10^{-4}	60
0.1N H_2SO_4	20.5	0.130		2×10^{-4} - 3×10^{-3}	61
1 N H_2SO_4	25	0.108		10^{-6}-10^{-1}	62
2 N H_2SO_4		0.106		10^{-5} - 1	63
1 N H_2SO_4	20	0.12		10^{-5} - 1	64
0.001N-0.1N H_2SO_4		0.083-0.097	$1.3\text{-}2.2 \times 10^{-10}$	10^{-10}-10^{-3}	52
2 N H_2SO_4	25	0.122	1.3×10^{-9}-	10^{-7} - 10^{-4}	65
0.1 N H_2SO_4		0.113	2.5×10^{-10}	10^{-10}-10^{-2}	66
0.1 N H_2SO_4		0.115		10^{-4}-10^{-2}	67
0.1 N H_2SO_4	25	0.086	9×10^{-12}	10^{-7}-10^{-5}	49
1 N H_2SO_4	25	0.09-0.12	$\sim10^{-9}$	10^{-5} - 1	55
0.2 N HNO_3	20	0.114	1×10^{-10}	10^{-7} - 1	68
5 M $HClO_4$	25	0.14		10^{-4}-10^{-1}	69
1 N $HClO_4$	25	0.110	4×10^{-10}	10^{-8}-10^{-3}	70
85% O-H_3PO_4	25.1	0.139	5.4×10^{-11}	10^{-8}-10^{-5}	71
0.1 N NaOH	25	0.064	3×10^{-13}	10^{-7}-10^{-5}	49
1 N KOH	20	0.3		10^{-5} - 1	64
1 M NaOH	25	0.057			10
1 N KOH		0.14, 0.21		10^{-3} - 1	72
1 N KOH		0.07, 0.28		10^{-5} - 1	73
0.5 N KOH		0.11		10^{-5}-10^{-3}	74
1 N KOH	25	0.055, 0.110	1×10^{-11}	10^{-7}-10^{-3}	70
1 M KOH		0.047	4×10^{-12}	10^{-6}-10^{-3}	75

include the following:

a. Different history and particularly pretreatment of electrodes
b. Composition and purity of electrolytes
c. The potential and time dependence of the state of electrode surface, which influences the catalytic activity of the Pt electrode for O_2 formation.

The exchange current density is very small, in the range 10^{-9} - 10^{-11} A/cm^2. At a current density of 10^{-6} A/cm^2, at least an overpotential of 300-400 mV is required. This indicates that the O_2 generation is a highly irreversible process with no sensitivity of the kinetics to the back reaction under measurable conditions. Thus it is not possible so far to obtain kinetic data following the rate-controlling step.

Several studies have been conducted on the pH dependence of the overpotential. The quantitative results are rather different between workers;[52,70,76] however, a positive pH dependence in low pH regions and a negative pH dependence at high pH values are shown, indicating O_2 comes from the water molecule in acid and from the OH^- ion in alkaline solution.

The overpotential decreases and the Tafel slope slightly increases with increasing temperature in the range 0-100°C. Bowden,[60] Rius, Llopis, and Giner,[77] Roiter and Yampolskaya,[61] and Appleby,[71] all have observed this behavior in their studies. No general agreement has been reached as to whether the activation energies in acid and in alkaline solution are of the same magnitude. This leads to difficulty in distinguishing the reaction mechanism in acid and in alkaline solution.

The involvement of anodically formed oxide in O_2 formation is rather unclear. Rosental and Veselovskii[78] have indicated, by means of O^{18}, that oxide film formed at high anodic potentials (> 1.5V) is directly involved in the O_2 formation, while an oxide film formed at lower potentials (< 1.5V) is not. Their results have been criticized by Vetter[57] with the argument that they have not checked the O^{18} exchange between enriched oxide and unenriched electrolyte. The O^{18} might come from the already exchanged electrolyte directly at the electrode surface.

The anodic oxide film has a large influence on the kinetics of O_2 formation. Schultze and Vetter[55] have proposed that the oxide film is a barrier for electron transfer in O_2 formation, and proposed a relationship involving a linear decrease of the logarithm of the current with increasing film thickness for a given applied potential. Damjanovic, Ward, and O'Jea[67] have also found that the thickness of the oxide film affects the catalytic activity for O_2 formation in a manner similar to that described by Schultze and Vetter. Charge transfer through the anodic film, however, in itself is not the only process responsible for the irreversibility of the O_2 electrode.

(2) Possible Reaction Mechanism Proposed for O_2 Generation

From Table 1, the kinetic data for O_2 generation are diverse, despite a relatively large number of studies conducted. These discrepancies lead to the proposition of various reaction mechanisms. Even with the same kinetic parameters obtained, many alternative reaction mechanisms are still possible. However, most workers

agree that the rate-controlling step is an electron transfer, and the most likely step is a charge transfer step involving H_2O molecules in acid or OH^- ions in alkaline solution to form hydroxyl radicals on the electrode surface,

Acid solution: $H_2O \longrightarrow (OH)^* + H^+ + e^-$ (II-13)

Alkaline solution: $OH^- \longrightarrow (OH) + e^-$ (II-14)

This step is then followed by several possible steps leading to the formation of O_2, but no means are available to distinguish these steps. The controversies emerge from the speculation as to the further steps.

There are two different views concerning the intermediates formed after the rate-controlling steps. One is that the intermediate is principally an O species, in a form of either a metal oxide or hydroxide, or an adsorbed species such as O or OH radicals; no peroxide is involved. Bockris and Huq,[52] and Damjanovic, Dey, and Bockris,[70] support this view. The other is that H_2O_2 or a peroxide ion is formed as an intermediate produced from hydroxyl radical or from the O atom. Hoar ,[49] and Vetter[57] prefer to have peroxide involved in the overall reaction. (The peroxide mechanism will be discussed further later in this chapter.)

Even for a given type of intermediate, a large number of reaction paths are still possible for the overall reaction to proceed.

---

*The parenthesis simply indicates the species adsorbed on the electrode surface.

According to the analysis of Milner,[80] several thousand reaction paths are possible with OH, O, O_2H, and O_2H^- considered as intermediates. By applying the most drastic assumptions, the number only reduces to eleven. Damjanovic et al.[70] has summarized fourteen paths (including five paths proposed by Bockris[81] and the rest from others) for O_2 generation with theoretically calculated Tafel parameters and stoichiometric numbers. These reaction mechanisms are listed in Table II-2.

A further severe complication arises from the fact that O_2 generation reaction occurs at significant rates only at potentials so anodic that the Pt surface is covered with an oxide layer, while the reverse O_2 reduction occurs at appreciable rate in the potential range 0.8-0.0V, where the state of the electrode surface is quite different. Thus, the anodic O_2 generation and cathodic O_2 reduction reaction paths may be different. Therefore, it is not possible to obtain the stoichiometric numbers from a comparison of the anodic and cathodic Tafel slopes. The other alternative to evaluate the stoichiometric number is from the current-overpotential relation at potentials near reversible O_2 electrode potential, where the back reaction is appreciable. This technique has not proved practical for O_2generation, because of the very low exchange current density and interference from impurity effects and competing processes intrinsic to the Pt electrode surface (anodic film).

In 1937, Glasstone and Hickling[83] proposed that discharge of hydroxyl ions led to the irreversible formation of H_2O_2, by combination of the radical in pairs; O_2 was then generated by decomposi-

Table II-2. Various paths in O_2 generation, Tafel parameters and stoichiometric numbers (from Ref. 70).

	$\partial V/\partial \ln i$ Anodic low η	Anodic high η	Cathodic	ν
(1) The "Oxide" path				
$S + H_2O \rightarrow SOH + H^+ + e^-$ —	$2RT/F$		$2RT/F$	4
$2SOH \rightarrow SO + SH_2O$	$RT/2F$		∞	2
$2SO \rightarrow O_2 + 2S$	$RT/4F$		∞	1
(2) The "Electrochemical Oxide" path				
$S + H_2O \rightarrow SOH + H^+ + e^-$	$2RT/F$		$2RT/3F$	2
$SOH + S + H_2O \rightarrow SO + SH_2O + H^+ + e^-$	$2RT/3F$	$2RT/F$	$2RT/F$	2
$2SO \rightarrow O_2 + 2S$	$RT/4F$		∞	1
(3) The "Hydrogen Peroxide" path				
$4S + 4H_2O \rightarrow 4SOH + 4H^+ + 4e^-$	$2RT/F$		$2RT/F$	4
$2SOH \rightarrow SH_2O_2 + S$	$RT/2F$		$RT/2F$	1
$SH_2O_2 + SOH \rightarrow SOH_2 + SO_2H$	$RT/3F$		RT/F	1
$SO_2H + SOH \rightarrow SH_2O + S + O_2$	$RT/3F$		∞	1
(4) The "Metal Peroxide" path				
$4S + 4H_2O \rightarrow 4SOH + 4H^+ + 4e^-$	$2RT/F$		$2RT/F$	4
$SOH \rightarrow SO + SH_2O$	$RT/2F$		$RT/2F$	1
$SO + SOH \rightarrow S + SHO_2$	$RT/3F$		RT/F	1
$SHO_2 + SOH \rightarrow O_2 + S + SH_2O$	$RT/4F$		∞	1
(5) The "Electrochemical Metal Peroxide" path				
$3S + 3H_2O \rightarrow 3SOH + 3H^+ + 3e^-$	$2RT/F$		$6RT/5F$	3
$2SOH \rightarrow SO + SH_2O$	$RT/2F$	RT/F	$RT/2F$	1
$SO + H_2O \rightarrow SHO_2 + H^+ + e^-$	$2RT/5F$	$2RT/F$	$2RT/3F$	1
$SHO_2 + SOH \rightarrow S + O_2 + SH_2O$	$RT/4F$		∞	1
(6) The "Alkaline" path of Hoar				
$S + H_2O \rightarrow SOH + H^+ + e^-$	$2RT/F$		$2RT/3F$	2
$SOH + H_2O \rightarrow SH_2O_2^- + H^+$	RT/F		RT/F	2
$2SH_2O_2^- \rightarrow S + SO_3^{2-} + 2H_2O$	$RT/2F$	RT/F	$RT/2F$	1
$SO_3^{2-} \rightarrow S + O_2 + 2e^-$	$RT/3F$		RT/F	1
(7) Path suggested by Conway & Bourgault				
$3S + 3H_2O \rightarrow 3SOH + 3H + 3e^-$	$2RT/F$		$6RT/5F$	3
$SOH \rightarrow SO + H^+ + e^-$	$2RT/3F$	$2RT/F$	$2RT/5F$	1
$SO + SOH \rightarrow SHO_2$	$RT/3F$	RT/F	RT/F	1
$SHO_2 + SOH \rightarrow S + SH_2O + O_2$	$RT/4F$		∞	1
(8) Alternative path suggested by Conway & Bourgault				
$2S + 2H_2O \rightarrow 2SOH + 2H^+ + 2e^-$	$2RT/F$		$2RT/3F$	2
$SOH \rightarrow SO + H^+ + e^-$	$2RT/3F$	$2RT/F$	$2RT/5F$	1
$SO + H_2O \rightarrow SHO_2 + H^+ + e^-$	$2RT/5F$		$2RT/3F$	1
$SHO_2 + SOH \rightarrow S + SH_2O + O_2$	$RT/4F$		∞	1
(9) Path suggested by Riddiford				
$S + H_2O \rightarrow SOH + H^+ + e^-$	$2RT/F$		$2RT/3F$	2
$2SOH \rightarrow SO + SH_2O$	$RT/2F$		$RT/2F$	1
$SO + H_2O \rightarrow SHO_2 + H^+ + e^-$	$2RT/5F$	$2RT/F$	$2RT/3F$	1
$SHO_2 + H_2O \rightarrow O_2 + SH_2O + H^+ + e^-$	$2RT/F$		$2RT/F$	1
(10) Krasilshchikov path (for Ni electrodes)				
$S + H_2O \rightarrow SOH + H^+ + e^-$	$2RT/F$		$2RT/3F$	2
$SOH \rightarrow SO^- + H^+$	RT/F		RT/F	2
$SO^- \rightarrow SO + e^-$	$2RT/3F$	$2RT/F$	$2RT/F$	2
$2SO \rightarrow O_2 + 2S$	$RT/4F$		∞	1
(11) Wade & Hackerman's path				
$2S + 2H_2O \rightarrow SO + SH_2O + 2H^+ + 2e^-$	RT/F		$RT/3F$	1
$SO + 2SOH^- \rightarrow 2S + SH_2O + O_2 + 2e^-$	$RT/3F$		RT/F	1
(12) $S + H_2O \rightarrow SOH + H^+ + e^-$	$2RT/F$		$2RT/7F$	1
$SOH \rightarrow SO + H^+ + e^-$	$2RT/3F$	RT/F	$2RT/5F$	1
$SO + H_2O \rightarrow SO_2H + H^+ + e^-$	$2RT/5F$	$2RT/F$	$2RT/3F$	1
$SO_2H \rightarrow S + O_2 + H^+ + e^-$	$2RT/7F$		$2RT/F$	1
(13) $S + H_2O \rightarrow SOH + H^+ + e^-$	$2RT/F$		$2RT/3F$	2
$SOH + H_2O \rightarrow SO{-}H{-}OH^- + H^+$	RT/F		RT/F	2
$SO{-}H{-}OH^- \rightarrow SO{-}H{-}OH + e^-$	$2RT/3F$	$2RT/F$	$2RT/F$	2
$SO{-}H{-}OH \rightarrow SO + H_2O$	$RT/2F$	RT/F	∞	2
$2SO \rightarrow S + O_2$	$RT/4F$		∞	1
(14) $S + H_2O \rightarrow SOH + H^+ + e^-$	$2RT/F$		$2RT/7F$	1
$SOH + H_2O \rightarrow SO{-}H{-}OH^-$	RT/F		$RT/3F$	1
$SO{-}H{-}OH^- \rightarrow SO{-}H{-}OH + e^-$	$2RT/3F$	$2RT/F$	$2RT/5F$	1
$SO{-}H{-}OH \rightarrow SO + H_2O$	$RT/2F$	RT/F	$RT/2F$	1
$SO + H_2O \rightarrow SHO_2 + e^-$	$2RT/5F$	$2RT/3F$	$2RT/3F$	1
$SHO_2 \rightarrow S + O_2 + H^+ + e^-$	$2RT/7F$		$2RT/F$	1

tion of the peroxide. This interpretation was criticized by Walker and Weiss[84] with the argument that the combination of hydroxyl radicals to form H_2O_2 was highly improbable, since the anodic formation of H_2O_2 had not been detected. They then suggested a reaction path as

$$OH^- \rightleftharpoons (OH) + e^- \quad \text{rate-controlling} \qquad \text{(II-14)}$$

$$(OH) + (OH) \rightleftharpoons H_2O + (O) \qquad \text{(II-15)}$$

$$(O) + (O) \rightleftharpoons O_2 \qquad \text{(II-16)}$$

Considering the cathodic O_2 reduction, Vetter[57] has proposed a reaction path with H_2O_2 as intermediate:

$$OH^- \rightleftharpoons (OH) + e^- \qquad \text{(II-14)}$$

$$OH^- + (OH) \rightleftharpoons H_2O_2 + e^- \qquad \text{(II-17)}$$

$$H_2O_2 \rightleftharpoons HO_2^- + e^- \qquad \text{(II-18)}$$

$$HO_2^- \rightleftharpoons (HO_2) + e^- \qquad \text{(II-19)}$$

$$(HO_2) \rightleftharpoons O_2^- + H^+ \qquad \text{(II-20)}$$

$$O_2^- \rightleftharpoons O_2 + e^- \qquad \text{(II-21)}$$

He reasons that the subsequent steps after the formation of H_2O_2 are very fast, causing H_2O_2 to be undetectable. In contrast, Bockris and Huq[52] have concluded that the discharge of OH^- ion is the rate-controlling step for O_2 formation in H_2SO_4 at Pt, followed by the formation of O atoms which then combine to form O_2.

Hoar [49] has studied the generation of O_2 in NaOH solutions at Pt and his data do not correspond to any of the five mechanisms proposed by Bockris.[81] Hoar proposes that the step

$$(OH) + OH^- \longrightarrow (H_2O_2^-) \qquad \text{(II-22)}$$

is rate-controlling. This raises the question as to whether the mechanism of O_2 formation in acid and alkaline solutions is along the same paths or not. By determining the activation energies, Stout[85] has concluded that the mechanisms are different in acid and in alkaline solutions with different activation energies in each solution. On the contrary, Yoneda[86] has argued that the mechanisms are usually the same in both solutions with similar measured activation energies.

In an attempt to resolve this controversy, Riddiford[79] analyzed the results of Bockris and Huq and of Hoar , and suggests that the mechanism is the same in all solutions with the step

$$(OH) + OH^- \rightleftharpoons (O) + H_2O + e^- \qquad \text{(II-23)}$$

rate-controlling.

Damjanovic et al.[70] have re-examined the O_2 generation on Pt in acid and in alkaline solutions. Their results support the mechanisms proposed by Bockris and Huq in acid solution and by Hoar in alkaline solution. However, three reaction paths are still possible in acid and another three possible in alkaline solution.

(3) The Effects of Ions on Oxide Film Formation and Oxygen Generation

The previous studies of ion effects at a Pt electrode have principally concentrated on the adsorption behavior of halide anions. It has been demonstrated by various techniques[87-89] that anions ad-

sorbed on Pt are in the order $I^- > Br^- > Cl^- > SO_4^= > ClO_4^-, F^-$ at the same electrode potential and the same concentration of ions.

Halide ions except F^- ion have a retarding effect on anodic oxygen film formation on Pt in acids.[90,91] Breiter[91] was the first to use linear potential sweep to show the effect of halide anions on anodic oxygen film formation. This technique has the advantage of bringing the electrode to a more reproducible surface state than generally achieved with other methods.

A study has been made by Podlovchenko, Epstein and Frumkin[92] to compare the adsorption properties of F^- anions and $SO_4^=$ anions on Pt. They have shown that $SO_4^=$ anions are more strongly adsorbed on Pt than F^- ions, and that the anodic oxygen film formation in HF begins at more cathodic potentials than that in H_2SO_4 with solutions of similar pH. Recently, Lane and Hubbard[93] have indicated that F^- anions have a strong retarding effect on anodic film formation in H_2SO_4 solution. This result is rather surprising, as judging from the results of Podlovchenko et al.[92] The F^- anion effect shown by Lane and Hubbard is probably due to the presence of Cl^- anions, either in the fluoride salt used or adsorbed during rinsing processes.

Anions in high concentration are believed to be involved in oxygen generation. Gerovich, Kaganovich, Vegelesov, and Gorokhov,[94] Kasatkin, Rozental, and Veselovskii[95] have observed two Tafel regions in O_2 overpotential measurements in concentrated $HClO_4$ solutions at Pt in the potential range 1.5-3.0 V. They consider that the high Tafel region is due to the firect participation of ClO_4^- anions in the electrode process. This is confirmed

by using O^{18} enriched $HClO_4$ solution and finding that the O_2 evolved in the upper Tafel region is enriched with the O^{18} isotope. A similar situation occurs in concentrated H_2SO_4 (7-15 N) at high anodic potentials (2.5-3.0 V) along with the production of $H_2S_2O_8$ and H_2SO_5.[96,97]

Hickling and Hill[98] reported that oxygen overpotential at Pt increased by 10-110 mV in 1 N KOH and 40-310 mV in 1 N H_2SO_4 in the presence of 0.02-0.1 N KF, and that this phenomenon was unique as compared to other metals of the Pt family. No explanation was attempted by these workers.

Erdey-Gruz and Shafarik[63] showed that oxygen overpotential on Pt in 1N H_2SO_4 increased in the presence of large amounts (0.3-1.0 N) of cations in the following order: $K^+ > Al^{+++} > NH_4^+ > Zn^{++} > Na^+ > Mg^{++} > Li^+$. Their interpretation was that metal cations are incorporated in the double layer by association with the already adsorbed $SO_4^=$ ions. They propose that this results in deforming water molecules adsorbed on the electrode surface and changing their bonds with other water molecules. The attractive action of metal cations, affecting the electrons of adsorbed water molecules, hinders the transfer of electrons to the electrode, and increases the activation energy of the O_2 formation (i.e., the potential distribution across the interface is changed).

In the high anodic potential range (2.0-3.5 V), Frumkin[99] has shown that the alkaline metal cations increase the O_2 overpotential on Pt in the order $Cs^+ > Li^+ > Na^+ > K^+$. This cation effect has been interpreted on the basis that chemisorption of oxygen species

with negative charge overcompensates the positive potential of the electrode relative to the bulk solution and leads to the adsorption of cations.

Rozawa[10] has shown that O_2 overpotential on Pt is increased by 15-90 mV when Ba^{++}, Sr^{++}, Ca^{++} ions are added to 1 M NaOH. This effect has been explained in terms of ion-exchange mechanisms. The metal cations exchange for protons in the hydroxyl groups which exist on the electrode surface to form a surface complex. The O_2 formation is thus depressed. The anodic film on Pt should have ion exchange properties and this explanation appears quite logical.

CHAPTER III

EXPERIMENTAL PROCEDURES

The experimental procedures and equipment employed in carrying out the electrochemical measurements are described in this chapter. The equipment is essentially the same as that used in the thesis research of R. Zurilla for O_2 electrode studies on Au. The description is divided into the following categories:

1. Mechanical Equipment
2. Preparation and Purification Techniques
3. Electronic Equipment and Measurements

A. Mechanical Equipment

1. The Electrochemical Cell

The experimental cell was designed and built at Case Western Reserve University by prior workers and has been described by Zurilla and Yeager.[100] This cell, which was constructed entirely from Teflon, consisted of a main compartment for the rotating disc Pt electrode and two separate compartments for the counter and reference electrodes. The main compartment of the cell and the position of the assembled disc electrode are illustrated in Fig. III-1. The volume of the main compartment was approximately 500 cc. A volume of 400 cc of electrolyte was used for the experiments. Teflon connectors CE and RE were used for jointing the counter electrode and reference electrode compartments to the main cell. A Pd foil (99.99%), 2.9 cm diameter x 0.01 cm, was used as

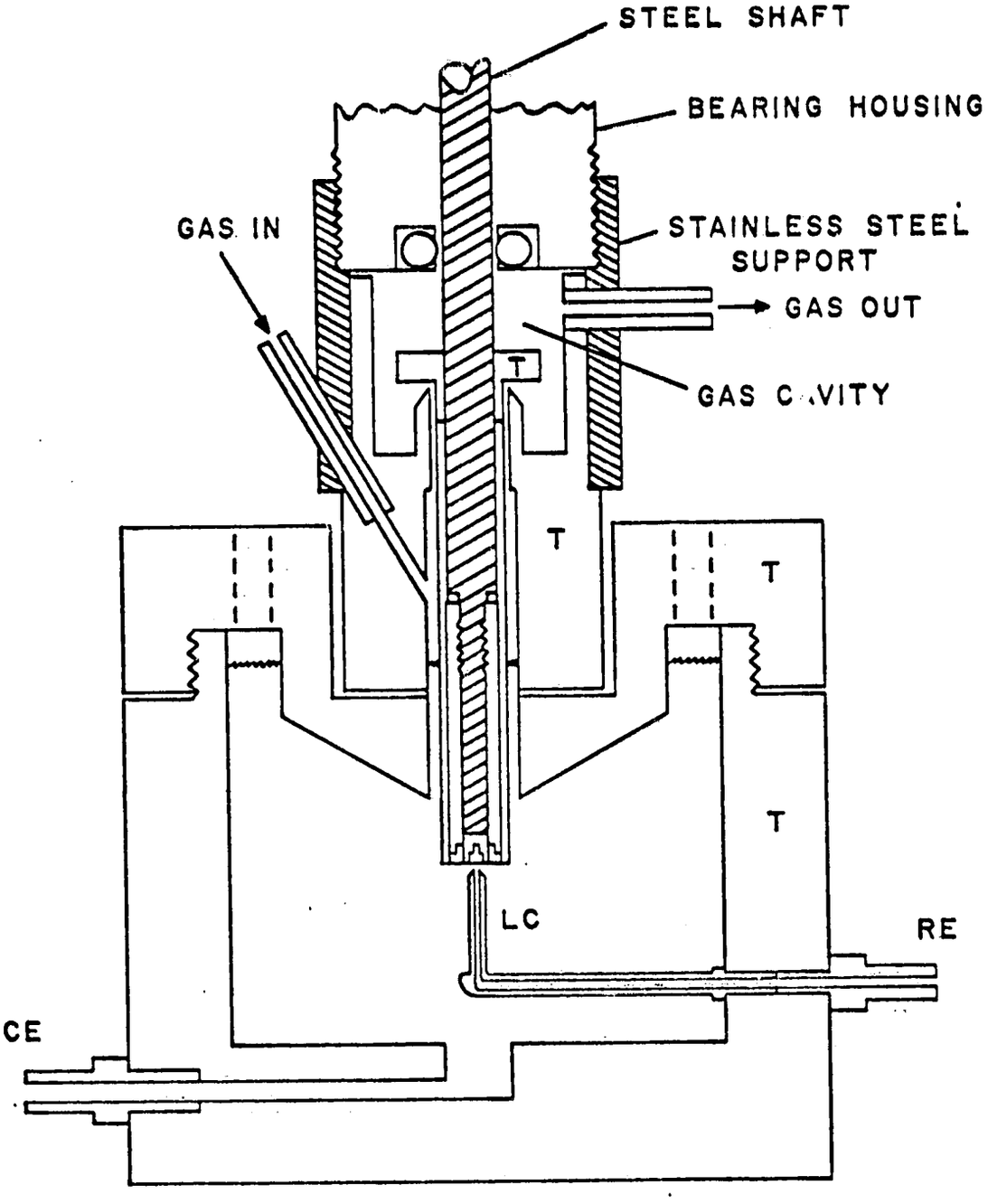

Fig. III-1. Main compartment of Teflon cell. T - Teflon. RE - Reference electrode compartment connector. compartment connector. LC - Luggin capillary. CE - Counter electrode

a counter electrode with the back side charged with purified H_2. After prolonged charging with purified H_2, the electrode behaves as a β-Pd-H electrode, as will be described later. The Pd electrode is cathodically protected against dissolution and contamination of the electrolyte with Pd is quite unlikely with this arrangement.

The reference electrode was connected to the main compartment via a Luggin capillary, placed approximately 3 mm below the surface of the working electrode. The reference electrode was a Pd foil electrode (99.99%), 2.5 cm diameter x 0.01 cm, also with purified H_2 on the back side. During the charging of H_2, the solution side was filled with purified He.

Normally the reference and counter electrodes were charged with purified H_2 for 24 hours in advance of a run. This charging method results in the formation of a stable H-Pd alloy commonly referred to as the β-phase of the alloy.[101] This Pd electrode is designated as β-Pd-H and attains the potential of a reversible hydrogen electrode (RHE). Another Pd hydrogen reference electrode was fabricated, also consisting of a small Pd bead mounted on Teflon. With short time cathodic charging with H_2 evolution, the Pd bead formed an α-phase of the H-Pd alloy as described by Hoare.[102] This α-Pd-H electrode shows a potential of +0.050V vs. RHE. Provisions were made so that the α-Pd-H electrode could be inserted into the reference electrode compartment, either for use as a reference electrode or for checking the potential of the β-Pd-H electrode. The counter and reference electrode compartments are shown in Fig. III-2.

COUNTER ELECTRODE COMPARTMENT

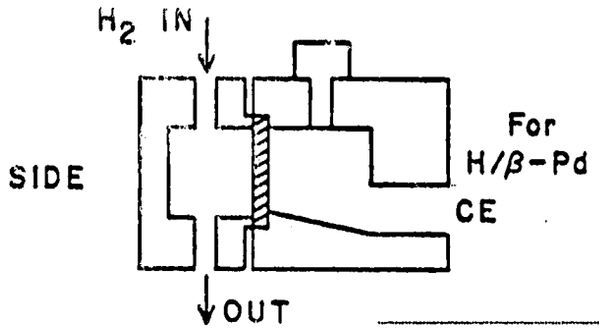

REFERENCE ELECTRODE COMPARTMENT

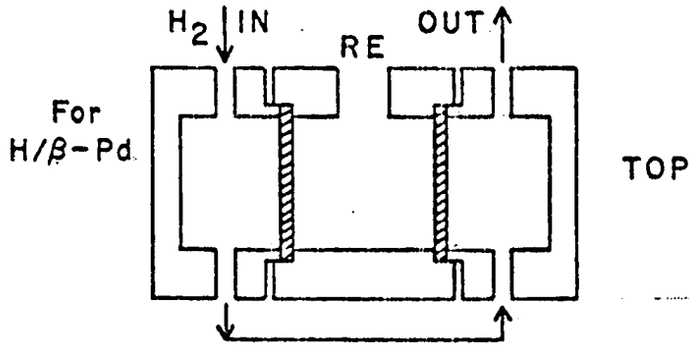

Fig. III-2. Counter and reference compartments.

2. The Rotating Electrode Assembly

The rotating electrode assembly consisted basically of a hard tempered steel shaft, mounted on sealed precision bearings, which was rotated via a belt and pulley system by a 1/15 HP high speed Bodine universal motor, type NSE-12. The motor speed was controlled by a General Radio speed control, type 1701-AU. Shaft rotation rates were measured by means of a light beam which was transmitted onto a photocell through sixteen equally spaced holes in an aluminum disc attached to the upper part of the shaft. The frequency of the pulsed output from the photocell was measured with a Fluke 1941 A digital counter. An aluminum framework was used to mount the motor, shaft, and bearings, and the bearing housing was electrically insulated from the framework by use of a 5/8 inch thick Lucite spacer.

The electrical connection from the working electrode was made at the top end of the shaft by means of spring-loaded Ag-graphite brushes. This arrangement generated negligible electrical noise even at high rotation speed.

3. The Nitrogen Atmosphere Box

The electrochemical experiments were performed in a N_2 atmosphere box to prevent CO_2 and dust contamination. A Forma Scientific enclosure box was modified to accommodate the rotating electrode assembly. The box was equipped with rubber gloves and a vacuum interchange to facilitate the transfer of materials in and out. A water aspirator was used to evacuate the interchange. All

electrical jacks and tubing connections were made gas tight with rubber gaskets. The box was purged with N_2 from liquid N_2 at about 20 cc/min, except when the gloves were in use. A heater-blower assembly which was able to control the temperature of the environment of the cell was provided in the box.

B. Preparation and Purification Techniques

1. Electrode Preparation

The working electrode was the Pt disk of a Pt ring-disk assembly. While the measurements were made with a ring-disk assembly, only the disk was used. The ring-disk electrodes consisted of a Pt disk (0.492 cm diameter) press-fitted into Teflon which had in turn been press-fitted into a Pt ring (0.556 cm internal diameter, 0.724 cm external diameter). The Pt ring and disk were reference grade (99.999%). The ring-disk assembly was then in turn firmly press-fitted into an outer Teflon cylinder (1.27 cm diameter).

After the construction of ring-disk electrodes from the machine shop, the electrode surface was first polished with Buehler METADI polishing material (1/4 μ) on nylon cloth, lubricating with Buehler AB METADI fluid, and followed by polishing with Buehler AB Gamma alumina (0.05 μ) suspensions on Buehler Microcloth. When the electrode surface attained a mirror finish, it was washed with distilled water, degreased with isopropyl alcohol (spectro grade), cleaned with 1:1 H_2SO_4-HNO_3 mixture (volume ratio, reagent grade) and rinsed with triply distilled water, followed by pyrolyzed water. (The preparation of pyrolyzed water is described in a later section.)

The electrodes were further cleaned with ultrasound in a solution of the same composition as the electrolyte to be used and then either mounted on the steel shaft for experiment or stored in pyrolyzed water. When the measurements were finished, the electrodes were again polished with the gamma alumina suspensions, followed by chemical and ultrasonic treatment as previously mentioned.

2. Gas Purification

Purification trains were constructed to purify H_2, He, and O_2.

The tank H_2 (Air Products) used for charging the Pd counter and reference electrodes was purified with an Engelhard Industries Pd-Ag alloy diffuser.

The tank He (Bureau of Mines Helium Plant) was purified with the use of the following traps:

1. copper turnings in a Vycor trap maintained at ~450°C for removal of O_2.
2. molecular sieves (Linde type 13X) maintained at liquid N_2 temperatures for removal of organic contaminants.
3. molecular sieves (Linde type 3A) for adsorption of remaining O_2.
4. glass wool filters.

The tank O_2 (Linde) was purified to remove trace contaminants such as CO, CO_2, and organic substances. The purification train consisted of the following traps:

1. silica gel (Fisher Scientific Co., 6-16 mesh) for removal of water to protect trap 2.
2. hopcalyte (Mine Safety Appliances Co., 14-20 mesh), an active mixed oxide catalyst for oxidation of CO to CO_2.

3. same as trap 1.

4. ascarite (Arthur Thomas Co., 20-30 mesh), NaOH on asbestos, for removal of CO_2.

5. rutile (Fisher Scientific Co.,), TiO_2 maintained at acetone-dry ice bath temperatures, for removal of most organic substances.

6. glass wool filter.

All of the gas lines were constructed of glass or Cu and the traps were made of glass. Glass to Cu connections were attained using Swagelok fittings coupled to glass-to-metal seals. For the electrochemical measurements, purified He or O_2 was passed through bubblers containing pyrolyzed water before entering the cell.

3. Glassware and Teflon Cleaning

All Pyrex glassware used in this work was cleaned with 1:1 H_2SO_4-HNO_3 mixture for one week. Before use, each piece was thoroughly rinsed with triply distilled water.

The Teflon cell and all other Teflon parts were initially degreased in 4 M KOH for one day. After thoroughly washing with distilled water, the cell and parts were cleaned with 1:1 H_2SO_4-HNO_3 mixture, followed with thorough rinsing with triply distilled water until all the acid was leached from Teflon.

4. Chemical Purification

The purification procedures involved for the various substances were as follows:

a. Triply distilled water. Triply distilled water was obtained by distillation of tap water three times, the second distil-

lation being from an alkaline $KMnO_4$ solution. The last two stages were carried out in an all-Pyrex apparatus in a N_2 atmosphere.

b. Pyrolyzed water. Pyrolyzed water was prepared by distilling the triply distilled water through a pyrolysis quartz column, packed with Pt/Rh gauzes with O_2 purging, and maintained at ∿800°C. Final distillation was followed after pyrolysis in a N_2 atmosphere. This procedure has been described by Conway, Kozlowska, Sharp, and Criddle[103] to ultrapurify water for electrochemical work.

c. Activated charcoal. Commercial cocoanut charcoal (Barnebey-Cheney Co., Columbus, Ohio) was purified by refluxing in a Soxhlet extractor tube with azeotropic HCl solution (∿6 N) for at least four weeks followed by refluxing with triply distilled water for at least four weeks. During the refluxing operations the solutions were changed frequently. The activated charcoal was used to absorb impurities in the electrolyte.

5. Solution Preparation and Pre-electrolysis

Solutions of various acids were used in this work. Acid solutions were mostly prepared with ultrapure acids (Ultrex H_2SO_4 from J. T. Baker, ultrapure 49% HF and ultrapure 85% H_3PO_4 from Apache Chemicals, ultrapure 70% $HClO_4$ from Ventron Alfa Products) and pyrolyzed water. The H_2SO_4, $HClO_4$, and H_3PO_4 solutions were prepared in cleaned glassware and used without further chemical purification. All HF solutions were prepared in Teflon bottles and treated with activated charcoal to remove trace chloride. A 10 N HF solution was first prepared and activated charcoal (1 g/100 ml

solution) was then added to the first solution. This solution was stirred and allowed to stand overnight to permit the charcoal particles to settle to the bottom of the bottle. The clear portion of the solution was used to prepare diluted HF solutions. In some early overpotential measurements of O_2 generation, triply distilled water was used to prepare HF solutions because pyrolyzed water was not available at that time. However, the results obtained showed no significant difference as compared to those in solutions prepared with pyrolyzed water.

Solutions of 0.1 N NaOH were prepared in Teflon bottles by dilution of activated charcoal-pretreated 1 N NaOH with triply distilled water. A 50% stock solution of NaOH was first formulated from special low carbonate NaOH pellets (J. T. Baker). After allowing the 50% solution to stand over several weeks, the solution was decanted many times to remove precipitated Na_2CO_3. A 1 N NaOH solution was prepared from this 50% solution, then treated with activated charcoal to remove remaining impurities. The carbonate solubility with 50% NaOH is $\sim 10^{-4}$ M and hence the carbonate concentration in the first 1 N NaOH should have been $\sim 5 \times 10^{-6}$ M.

Various additive acids, bases, and salts were employed in the experiments. Dilute solutions of these chemicals were prepared with commercially available ultrapure chemicals (Apache Chemicals or Ventron Alfa Products) or with activated charcoal pretreated reagent grade chemicals when ultrapure ones were not available. Before each measurement, the solution was pre-electrolyzed at a potential of about 1.5 V between two auxiliary Pt (99.99%) electrodes

within the Teflon cell. Each auxiliary electrode was in the form of a sheet (4 cm x 2 cm x 0.01 cm), which was spot welded to a Pt wire. Prior to pre-electrolysis, purified He was bubbled through the solution for at least one hour to deoxygenate, at least partially, the solution; the bubbling was continued throughout the pre-electrolysis to provide the agitation and the inert atmosphere in the solution. Before placing the ancillary electrodes in the cell, they were cleaned with a 1:1 H_2SO_4-HNO_3 mixture, followed by thorough rinsing with pyrolyzed water or triply distilled water. The pre-electrolysis was carried out for at least 24 hr for acid solutions and 48 hr for NaOH solutions. The auxiliary electrodes were raised above the solution level before disconnecting the pre-electrolysis current. The use of platinum as pre-electrolysis electrodes leads to contamination of the solution with platinum, but it is very difficult to find other electrode materials that do not present similar difficulties. In the present work with Pt working electrodes, Pt contamination in solution was not considered a problem.

C. Electronic Equipment and Measurements

The experimental results reported in this work were obtained by linear potential sweep and quasi-steady-state potentiostatic techniques. The current-potential curves obtained from linear potential sweep techniques yield information concerning adsorption-desorption of species present in the solution and oxide film formation and reduction.

In linear sweep voltammetry, the potentiostat used was a Princeton Applied Research Potentiostat/Galvanostat, Model 173 with a Model 176 current-to-voltage converter and a digital readout. The potential sweep control was provided by a PAR universal programmer Model 175 or by a triangular sweep generator designed and built by B. D. Cahan at Case Western Reserve University. The current-potential curves were recorded on an X-Y recorder (Houston Instrument Omnigraphic 2000).

The quasi-steady-state potentiostatic measurements were performed by employing the PAR Model 173 potentiostat with digital readout. Two potentiometers which can be used interchangably are provided with this potentiostat. The electrode potential can be stepped to a selected value by presetting one of the potentiometers while the other is controlling the electrode at certain potential. Usually the Pt working disk electrode was pre-polarized at 2.0 V vs. α-Pd-H before the potentiostatic measurements were started toward lower potentials. The disk electrode was rotated during the measurement at 3600 rpm unless otherwise noted. The current reading was taken after the electrode potential had been maintained at the desired potential for 2 min. On some occasions, the electrode potential was driven by a slow potential sweep and the current-potential curve was recorded on a recorder.

CHAPTER IV

PRESENTATION OF RESULTS

The experimental results to be presented were obtained principally by linear sweep voltammetry for anodic oxide film formation on Pt and potentiostatic overpotential measurements in conjunction with the rotating disk electrode technique for O_2-generation on Pt.

A. Linear Sweep Voltammetry in Acids

1. Voltammograms of Pt in Various Acids

Voltammograms in 0.1 N H_2SO_4, H_3PO_4, HF, and $HClO_4$ are shown in Figs. IV-1 - 4. A comparison of the voltammograms reveals the prominent changes occurring with the change of anions in these acids. More fine structure is observed in both the hydrogen region and anodic oxide formation region in H_2SO_4 and H_3PO_4 solutions. With the stronger adsorbability of sulfate and phosphate, sharper peaks occur in the hydrogen adsorption-desorption region in H_2SO_4 and H_3PO_4 solutions. The hydrogen peaks are designated in the order of their appearance in this anodic sweep in Fig. IV-1. The middle peak in H_2SO_4 (peak III) and H_3PO_4 does not show its counterpart in the cathodic sweep. In HF and $HClO_4$ solutions the hydrogen peaks are not as sharp as compared to those in H_2SO_4 and H_3PO_4 solutions, and the potential range for the hydrogen region is wider (0.02-0.4V). The hydrogen peaks are more or less showing their counterparts in both anodic and cathodic sweeps.

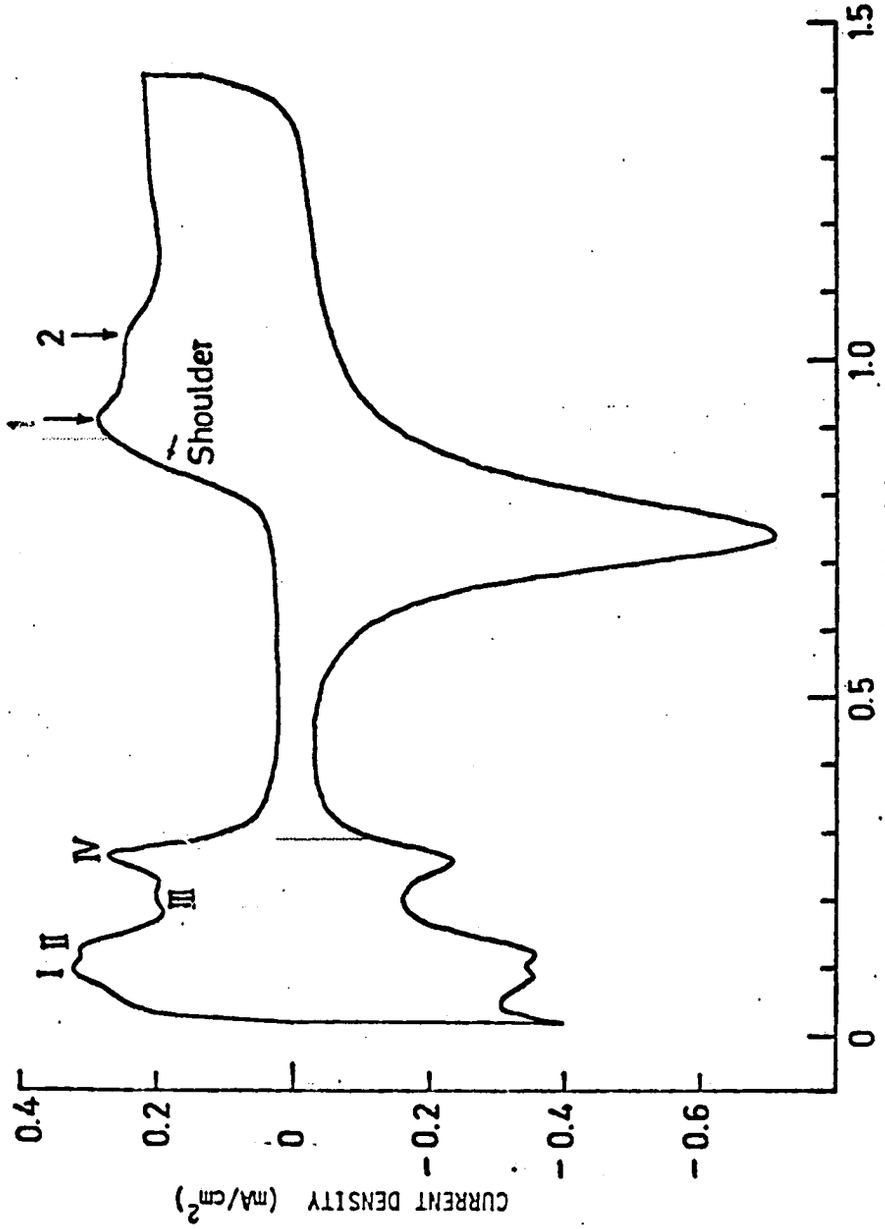

Fig. IV-1. Voltammogram for Pt in 0.1 M H_2SO_4. Sweep rate 100 mV/sec.

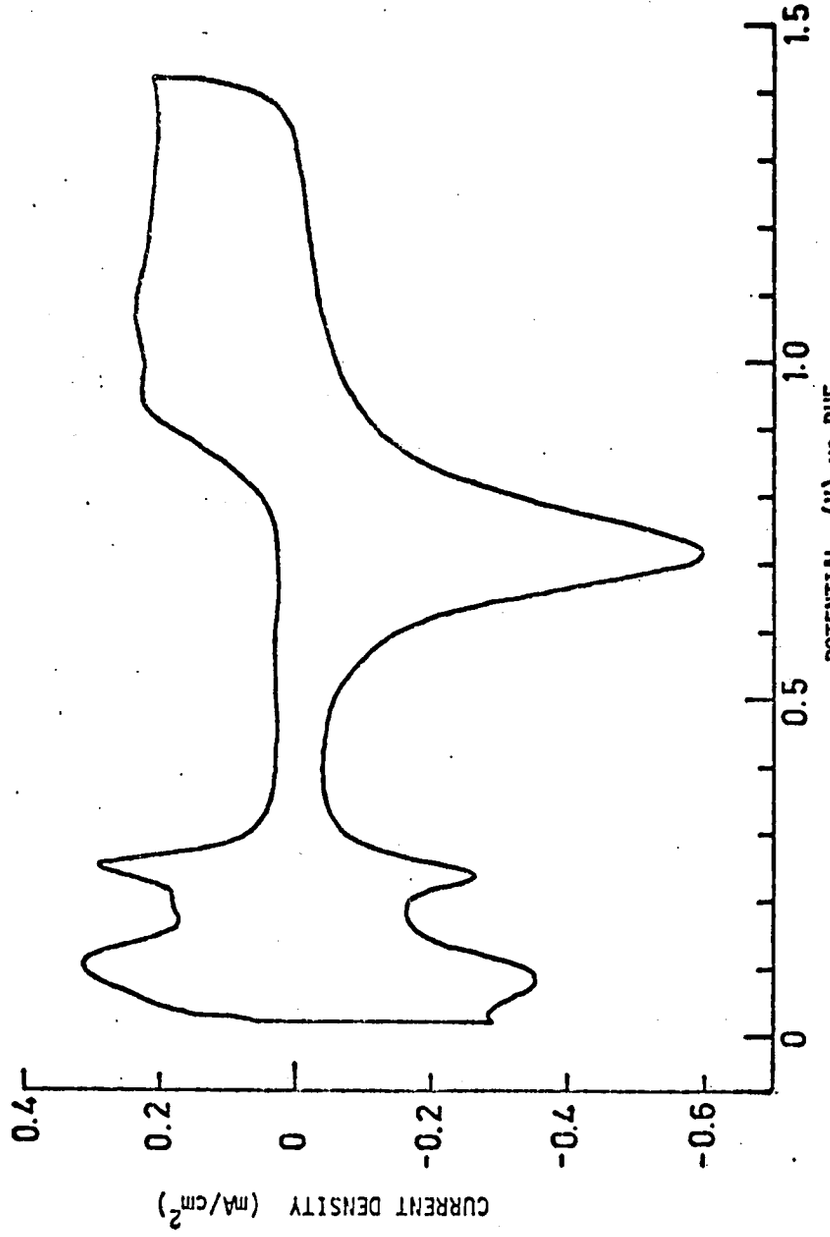

Fig. IV-2. Voltammogram for Pt in 0.1 N H_3PO_4. Sweep rate 100 mV/sec.

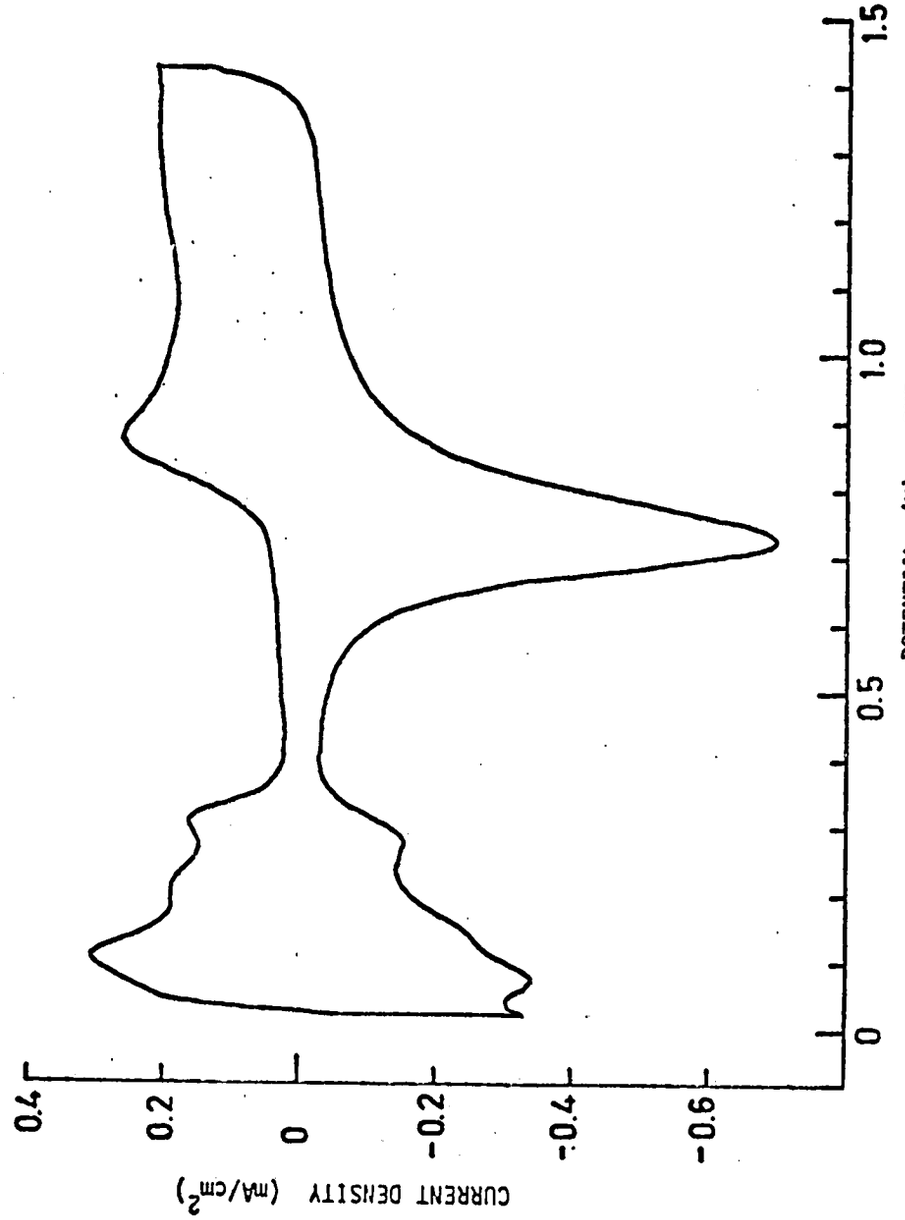

Fig. IV-3. Voltammogram for Pt in 0.1 N HF. Sweep rate 100 mV/sec.

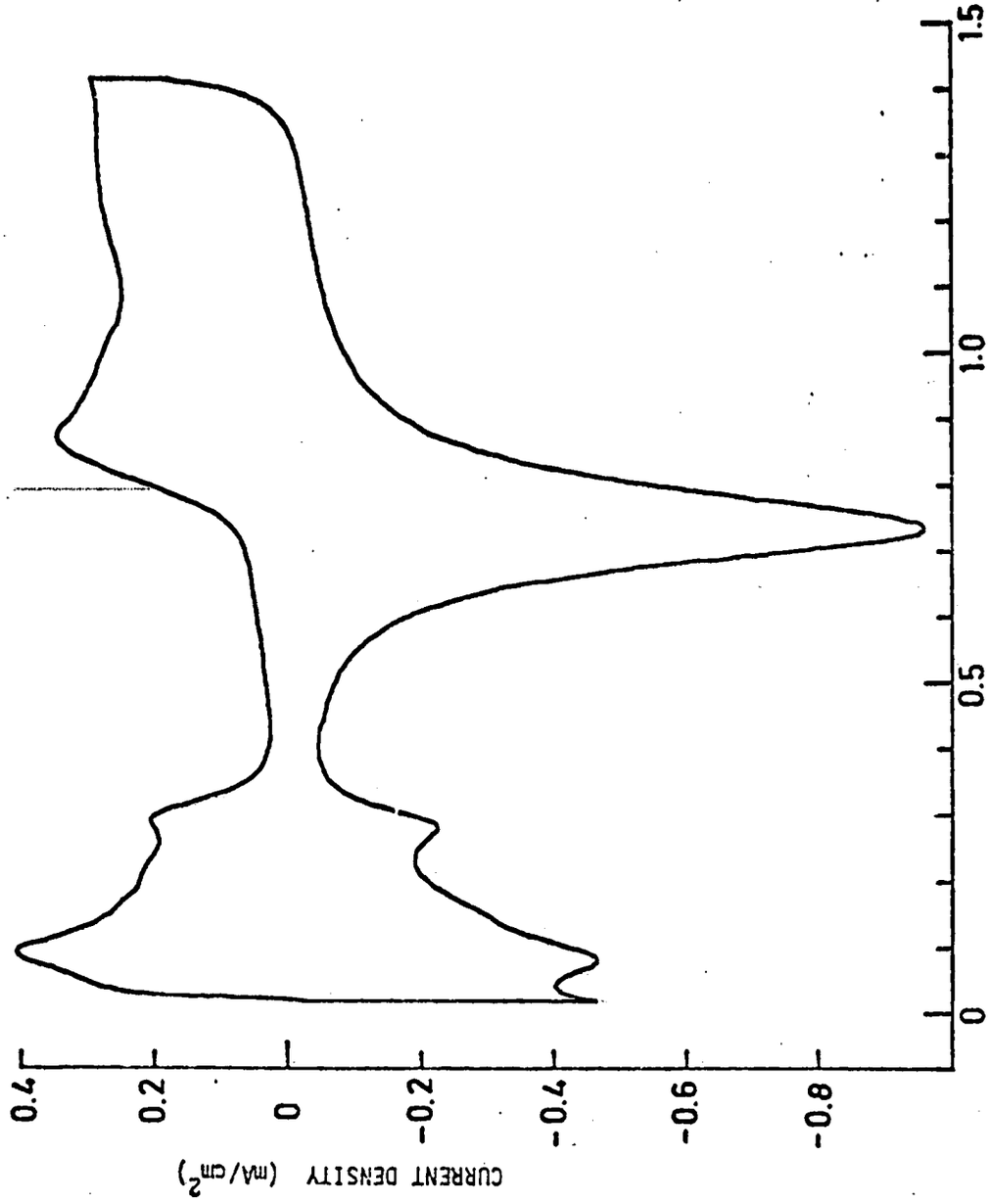

Fig. IV-4. Voltammogram for Pt in 0.1 N $HClO_4$. Sweep rate 100 mV/sec.

The double layer region in H_2SO_4 and H_3PO_4 solutions is essentially flat and wider in potential range, while that in HF and $HClO_4$ with less adsorbable anions is not flat and narrower in potential range. The anodic oxide formation in H_2SO_4 and H_3PO_4 begins at more anodic potential and shows more resolution as compared to the other two acids.

The presence of four peaks for the ionization of adsorbed hydrogen and two peaks in oxide formation region with the first one having a slight shoulder, verifies the results reported by Angerstein-Kozlowska et al.[5,104] However, this observation is not common for all acids. Two factors can contribute to the differences in the voltammetric curves in various acids: acidity and specific interactions of the acid or its anion with the electrode surface. Evidence will be presented that the specific adsorption of the anions is the principal factor.

In Fig. IV-5, the integrated charge for hydrogen adsorption Q'_H, expressed as the ratio Q'_H/Q_H, is shown as a function of potential in 0.1 N HF, $HClO_4$, and H_2SO_4. At most potentials, the charge associated with the hydrogen region is lower in 0.1 N H_2SO_4 while that in 0.1 N HF is higher at all potentials. This difference in charge may reflect the anion adsorption-desorption charge superimposed on the hydrogen charge. The Pt electrode employed had a roughness factor of ~3 after repeated potential cycling. The computation was based on the facts that a theoretical calculation of a monolayer coverage of hydrogen on Pt is ~220 $\mu C/cm^2$, assuming 1 H/surface Pt with predominantly 111 and 100 orientations. The

charge for hydrogen adsorption at various potential was thus expressed as a ratio relative to the total charge for hydrogen adsorption.

In Figs. IV-6, 7 voltammograms of Pt in 0.1 N HF and H_2SO_4 are shown with various reversal potentials in the oxide formation region. The anodic film formation is reversible in the beginning. As the potential sweeps become more anodic, irreversible character becomes evident with the reduction of anodic film showing as a single larger peak and the peak potential shifting more cathodic. The integrated oxide formation charge Q_a, expressed as the ratio Q_O/Q_H, is shown in Fig. IV-8 as a function of anodic potential in various acids. The ratio reaches unity at a potential of ∿1.1 V and shows linearity as the potential sweeps more anodic. The ratio $Q_O/Q_H = 1$ can be interpreted as indicating the Pt electrode surface is at full coverage of PtOH[5,27] or at half coverage of PtO.[21,31] The ratio $Q_O/Q_H \longrightarrow 2$ at potential ∿ 1.4V implies full coverage of PtO. However, electrochemical techniques alone cannot identify these species on a Pt surface. The results from ellipsometric studies[12] reveal that the nature of an anodic oxide film changes at potential ∿ 1.1V. The charge for oxide formation in the potential range 0.8-1.4 V is higher in 0.1 N $HClO_4$ and HF than that in 0.1 N H_2SO_4 and H_3PO_4, indicating an earlier oxide formation in the anodic sweep in those acids with less adsorbable anions.

Fig. IV-9 shows the ratio of the charges consumed for oxide formation and required for reduction, Q_a/Q_c, as a function of anodic potential in 0.1 N H_2SO_4 and HF. At potentials ≤ 1.2 V, the ratio

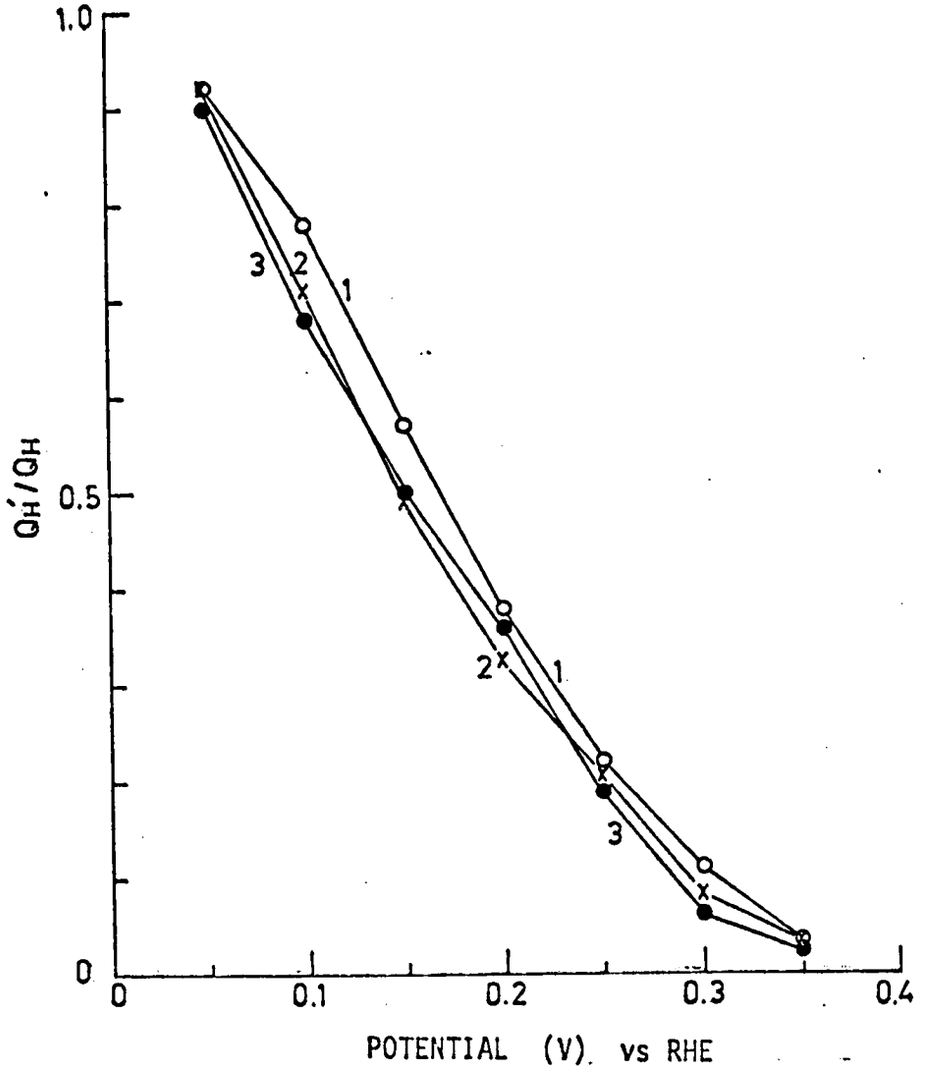

Fig. IV-5. The integrated charge for hydrogen adsorption as a function of potential in various acids.

1. 0.1 N HF 2. 0.1 N $HClO_4$ 3. 0.1 N H_2SO_4

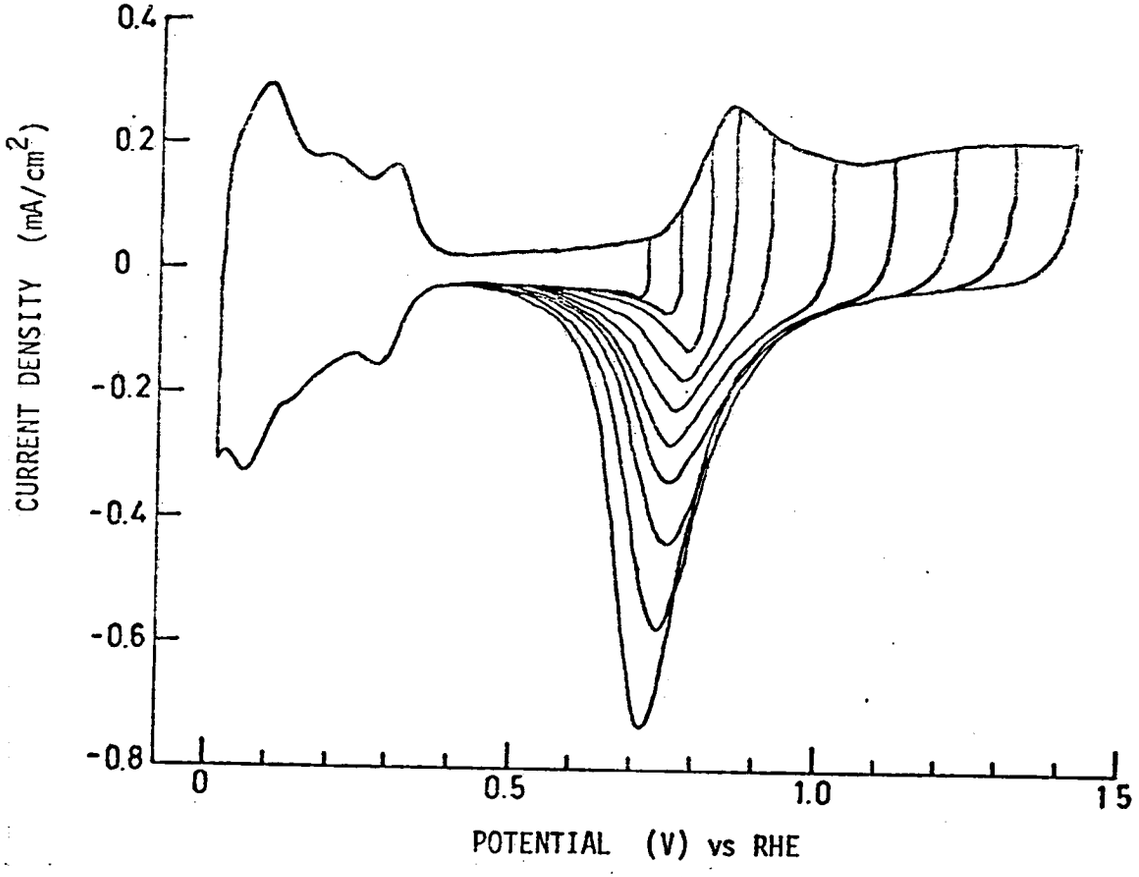

Fig. IV-6. Voltammogram of Pt in 0.1 N HF with various reversal potentials in oxide formation region.

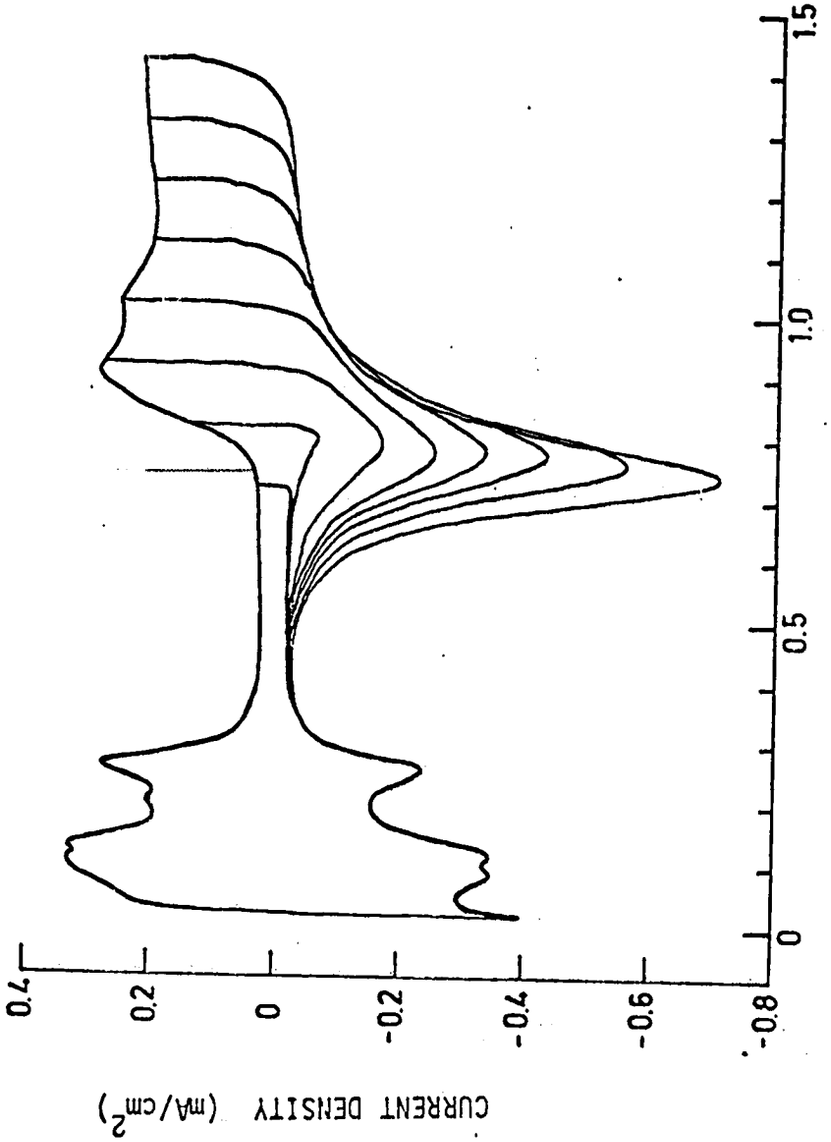

Fig. IV-7. Voltammogram of Pt in 0.1 N H_2SO_4 with various reversal potentials in oxide formation region.

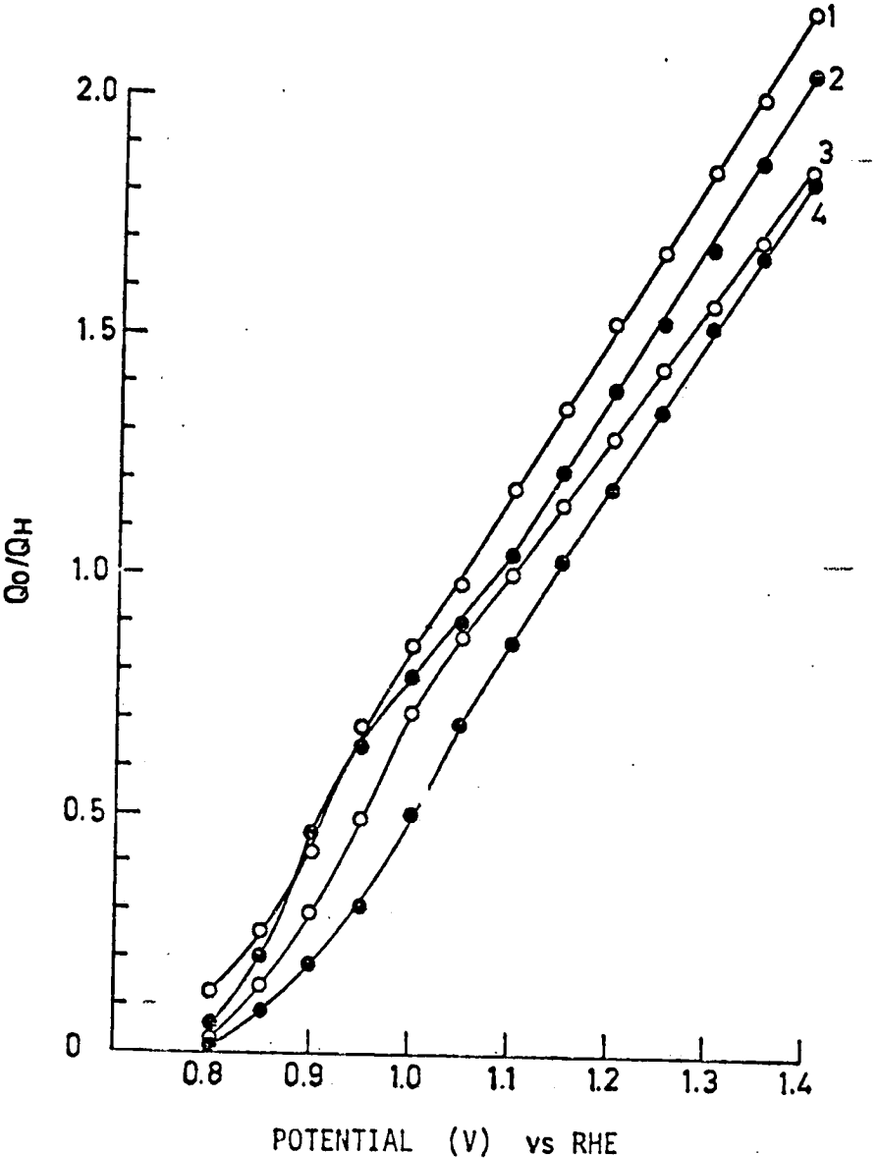

Fig. IV-8. The integrated oxide formation charge as a function of anodic potentials in various acids.

1. 0.1 N $HClO_4$
2. 0.1 N HF
2. 0.1 N H_2SO_4
4. 0.1 N H_3PO_4

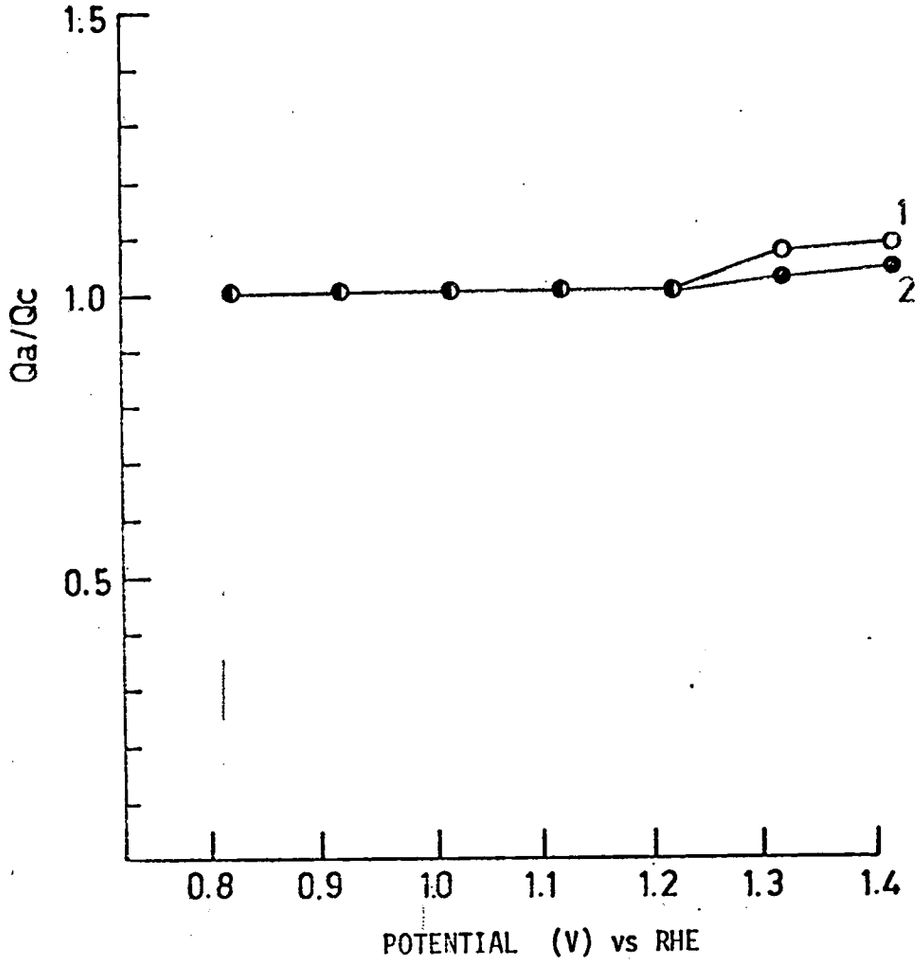

Fig. IV-9. The ratio of charges consumed for oxide formation and required for reduction as a function of anodic potential.

1. 0.1 N H_2SO_4 2. 0.1 N HF

Q_a/Q_c is essentially unity and increases at more anodic potentials. This same observation was made by Angerstein-Kozłowska et al.[5] in 1 N H_2SO_4. These results show that the reduction of Pt oxide film is not fully achieved within the cathodic sweep before the hydrogen adsorption region is reached after polarization at potentials > 1.2V.

The peaks for the oxide formation in 0.1 N H_2SO_4 have been deconvoluted using a du Pont 310 curve resolver with Gaussian distribution. The results are shown in Table IV-1.

TABLE IV-1.* The Deconvoluted Peak Potentials and Charges of Pt Anodic Oxide Formation in 0.1 N H_2SO_4

Peak	Peak Potential/V	$(Q_O/Q_H)_{peak}$
O_{A1}	0.87	0.15
O_{A2}	0.93	0.4
O_{A3}	1.05	0.8

*According to the notation of Angerstein-Kozlowska et al.[5]

The experimental values are in agreement with those reported by Angerstein-Kozlowska et al.[5] but the first two peak potentials are a little less anodic than their results. This difference in peak potential can be attributed to the difference in the concentration of H_2SO_4 used in both studies. This difference can be clearly shown from the potential for the onset of oxide formation. The oxide formation begins at 0.76 V in this study in 0.1 N H_2SO_4 as compared to 0.8 V in the current-potential curve of Angerstein-Kozlowska et al.[5] in 1 N H_2SO_4.

Attempts have been made to deconvolute the oxide formation curve for the other electrolytes beyond 1.2 V and are listed in Table IV-2 for 0.1 N $HClO_4$, HF, and H_3PO_4.

TABLE IV-2. The Deconvoluted Peak Potentials and Charges of Pt Anodic Oxide Formation in 0.1 N $HClO_4$, HF, and H_3PO_4.

Acid	Peak	Peak Potential/V	$(Q_O/Q_H)_{peak}$
$HClO_4$	O_{A1}	0.84	0.23
	O_{A2}	0.94	0.7
	O_{A3}	1.06	1.0
HF	O_{A1}	0.85	0.2
	O_{A2}	0.97	0.7
	O_{A3}	1.09	1.0
H_3PO_4	O_{A1}, O_{A2}	0.95	0.3
	O_{A3}	1.09	0.8

The Pt oxide formation beyond 1.2 V in most acids studied can be deconvoluted into three peaks except in H_3PO_4. In H_3PO_4, the first two stages of oxide formation probably occur simultaneously and form a single peak. A comparison between the results shown in two tables shows that the initial stages of Pt oxide formation proposed by Angerstein-Kozlowska et al.[5] are influenced by the anions presented in acids. The positions of peak potentials and charges at peak are different in various acids. Though acidity can be a dominant factor, evidence will be presented in a later section that anions are the principal factor.

2. Anion Effects on Voltammograms of Pt in Acids

Since different structures was observed in the current-potential curves for Pt in various acids, the addition of selected anions to various acids was performed to study their effects on the current-potential curves. Fig. IV-10 shows the effect of $SO_4^=$ in 0.1 N HF. As the concentration of $SO_4^=$ is increased, the current-potential curves gradually become similar to that in H_2SO_4. Four peaks in the ionization of adsorbed hydrogen become clearly evident when $SO_4^=$ concentration is increased up to 5×10^{-4} M. The integrated charge under the hydrogen portion of the voltammetry curve includes the faradaic component associated with the H_2 generation in the cathodic sweep and H_2 oxidation in the anodic sweep, although the latter is smaller in a solution essentially free of H_2 in the bulk. Deconvolution of the peaks could permit a correction for these faradaic components but such is difficult to accomplish quantitatively. Efforts at doing that lead to the conclusion that the total charge for hydrogen adsorption and ionization remains essentially unchanged if correction has been made to exclude the charge due to the formation and oxidation of H_2. The rightmost hydrogen peak (the so-called strongly bound hydrogen peak) occurs at more cathodic potential and becomes sharper and higher as the concentration of $SO_4^=$ is increased.

The double layer region becomes flatter and wider in potential range. The onset of oxide formation begins at more anodic potential when $SO_4^=$ is added to 0.1 N HF. The gradual appearance of a second peak and a shoulder on the first peak in oxide formation region

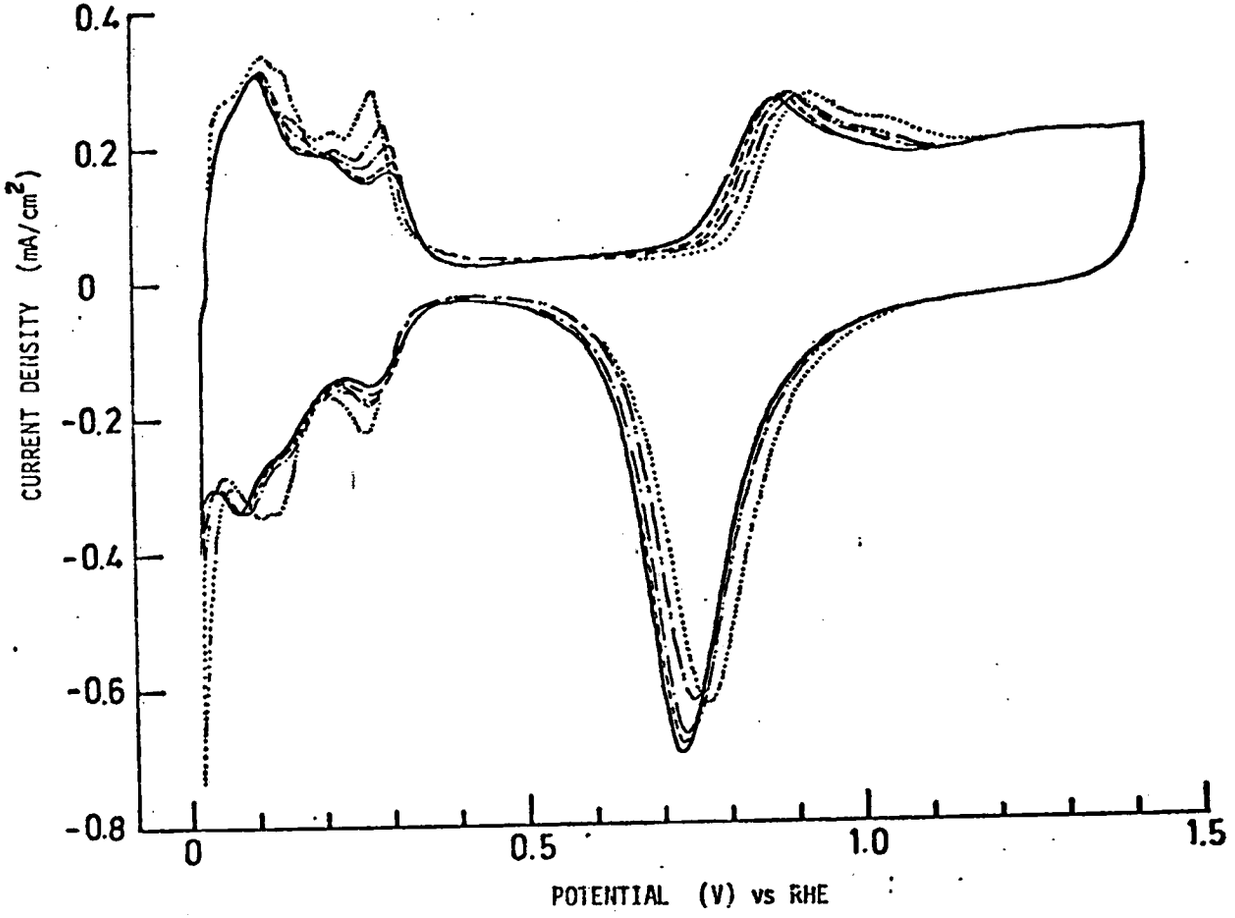

Fig. IV-10. Voltammograms for Pt in 0.1 N HF with various concentrations of H_2SO_4 added.

—— 0.1 N HF

— — 0.1 N HF + 10^{-4} N H_2SO_4

—·— 0.1 N HF + 10^{-3} N H_2SO_4

—·—·— 0.1 N HF + 10^{-2} N H_2SO_4

····· 0.1 N HF + 10^{-1} N H_2SO_4

shows that these two features observed with H_2SO_4 as the electrolyte are dependent on the interactions of the $SO_4^=$ with the Pt electrode.

The addition of different concentrations of F^- up to 0.1 N to 0.1 N H_2SO_4 was also studied. In Fig. IV-11 the current-potential curve after adding HF in 0.1 N H_2SO_4 shows no change in shape.

Another set of experiments was conducted to investigate the effects of $SO_4^=$ in solutions of 0.1 N $HClO_4$, since both H_2SO_4 and $HClO_4$ are much stronger acids than HF. The results are shown in Fig. IV-12. Similar effects are observed to those found with the addition of $SO_4^=$ to HF, confirming that these effects are not due principally to change in acidity.

In Fig. IV-13 the current-potential curves are shown for 0.04 N H_2SO_4 and 0.14 N HF. These two solutions have been shown[92] to have similar pH values. The difference in these two current-potential curves clearly shows the role of anions in the voltammograms.

Chloride anions have been known to be one of the common impurities present in the solutions in electrochemical studies. This anion was shown[88] to be specifically adsorbed on Pt. Consequently, the effects of this anion on the current-potential curves have been examined in 0.1 N HF and 1 N H_2SO_4. Fig. IV-14 shows the effects of Cl^- in 0.1 N HF on the voltammetry curves of Pt. The presence of Cl^- in HF solutions causes the rightmost hydrogen peak occurring at more cathodic potential with the hydrogen peak heights becoming higher as the concentration of Cl^- is increased. The charge for hydrogen adsorption and ionization is essentially unchanged. The

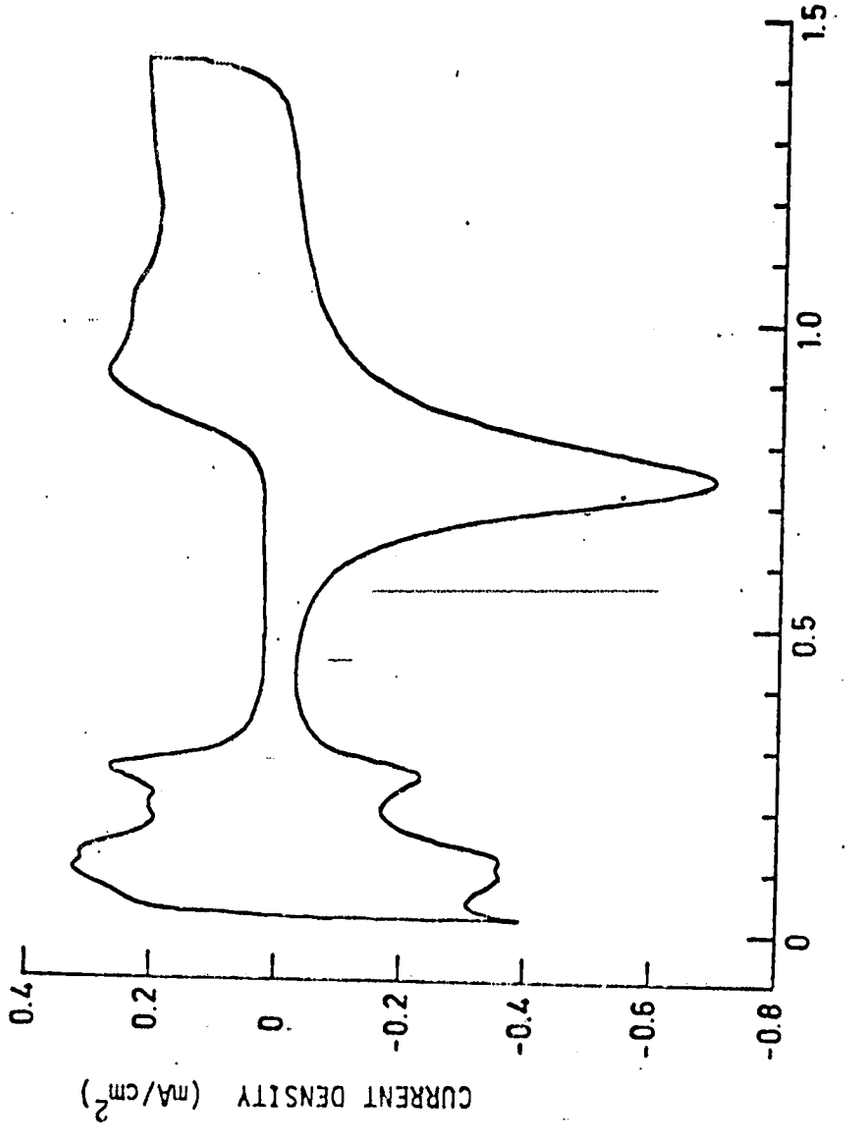

Fig. IV-11. Voltammogram for Pt in 0.1 N H_2SO_4 with 0.1 N HF added.

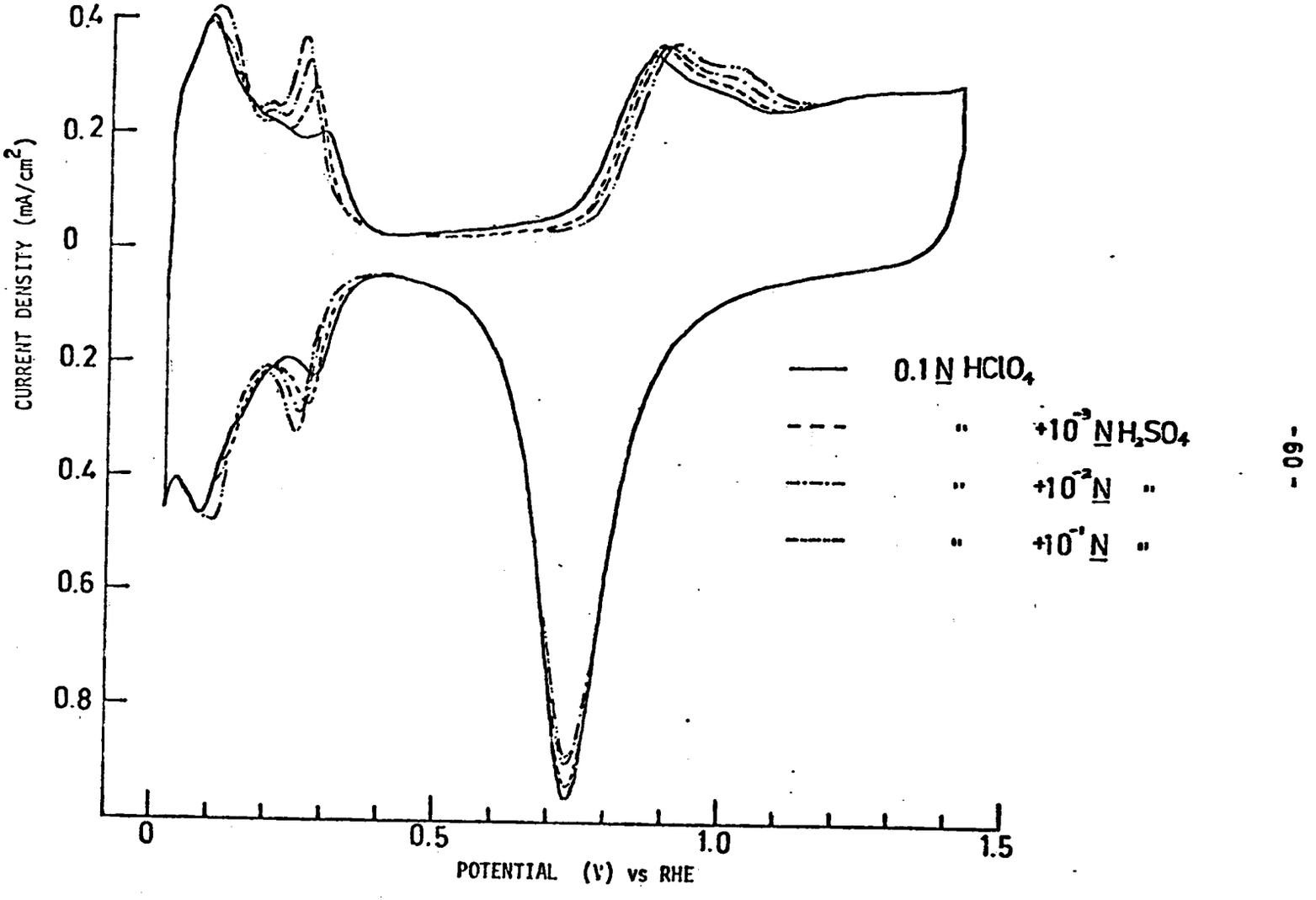

Fig. IV-12. Voltammograms for Pt in 0.1 N $HClO_4$ with various concentrations of H_2SO_4 added.

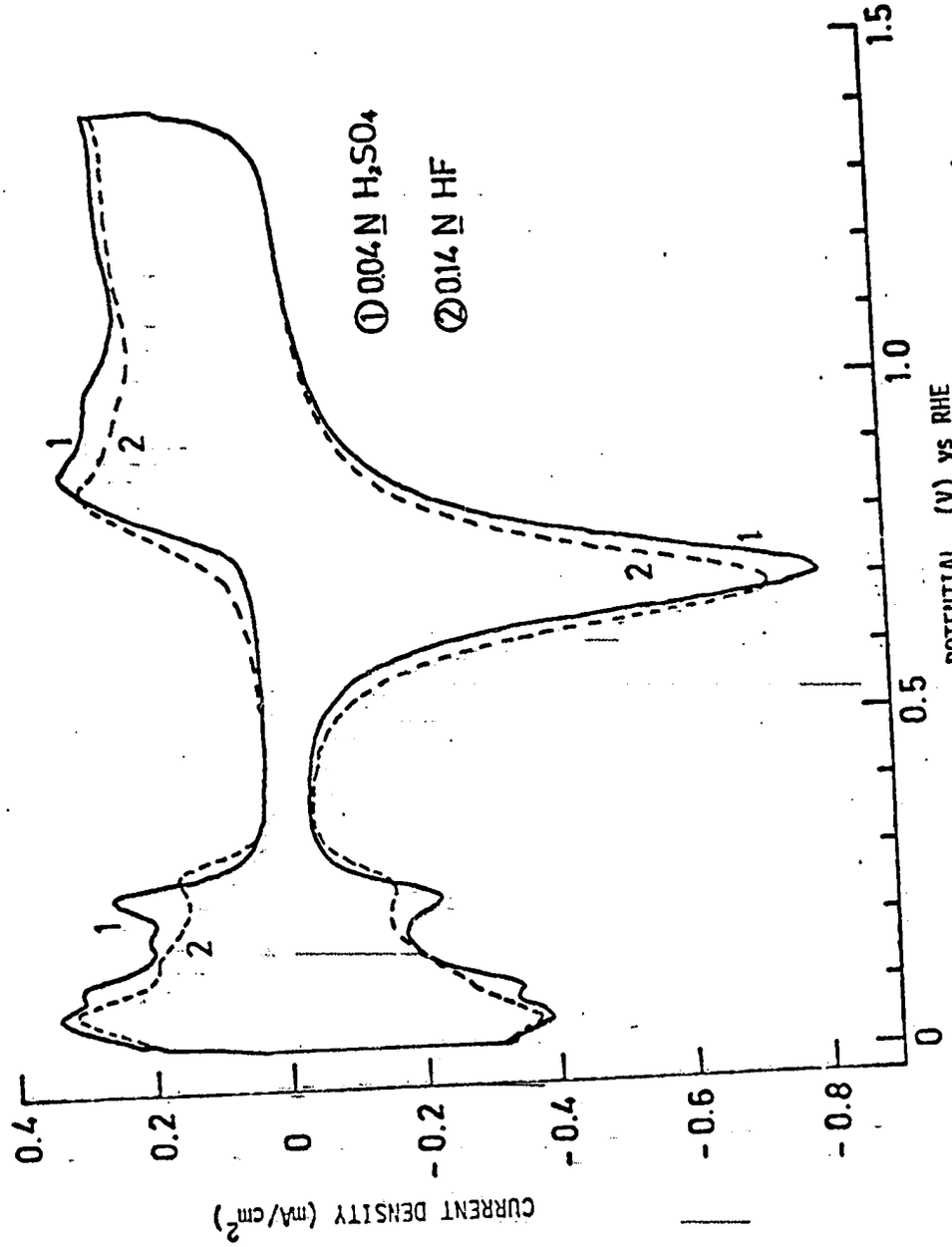

Fig. IV-13. Voltammograms for Pt in 0.04 N H_2SO_4 and 0.14 N HF. Sweep rate 100 mV/sec.

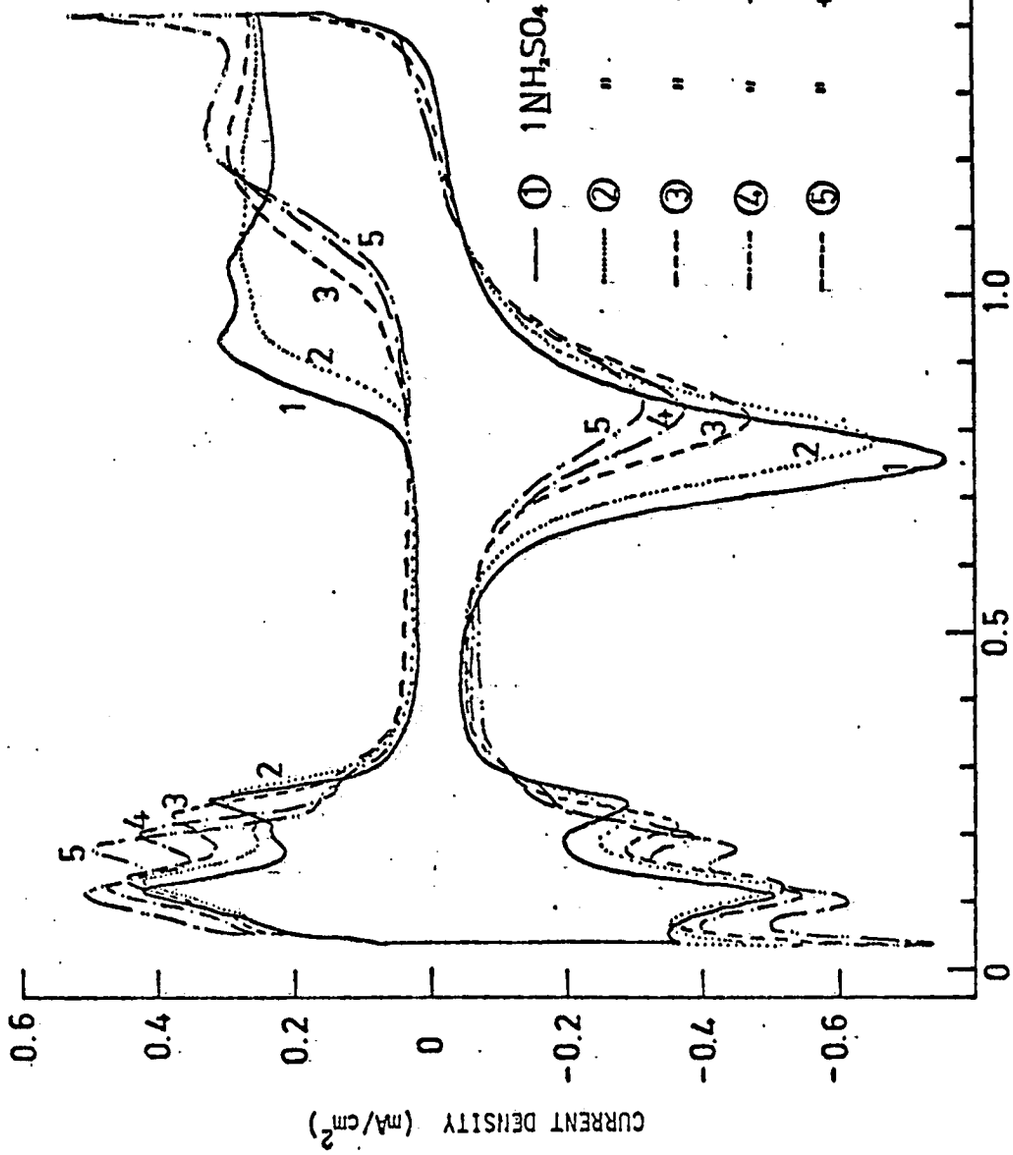

Fig. IV-14. Voltammograms for Pt in 1 N H_2SO_4 with various concentrations of HCl added.

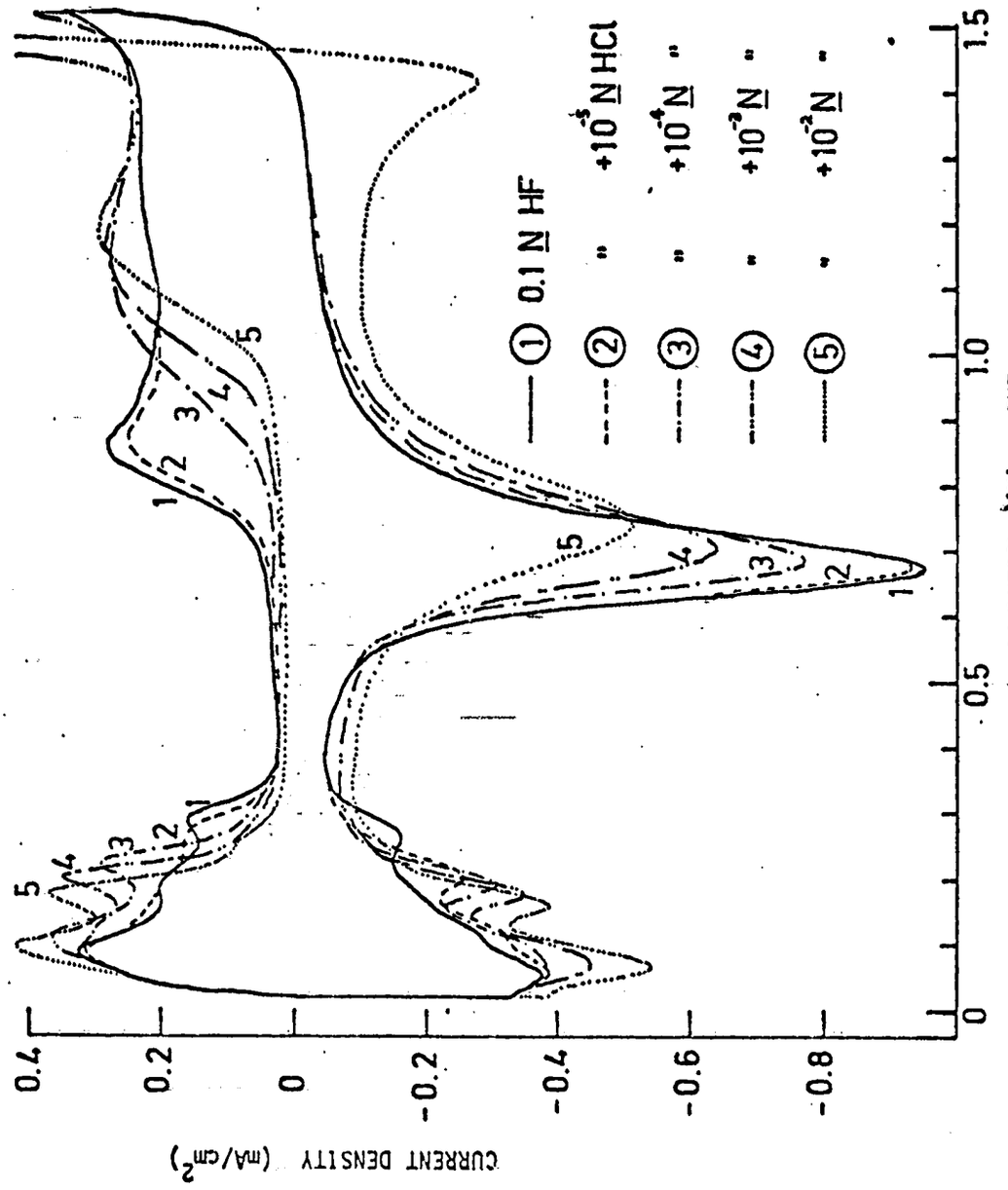

Fig. IV-15. Voltammograms for Pt in 0.1 N HF with various concentrations of HCl added.

double layer region in the anodic sweep becomes flatter and the potential range wider when Cl^- is added. The Cl^- anions strongly retard the oxide formation. When Cl^- is added up to 10^{-2} N, molecular chlorine formation and ionization are evident in the current-potential curve.

The effects of Cl^- in 1 N H_2SO_4 are shown in Fig. IV-15. Similar effects have been found with Cl^- in 0.1 N HF.

The effects of Cl^- in solutions of HF and H_2SO_4 in the hydrogen and double layer regions are similar to those of $SO_4^=$ in solutions of HF and $HClO_4$. With the stronger adsorbability of Cl^- on Pt than $SO_4^=$, the effects of Cl^- are more prominent. Anion adsorption has shown in this study to have a pronounced influence on the adsorption and ionization of hydrogen and oxide film formation on Pt. Possible mechanisms by which these effects occur will be discussed later.

In Fig. IV-16, the shift of strongly bound hydrogen peak potential is shown as a function of the concentration of added anions. The shift has a linear dependence on the logarithm of anion concentration. In Fig. IV-17, the potential for the onset of oxide formation is shown as a function of $SO_4^=$ concentration. The retardation of oxide formation also has a linear dependence on the logarithm of $SO_4^=$ concentration. These results imply that anion adsorption is competitive with hydrogen chemisorption and oxide film formation.

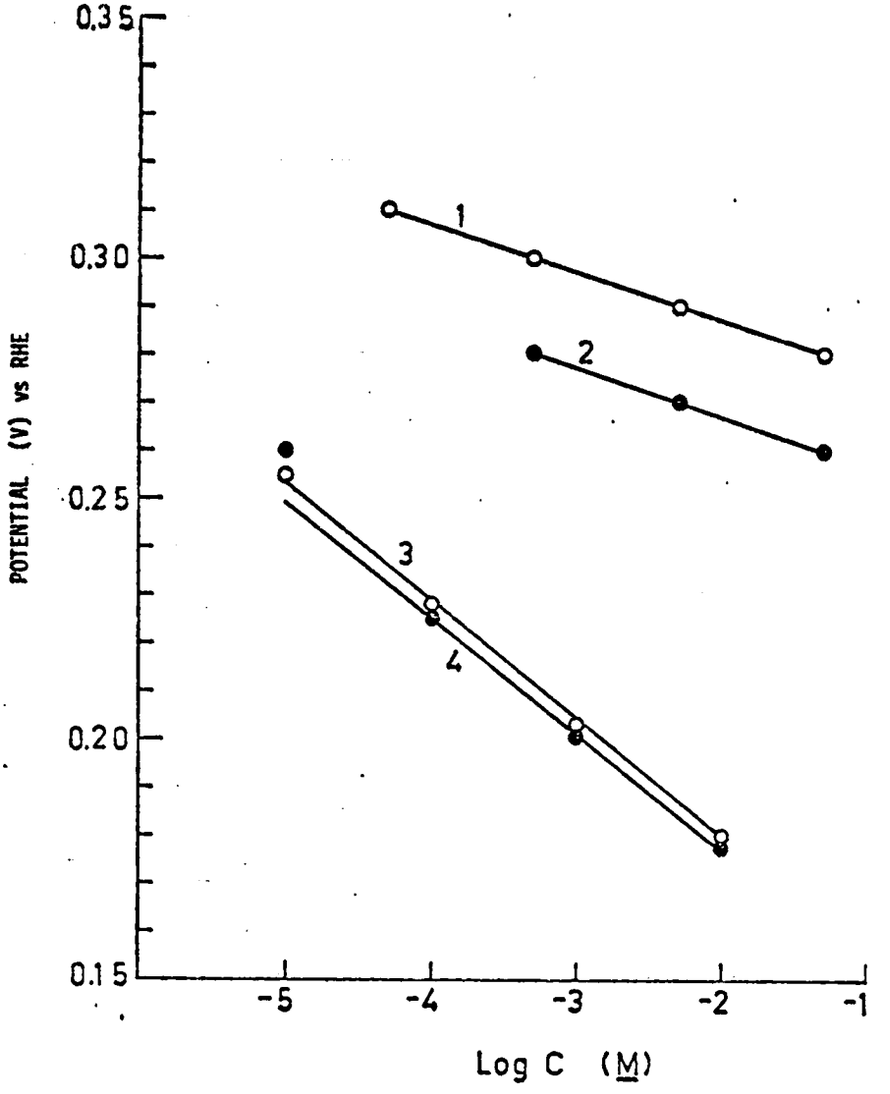

Fig. IV-16. The shift of strongly bound hydrogen peak potential as a function of the concentration of added anions.

1. 0.1 N HF + H_2SO_4
2. 0.1 N $HClO_4$ + H_2SO_4
3. 0.1 N HF + HCl
4. 1 N H_2SO_4 + HCl

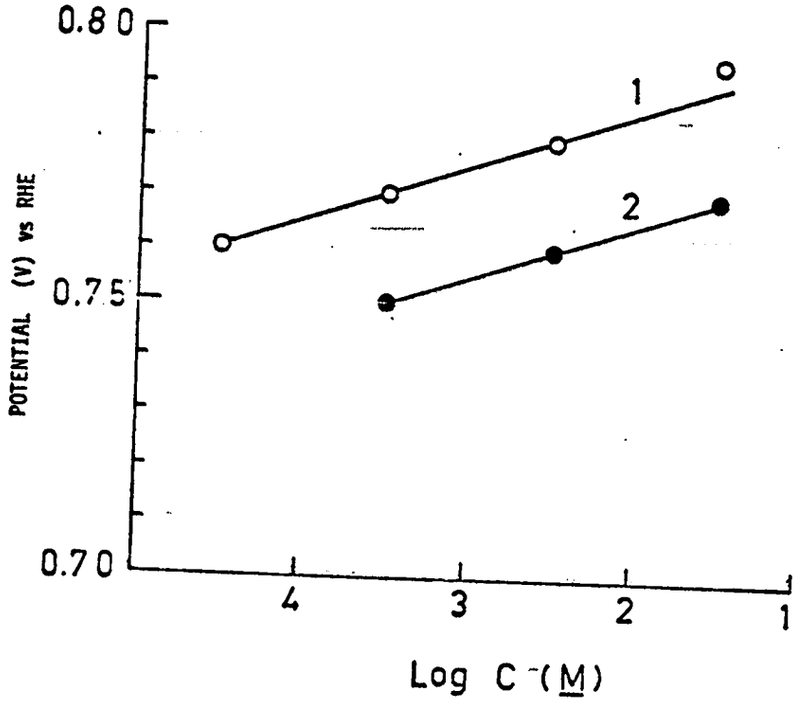

Fig. IV-17. The potential for the onset of oxide formation as a function of $SO_4^=$ concentration.

1. 0.1 N HF + H_2SO_4
2. 0.1 N $HClO_4$ + H_2SO_4

3. Cation Effects on Voltammograms of Pt in Acids

The voltammograms with Li^+ and Cs^+ cations added to the solutions of 0.1 N H_2SO_4 are shown in Figs. IV-18, 19. The presence of Li^+ cations in 0.1 N H_2SO_4, up to a concentration of 5×10^{-3} M, slightly lowers the first two peaks in hydrogen portion of the current-potential curve. The effect of Cs^+ cations in 0.1 N H_2SO_4 is more pronounced with the first two hydrogen peaks merged into one broad peak. No appreciable effect on oxide formation is observed with Li^+ and Cs^+ cations added. Specific adsorption of Cs^+ cations on Pt in the hydrogen region has been shown by Kazarinov and Balashova[105] in Cs_2SO_4 + H_2SO_4 solutions using radiotracer methods. The merger of two first hydrogen peaks into one can be attributed to this cation adsorption.

Figs. IV-20, 21 show the effect of Ba^{2+} and Sr^{2+} cations in 0.1 N $HClO_4$ on the hydrogen portion and the oxide formation portion of the voltammetry curve of Pt. The effects are small with the hydrogen peak potential somewhat shifted and the peak in oxide formation slightly lowered.

The effect of NH_4^+ and $N(C_2H_5)_4^+$ cations on the current-potential curves of Pt in 0.1 N HF are shown in Figs. IV-22, 23. The presence of NH_4^+ cations slightly affects the hydrogen and oxide formation portions of the voltammogram. The hump at 0.72 V may be due to impurities present in NH_4F solution. When $N(C_2H_5)_4^+$ cations are added to 0.1 N HF, the hydrogen peaks are shifted and become less well defined. The oxide formation is retarded and the peak lowered. Some portion of the effects indicated in Figs. IV-22, 23

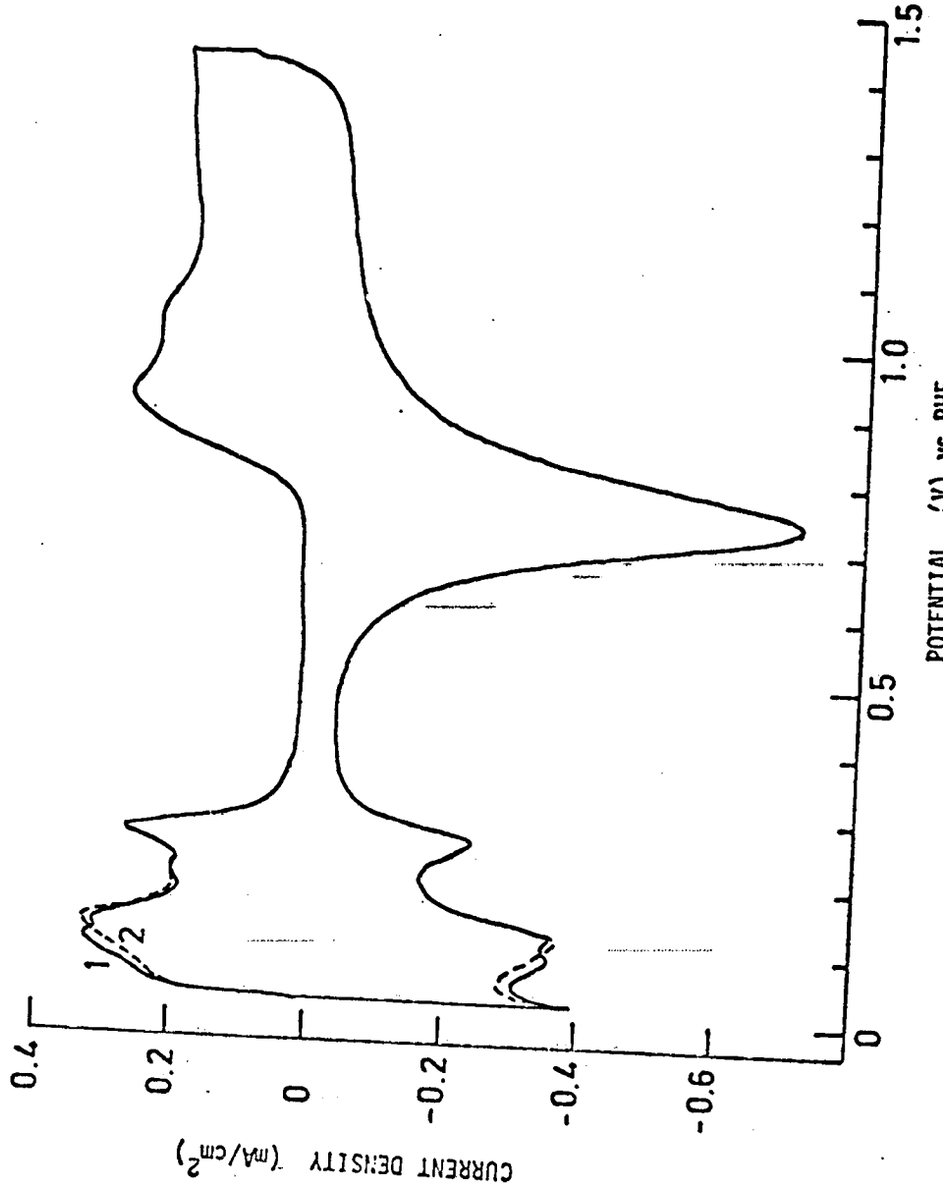

Fig. IV-18. Voltammograms for Pt in 0.1 N H_2SO_4 with Cs^+ cations added.

— 0.1 N H_2SO_4

— 0.1 N H_2SO_4 + 5 x 10^{-3} M Cs_2SO_4

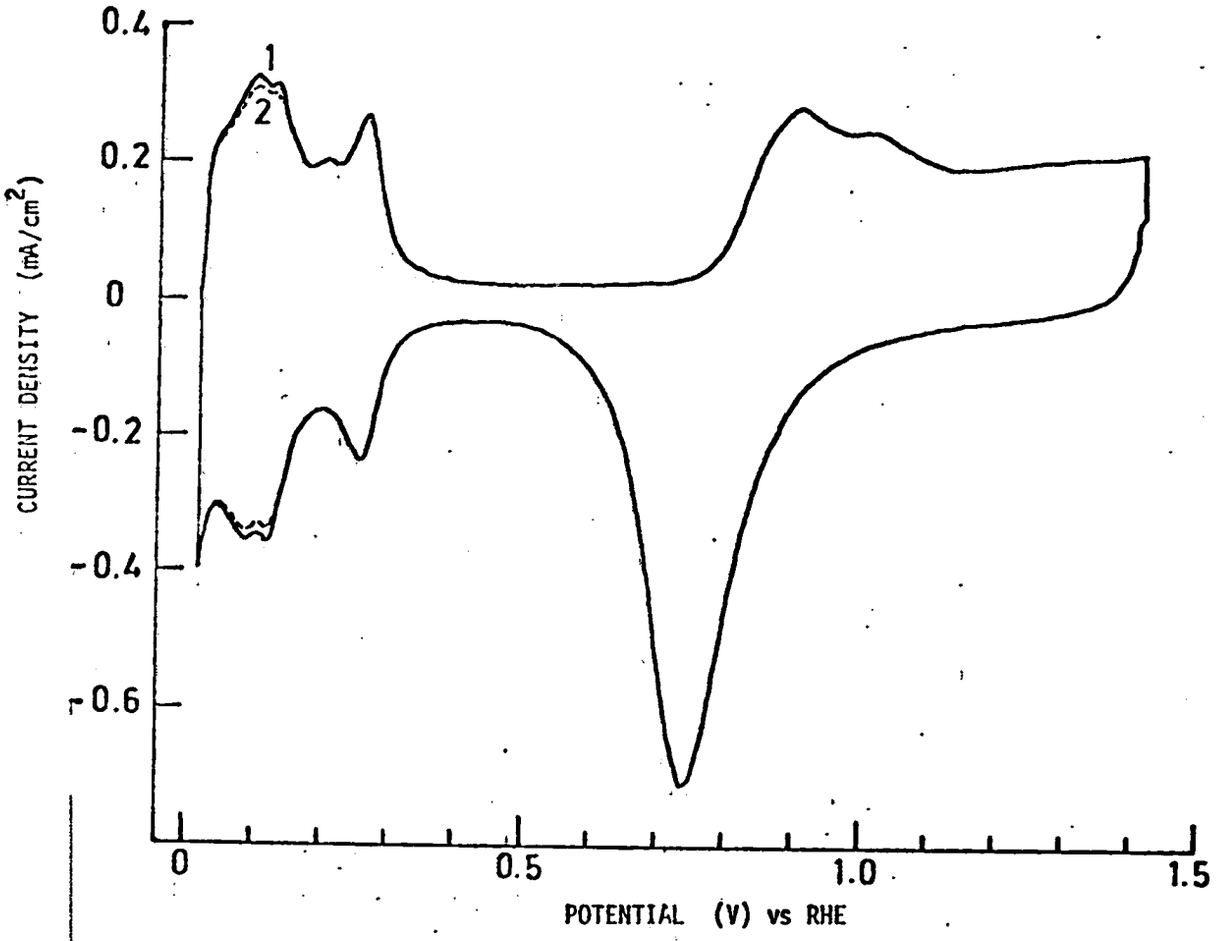

Fig. IV-19. Voltammograms for Pt in 0.1 N H_2SO_4 with Li^+ cations added.

—— 0.1 N H_2SO_4

--- 0.1 N H_2SO_4 + 5 x 10^{-3} M Li_2SO_4

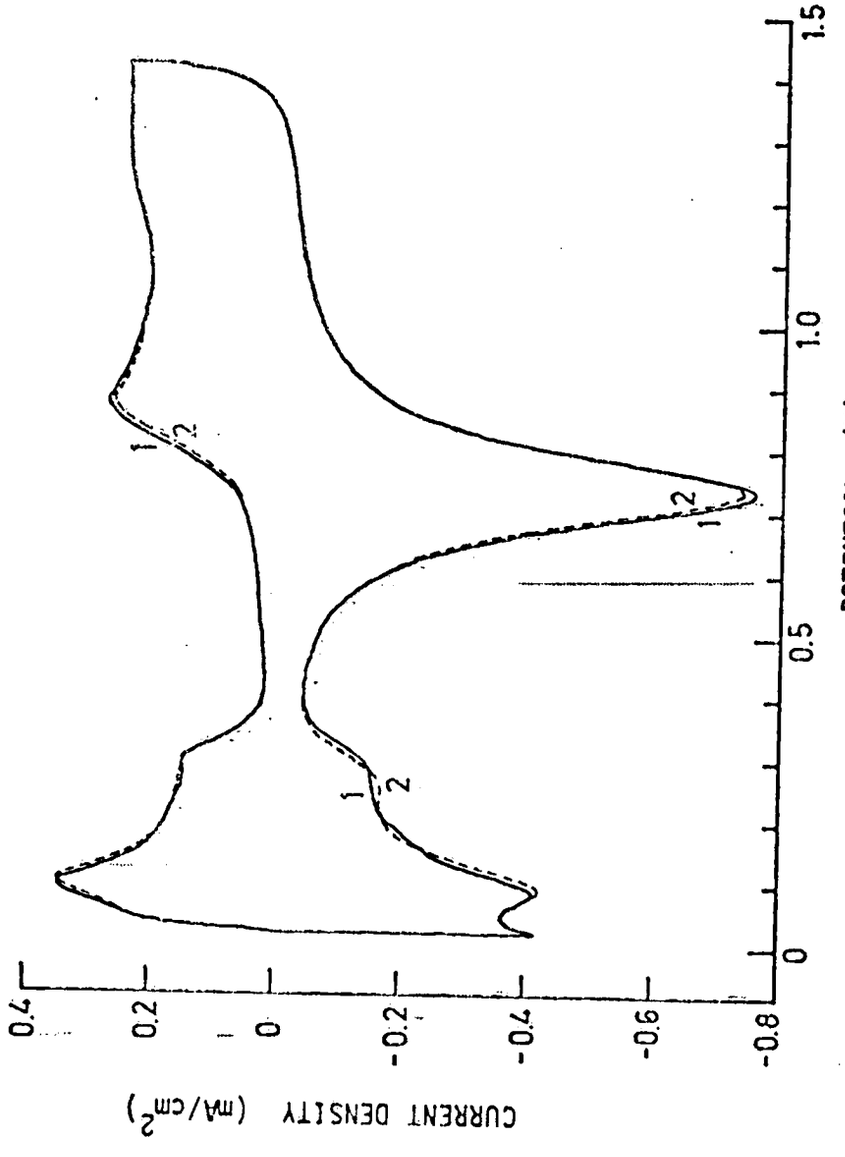

Fig. IV-20. Voltammograms for Pt in 0.1 N $HClO_4$ with 5×10^{-4} M $Ba(ClO_4)_2$ added.

1. 0.1 N $HClO_4$
2. 0.1 N $HClO_4$ + 5×10^{-4} M $Ba(ClO_4)_2$

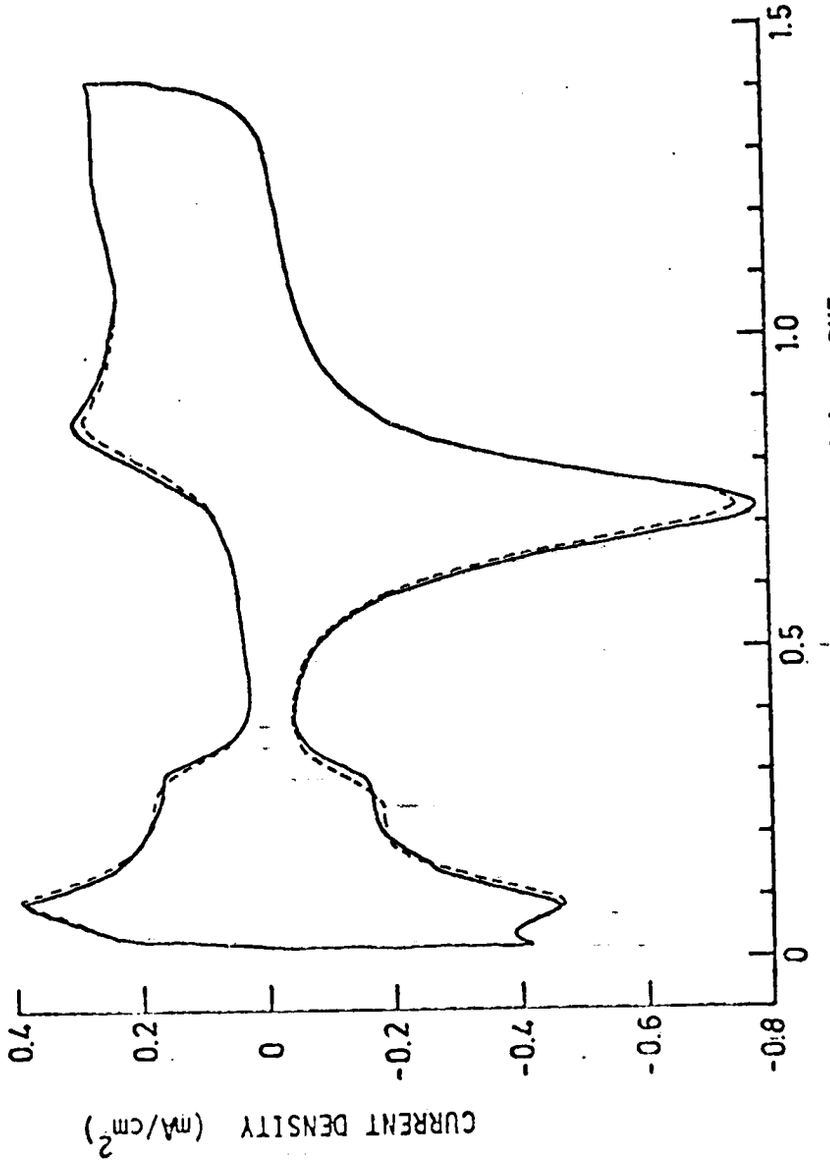

Fig. IV-21. Voltammograms for Pt in 0.1 N $HClO_4$ with 5×10^{-4} M $Sr(ClO_4)_2$ added.

1. 0.1 N $HClO_4$
2. 0.1 N $HClO_4$ + 5×10^{-4} M $Sr(ClO_4)_2$

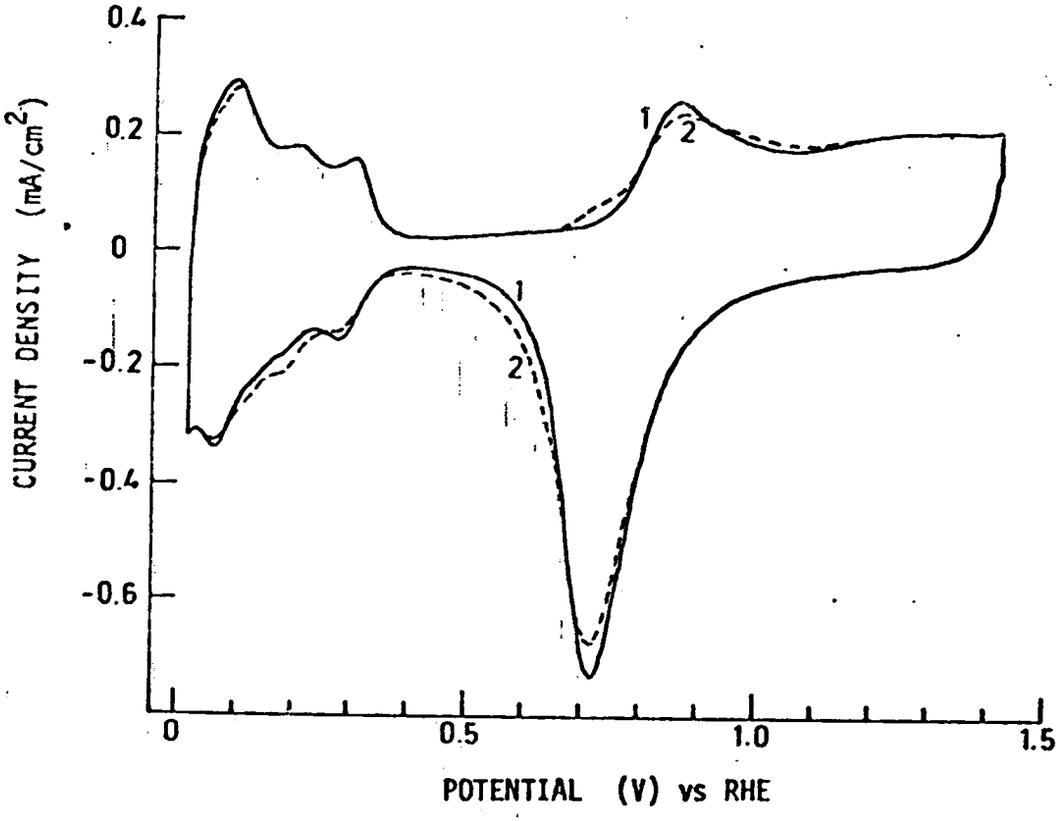

Fig. IV-22. Voltammograms for Pt in 0.1 N HF with NH_4^+ cations added.

1. 0.1 N HF 2. 0.1 N HF + 5×10^{-3} M NH_4F

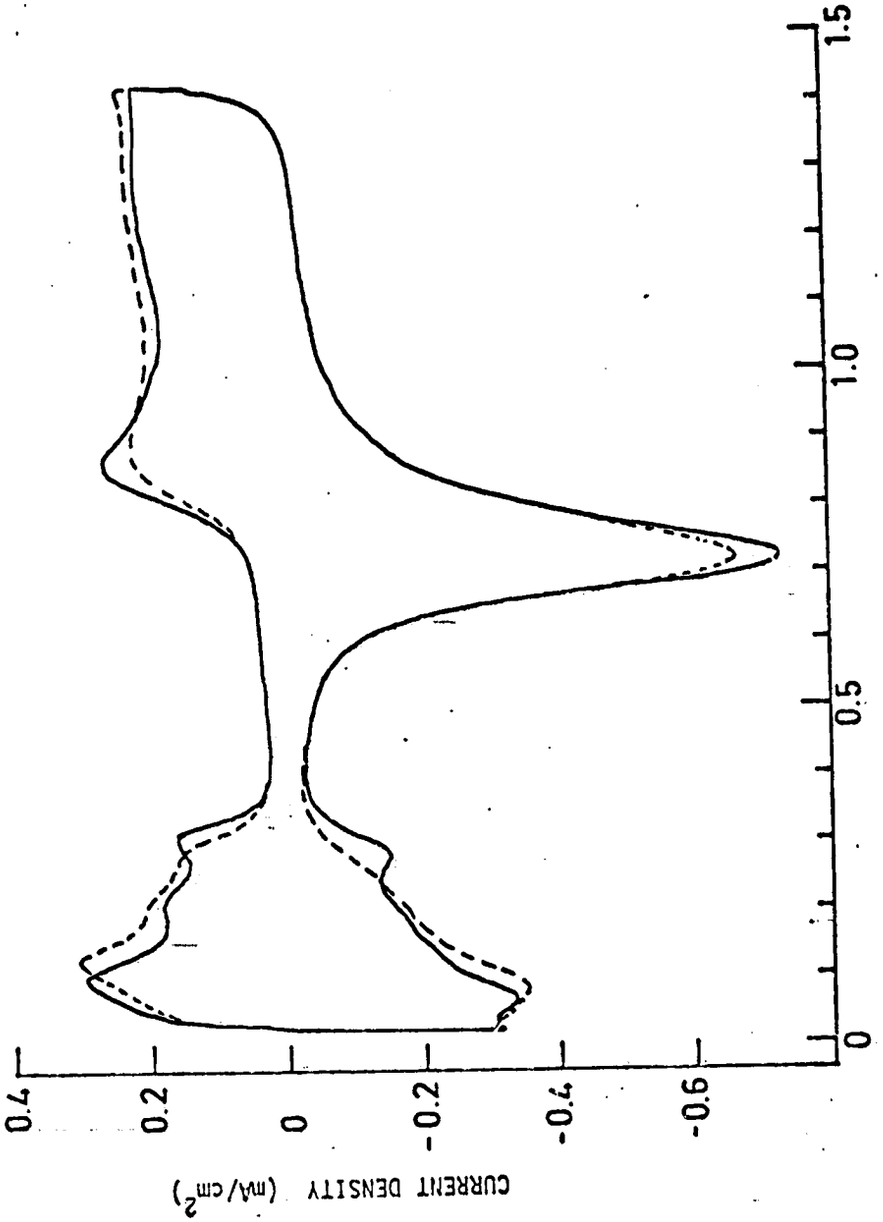

Fig. IV-23. Voltammograms for Pt in 0.1 N HF with $(C_2H_5)_4N^+$ cations added.

— 0.1 N HF

--- 0.1 N HF + 5×10^{-3} M $(C_2H_5)_4NF$

may be due to the change in acidity in the partially ionized HF, resulting from the addition of the salts.

B. Linear Sweep Voltammetry in Alkaline Solutions

1. Anion Effects on Voltammograms of Pt in Alkaline Solutions

Sodium salts of various anions were added to the solutions of 0.1 N NaOH to study the effects of anions on the current-potential curve of Pt in alkaline solution. The presence of iodide and cyanide anions in NaOH solution was found to have large effects on the voltammograms of Pt in 0.1 N NaOH. Bromide anions showed a slight influence on the voltammogram of Pt in 0.1 N NaOH. For the other anions studied, even concentrations up to 10^{-2} M did not show any pronounced change in the voltammograms of Pt in 0.1 N NaOH. These other anions included chloride, carbonate, sulfate, silicate, perchlorate and phosphate.

The results of adding iodide, cyanide and bromide anions to 0.1 N NaOH are shown in Figs. IV-24 - 26. Even with only 10^{-5} M of I^- present in 0.1 N NaOH, the hydrogen region is changed drastically. The peaks are diminished with a new peak appearing at a more cathodic potential. The onset of oxide formation is retarded and a new peak appears at a potential of 1.3 V. This new peak corresponds to iodide oxidation. When the concentration of I^- is increased to 10^{-3} M, the hydrogen peaks occur at more cathodic potentials. The oxide formation is totally blocked and I_2 formation becomes significant at potential > 1.2 V.

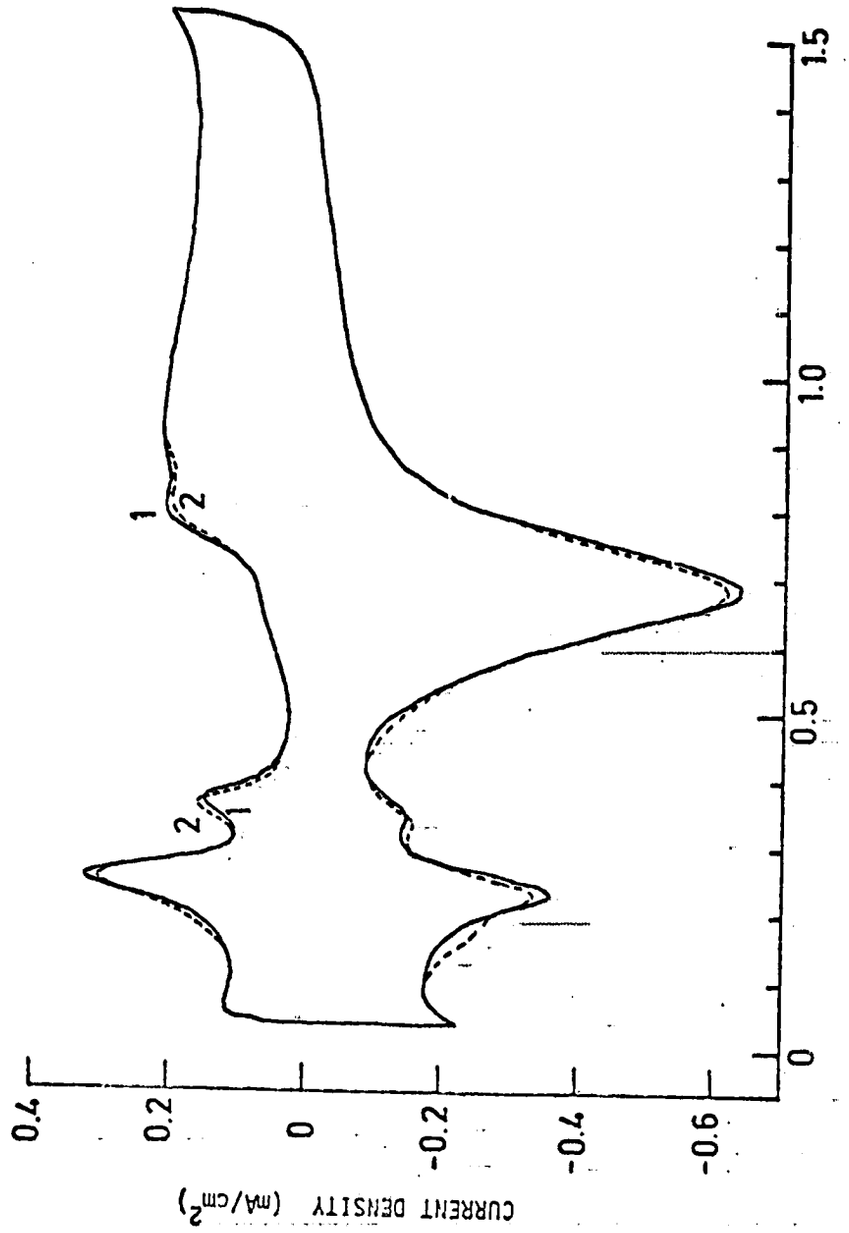

Fig. IV-24. Voltammograms for Pt in 0.1 N NaOH with Br^- anions added.

1. 0.1 N NaOH
2. 0.1 N NaOH + 10^{-3} M NaBr

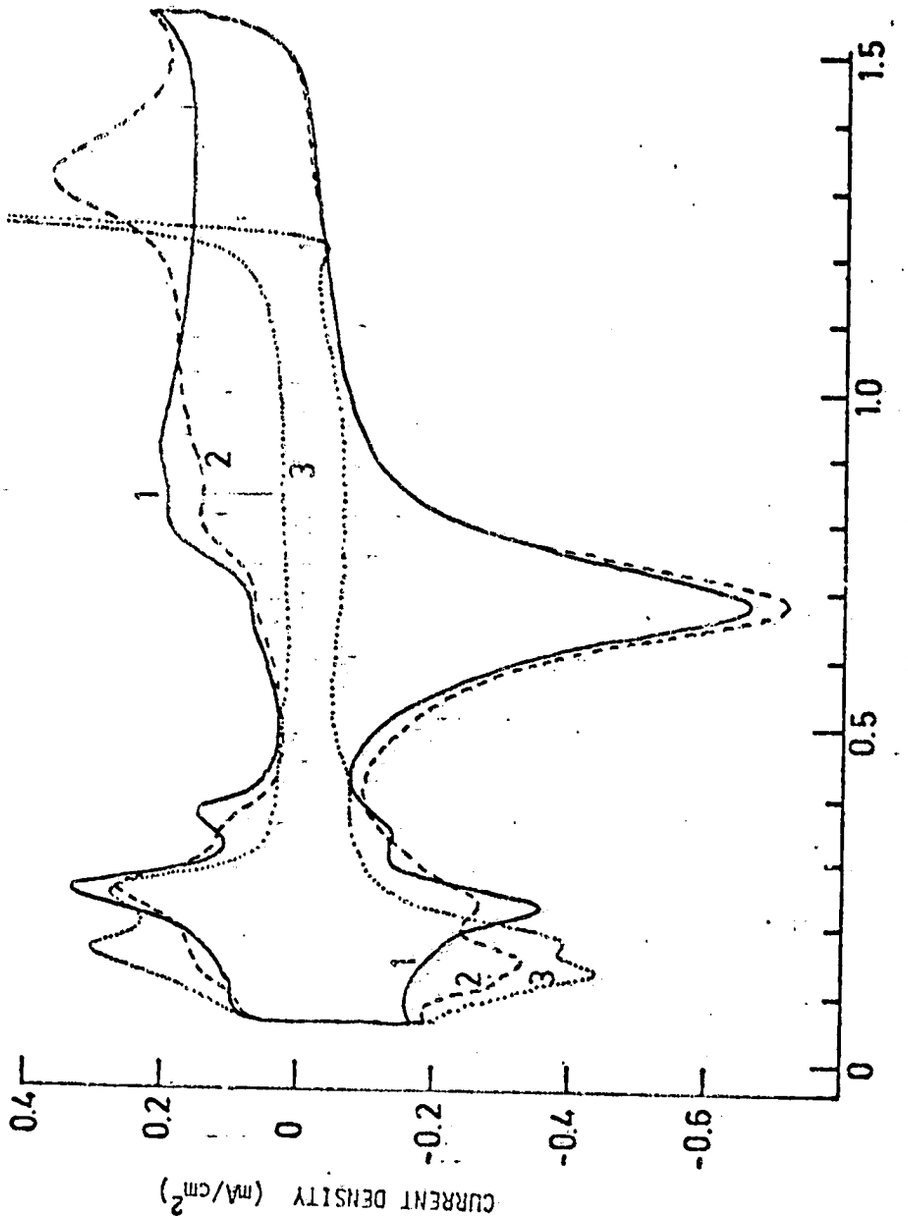

Fig. IV-25. Voltammograms for Pt in 0.1 N NaOH with I^- anions added.

1. 0.1 N NaOH
2. 0.1 N NaOH + 10^{-5} M NaI
3. 0.1 N NaOH + 10^{-3} M NaI

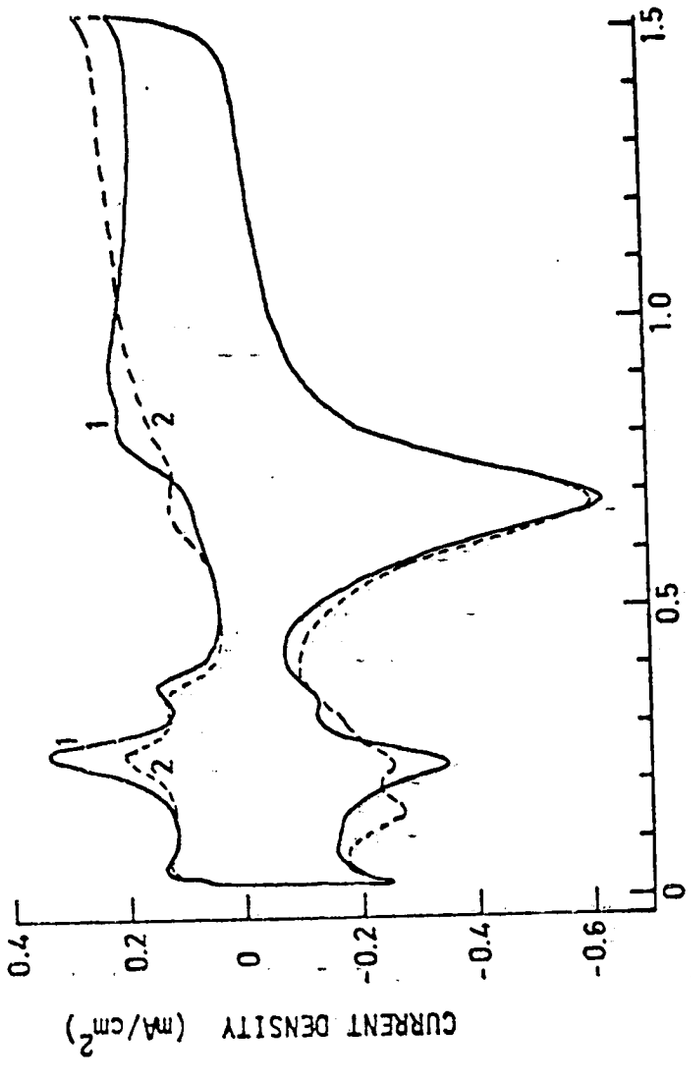

Fig. IV-26. Voltammograms for Pt in 0.1 N NaOH with CN^- anions added.

1. 0.1 N NaOH
2. 0.1 N NaOH + 1×10^{-5} M NaCN

A similar effect in the hydrogen region is observed when 10^{-5} M of CN^- is present in 0.1 N NaOH. The shape of the oxide formation region is changed while the total charge for oxide film reduction is essentially unchanged for a fixed sweep rate and range.

Slight changes are observed in the hydrogen and oxide formation regions when Br^- is added. As mentioned previously, Cl^- is a common impurity present in solutions. However, this anion does not have any significant effect on the voltammogram of Pt in alkaline solution.

On the basis of these voltammetric studies, the strength of the anion adsorption on Pt appears to be in the order I^-, $CN^- > Br^-$, $OH^- > Cl^- > SO_4^= > PO_4^{\equiv} > ClO_4^-$, F^-, showing good agreement with that reported in the literature.[87-89] Those anions which have weaker adsorbability on Pt than OH^- do not have any effect on the current-potential curve of Pt in 0.1 N NaOH in the concentration range (10^{-5} - 10^{-2} M) studied in this work.

It is well known that OH^- will attack glassware used as containers for alkaline solutions. This leads to the presence of silicate in alkaline solutions. Silicate anions up to 10^{-3} M, the highest added in 0.1 N NaOH, do not have any effect on voltammograms of Pt.

2. Cation Effects on Voltammograms of Pt in Alkaline Solutions

Figs. IV-27, 28 show the effects of Ba^{2+} and Ca^{2+} on the current-potential curves of Pt in 0.1 N NaOH. These two cations show pronounced effects with the hydrogen peaks shifted toward more cathodic and the oxide formation retarded.

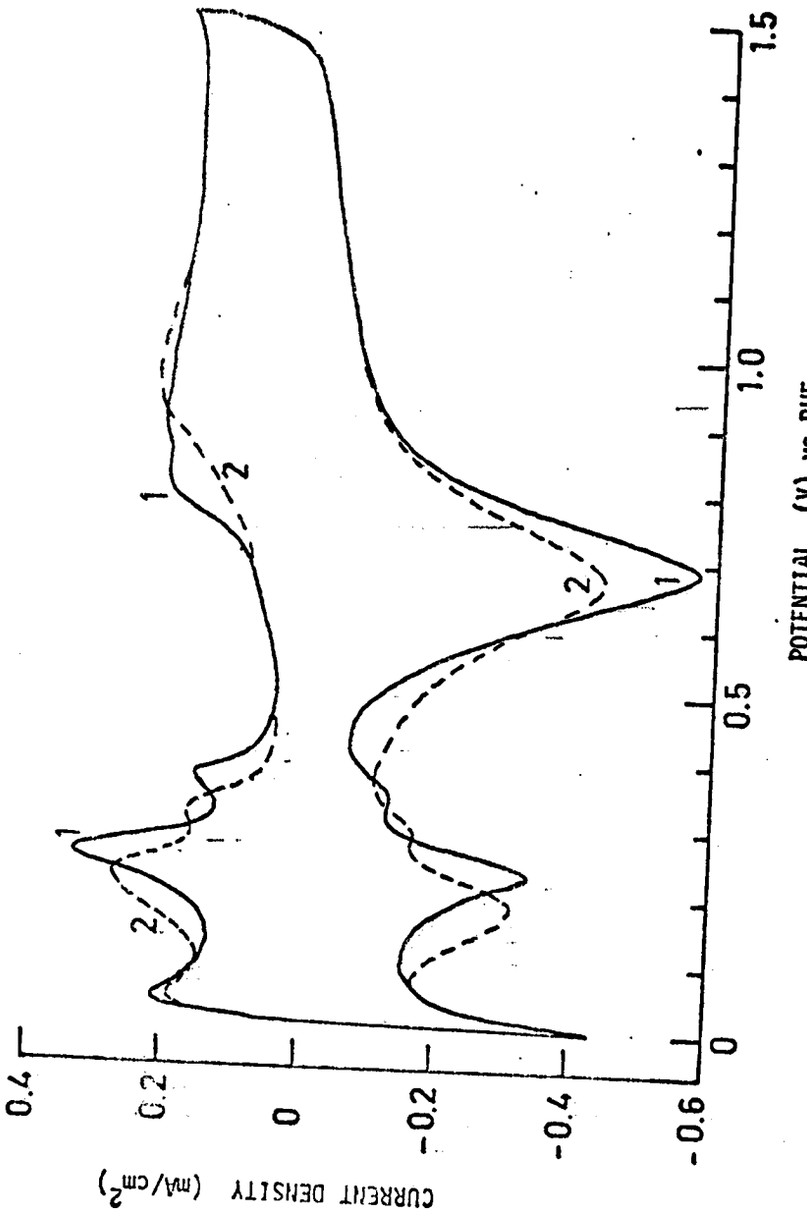

Fig. IV-27. Voltammograms for Pt in 0.1 N NaOH with Ba^{2+} cations added.

1. 0.1 N NaOH
2. 0.1 N NaOH + 5×10^{-3} M $Ba(OH)_2$

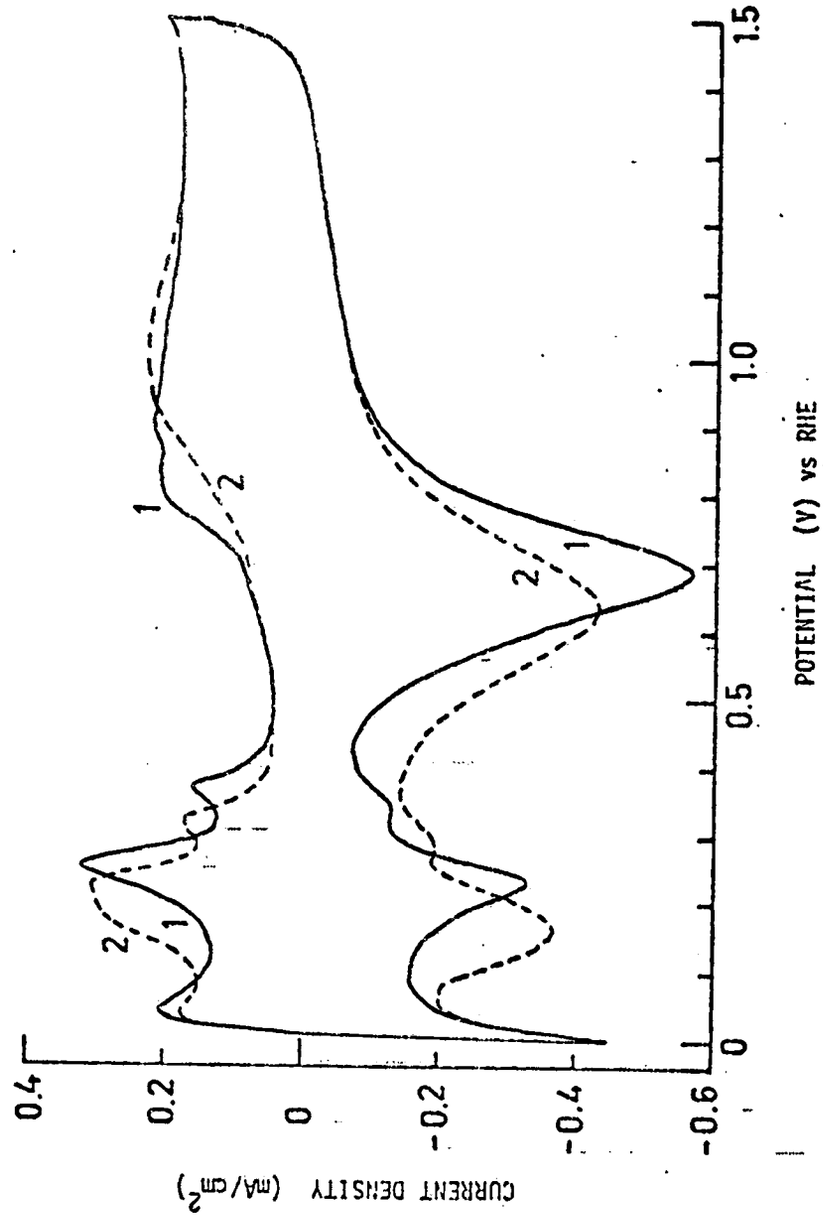

Fig. IV-28. Voltammograms for Pt in 0.1 N NaOH with Ca^{2+} cations added.

1. 0.1 N NaOH
2. 0.1 N NaOH + 5×10^{-3} M $Ca(OH)_2$

C. Potentiostatic Polarization Measurements on Oxygen Generation

1. Quasi-Steady State Potentiostatic Polarization Measurements of Oxygen Generation on Pt in HF

The quasi-steady state potentiostatic polarization curves in 0.1 N HF are shown in Figs. IV-29 - 31. Fig. IV-29 was obtained by polarizing the Pt electrode at specific potentials stepwise, increasing from 1.55 V to 2.05 V (curve A) then lowering the potential in steps (curve B) in He- and O_2-saturated 0.1 N HF solutions using the same electrode. The results show that the dependence on oxygen partial pressure of oxygen generation is insignificant. Though slight differences are observed in the lower portion of the polarization curve, this is probably caused by aging of the electrode surface while it remained at open circuit in the solution during the change of the saturation gas from He to O_2. A large hysteresis is observed in the anodic polarization curve as has been observed by other workers.[2] In the descending part of the curve, a well-defined Tafel region is observed (curve B). The Tafel slope is 130 mV/decade, similar to that obtained in both the present work and the literature in H_2SO_4 and $HClO_4$ solutions.

In Fig. IV-30, the electrode was first polarized at 2.0 V for 30 min.; next the potential was lowered in steps to 1.65 V and then returned in steps to higher values. A retraceable Tafel region is shown with a slope of 130 mV/decade. Upon polarizing the electrode at higher anodic potential, a quasi-steady state is reached on the electrode surface. The thickness of the Pt anodic oxide film is estimated as ~8Å from other studies[55,67] after polarizing the Pt

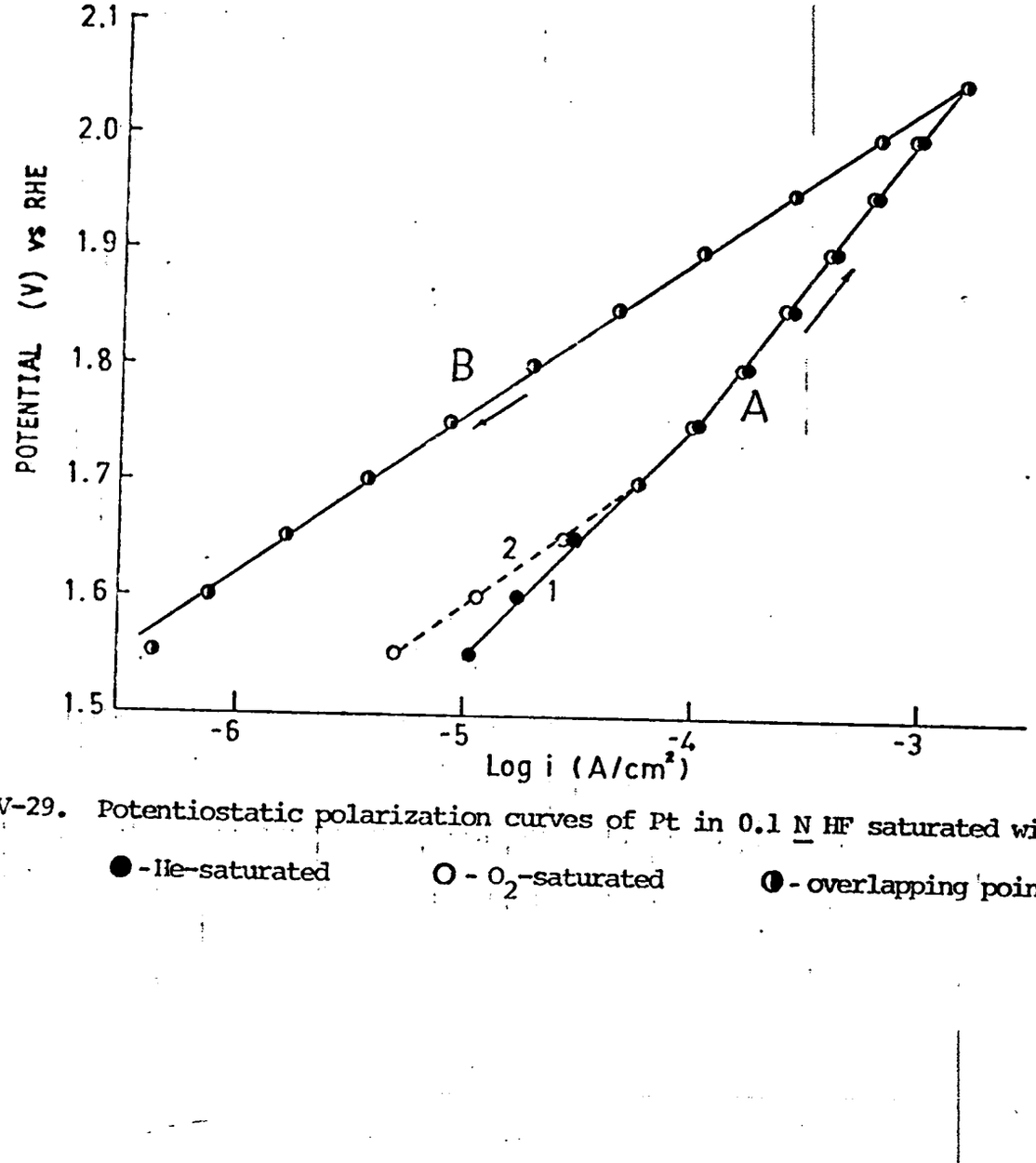

Fig. IV-29. Potentiostatic polarization curves of Pt in 0.1 N HF saturated with He and O_2.

● - He-saturated O - O_2-saturated ◑ - overlapping points

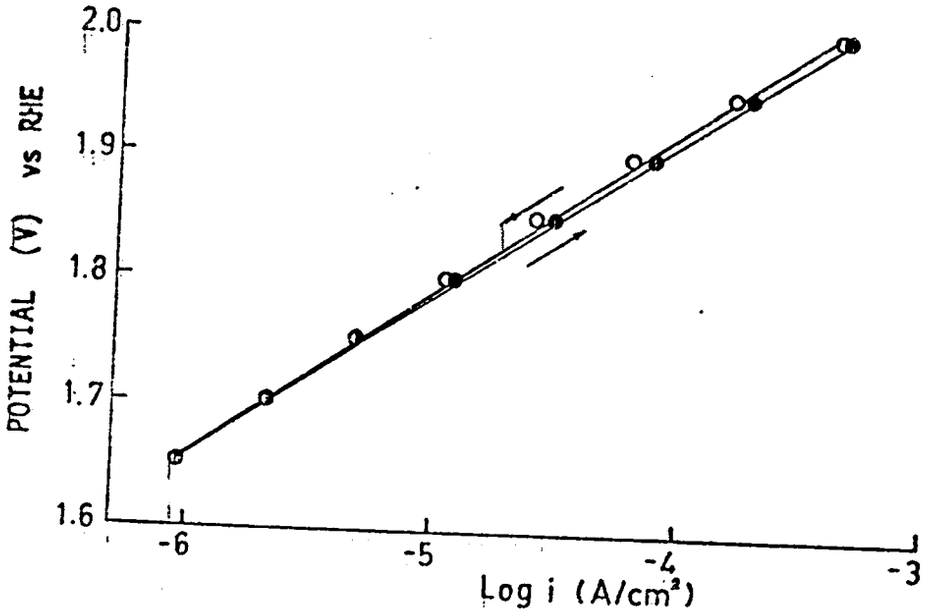

Fig. IV-30. Retraceable potentiostatic polarization curves of Pt in 0.1 N HF. The electrode has been prepolarized at 2.0 V for 30 min. and rotated at 3600 rpm in He-saturated solution.

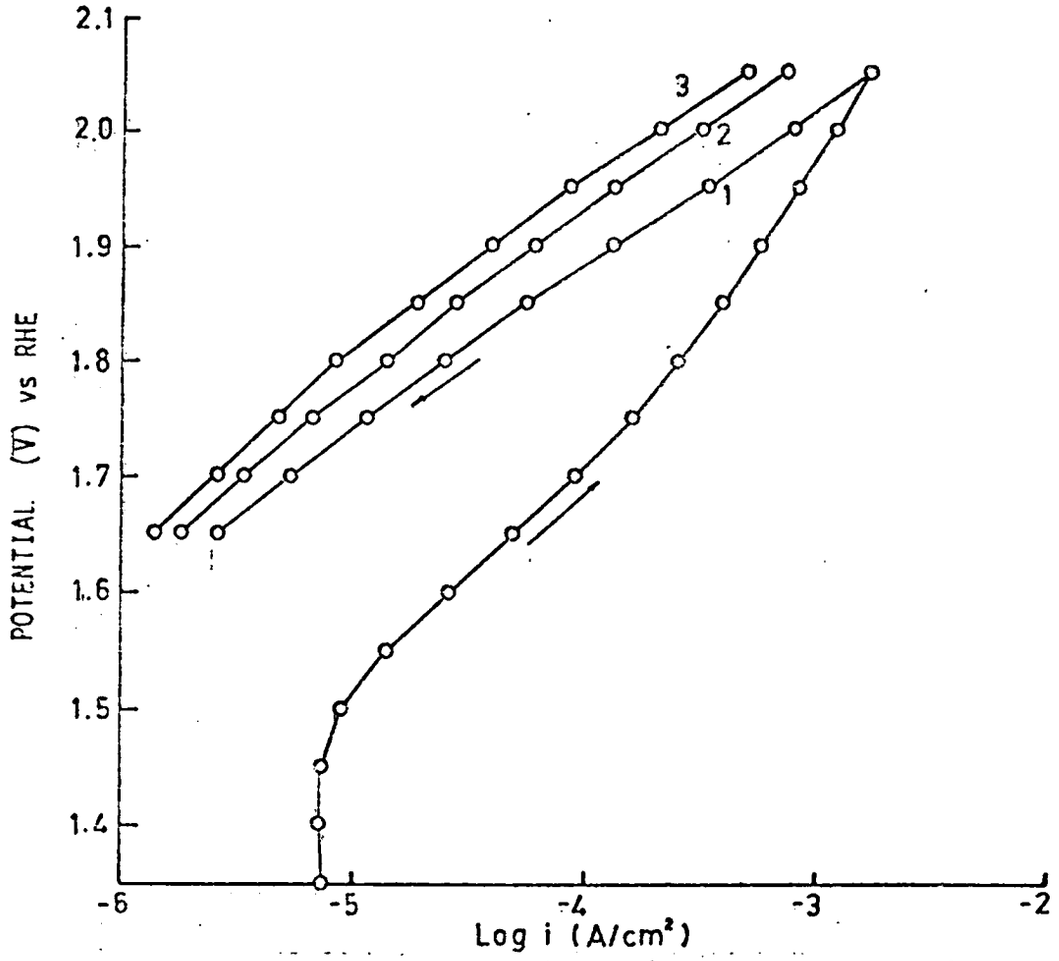

Fig. IV-31. Potentiostatic polarization curves of Pt in 0.1 N HF showing time effect. The curves are reconstructed from slow sweep voltammetry with the electrode rotated at 3600 rpm in He-saturated solution. Sweep rate 1.5 mV/sec. Staying time at 2.05V.

1. 0 min. 2. 10 min. 3. 30 min.

electrode at 2.0 V for 30 min.

Fig. IV-31 shows the effect of polarization time on oxygen generation, using slow linear potential sweep voltammetry (1.5 mV/sec). The potential was swept from 1.35 V to 2.05 V, then the potential was held for different times at 2.05 V, next swpet down to 1.6 V. Prior to each series of sweeps the electrode was reduced at 0.45 V for 10 min. The Tafel slopes shown in Fig. IV-31 remain independent of polarization time, but the exchange current density decreases as a function of polarization time. The mechanism of oxygen generation is thus unchanged and the electrocatalytic activity is decreased by longer prepolarization time. It can be seen that a standardized prepolarization treatment at high anodic potential is needed for reproducible electrocatalytic studies of oxygen generation on Pt. For the study of cation and anion effects on oxygen generation, the Pt electrode was first polarized at 2.05 V for 30 min. and the Tafel region was examined by lowering the potentials.

2. Cation Effect on Oxygen Generation

The effects of cations of oxygen generation are shown in Figs. IV-32 - 34. The effects are rather small with all the cations studied. The Tafel slope is unchanged except for $N(C_2H_5)^+$ and the catalytic activity is somewhat lowered by adding other cations in addition to H_3O^+. The initial attempt to study the effect of alkali metal cations in HF solutions was not successful, due to the presence of traces of chloride which were very difficult to remove in all of the fluoride salts, particularly CsF. This study instead was per-

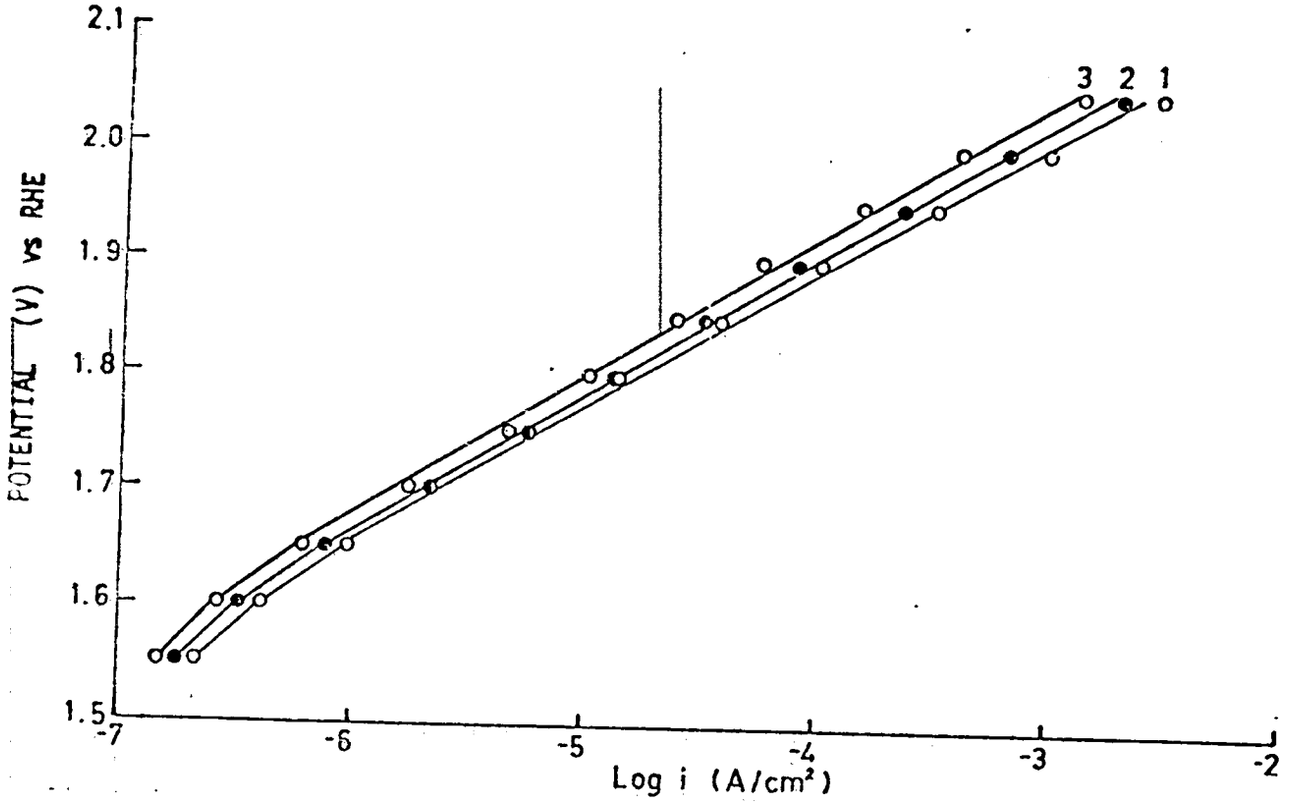

Fig. IV-32. The effect of Li^+ and Cs^+ cations on potentiostatic polarization curve of Pt in 0.1 N H_2SO_4.

1. 0.1 N H_2SO_4
2. 0.1 N H_2SO_4 + 5 x 10^{-3} M Li_2SO_4
3. 0.1 N H_2SO_4 + 5 x 10^{-3} M Cs_2SO_4

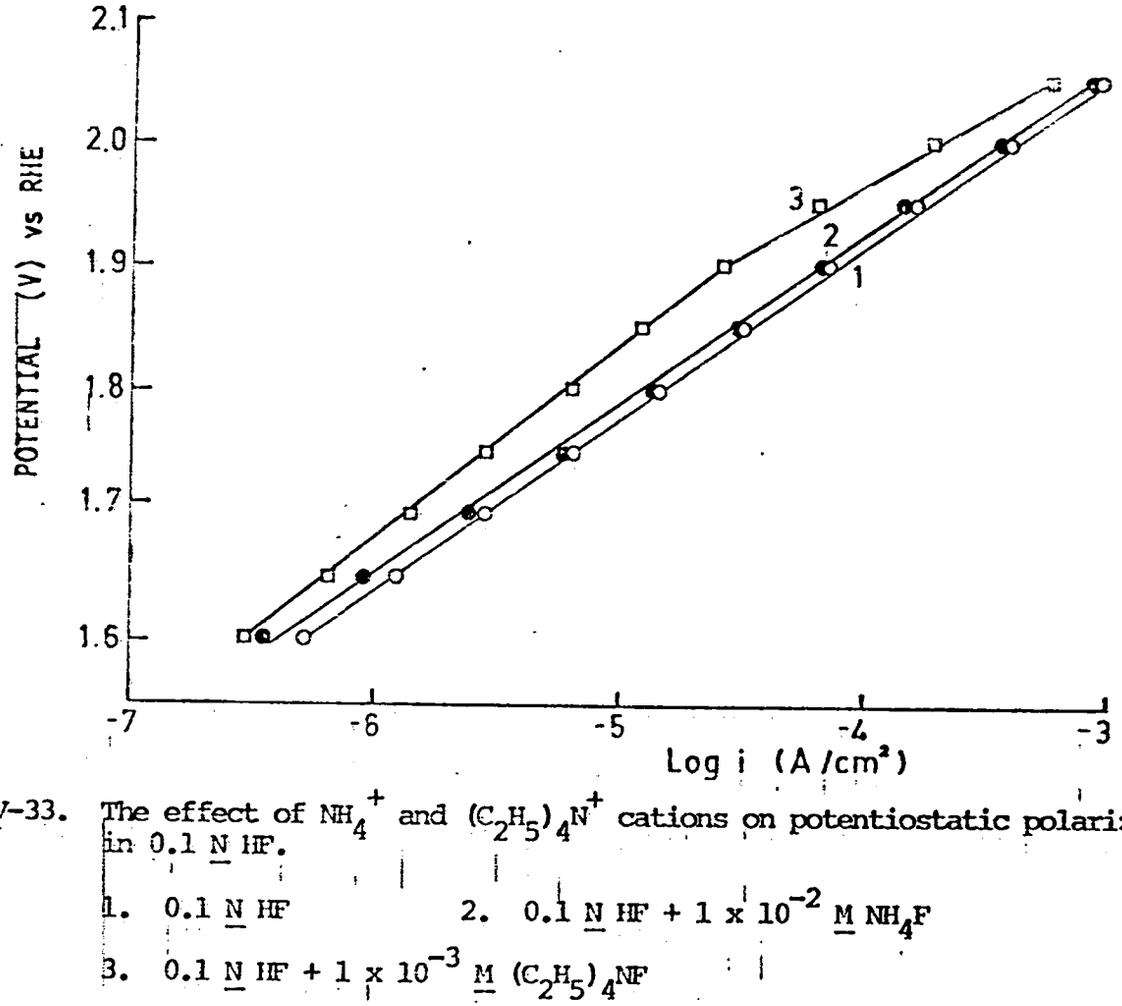

Fig. IV-33. The effect of NH_4^+ and $(C_2H_5)_4N^+$ cations on potentiostatic polarization curve of Pt in 0.1 N HF.

1. 0.1 N HF
2. 0.1 N HF + 1 x 10^{-2} M NH_4F
3. 0.1 N HF + 1 x 10^{-3} M $(C_2H_5)_4NF$

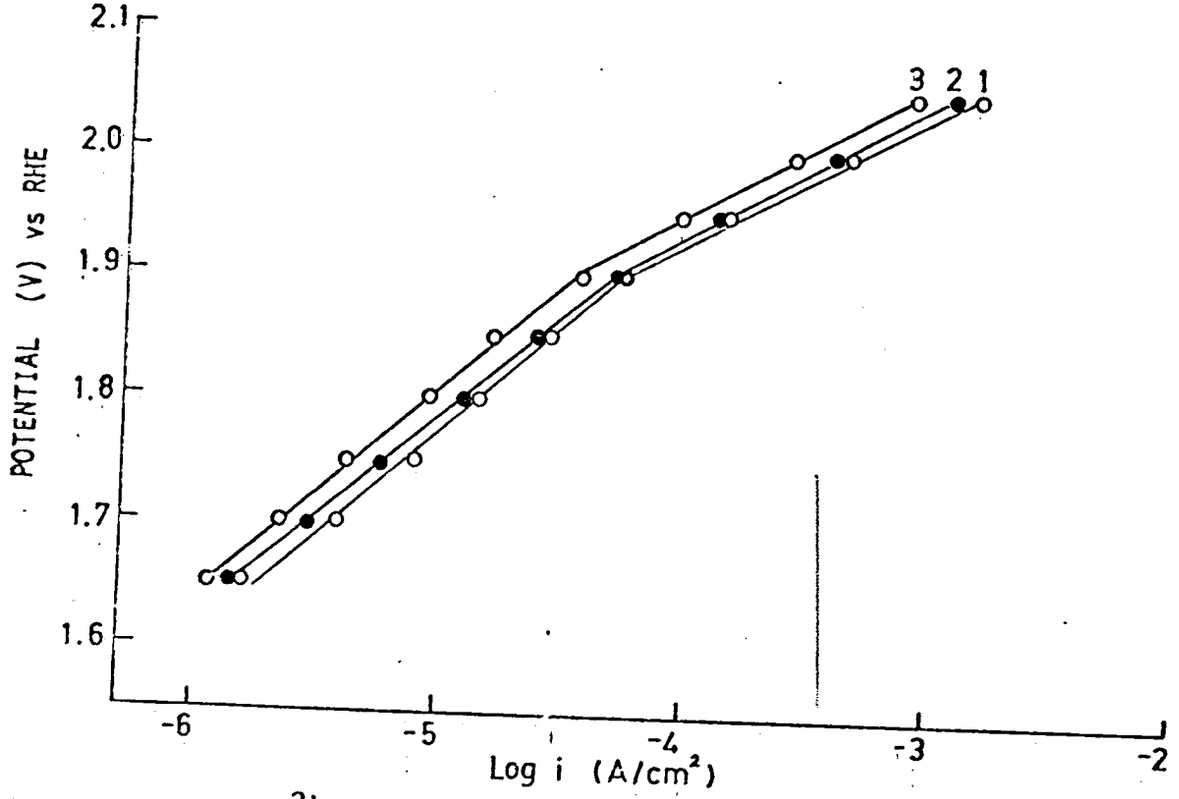

Fig. IV-34. The effect of Ba^{2+} cations on potentiostatic polarization curve of Pt in 0.1 N NaOH.

1. 0.1 N NaOH
2. 0.1 N NaOH + 5×10^{-4} M $Ba(OH)_2$
3. 0.1 N NaOH + 5×10^{-3} M' $Ba(OH)_2$

formed in H_2SO_4 with sulfate salts. The effect of Cs^+ cations is larger than that of Li^+ cations. This verifies the results of Erdey-Gruz, Gallyas and Szetey.[76] The effect of NH_4^+ cation is most probably due to the change of acidity in HF. The O_2 generation overpotential is 60 mV per pH.[106] The presence of $N(C_2H_5)_4^+$ cations causes a deviation of Tafel slope. This may be due to a partial blocking of the electrode surface by these large organic cations and/or modifications in the potential distribution across the solute-oxide-metal region.

While the majority of the O_2 anodic polarization studies have been carried out in acid solutions, a few measurements have also been made in alkaline solutions, despite the purification problems. Two Tafel regions are shown in 0.1 N NaOH, with a slope of 100 mV/decade in the upper region and a slope of 180 mV/decade in the lower region. Damjanovic et al.[70] have also observed slope change in alkaline solution and attributed the change to a change in mechanism of O_2 generation. An alternative explanation is that potential distribution across the solute-oxide-metal region has shifted, perhaps due to changes in the surface oxide properties at lower potentials. A third explanation is the adsorption or desorption of some impurities in NaOH solution in the region of 1.9 V.

The curves in Fig. IV-34 indicate that the effect of Ba^{++} is to increase the overpotential with very little modification of slope. The precision is not sufficient to establish the concentration dependence other than to note that the effect increases with Ba^{++} concentration in the range 10^{-4} - 10^{-3} M.

3. Anion Effect on Oxygen Generation

The effect of anions on oxygen generation is shown in Figs. IV-35 - 37. The Pt electrode was prepolarized at 2.05 V for 30 min in solutions free of added anions. The measurement was made after addition of anions. Chloride is a common impurity present in solutions. In HF solutions, traces (10^{-5} M) of Cl^- lower the catalytic activity for O_2 generation slightly without changing the Tafel slope. When Cl^- concentration reaches 10^{-2} M, Cl_2 formation is evident from the polarization curve. Even when Cl^- concentration present is 10^{-2} M, the effect on O_2 generation is small in the potential range 2.05 - 1.85 V. In the 10^{-2} M Cl^- containing solution, the current associated with Cl_2 generation probably corresponds to the differences in curves 1 and 3. This difference is much smaller than the diffusion limiting current calculated for Cl_2 generation. The overpotential for Cl_2 generation on the oxide covered Pt appears to be much higher than on Pt in a 10^{-2} to 10^{-1} M HCl solution.

In alkaline solution, the potential for Cl_2 generation is shifted anodically relative to O_2 generation. When 10^{-2} M Cl^- is present in 0.1 N NaOH, the overpotential for O_2 generation is increased slightly with the Tafel slope essentially unchanged.

The polarization for O_2 generation is also increased by silicates added during the run after the prepolarization at 2.05 V for 30 min. The effect is similar to Cl^- and the effect is so small that it is difficult to establish clearly whether a change in the Tafel slope is produced.

C2

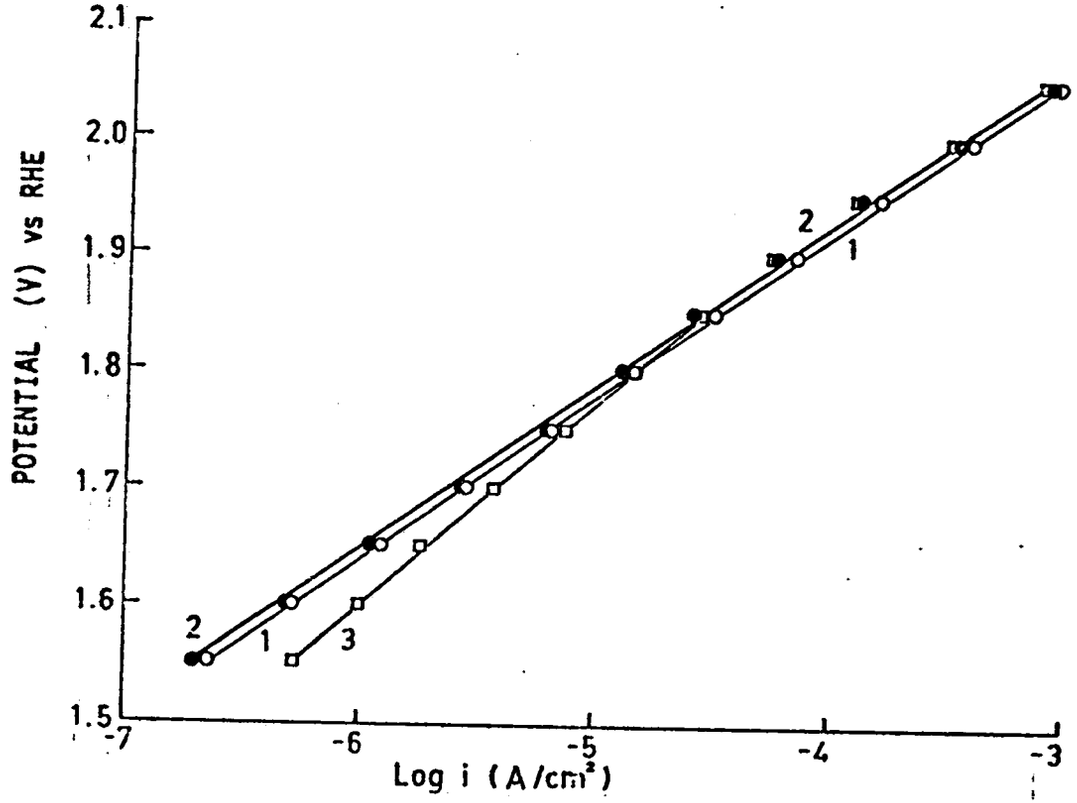

Fig. IV-35. The effect of Cl^- anions on potentiostatic polarization curve of Pt in 0.1 N HF.

1. 0.1 N HF
2. 0.1 N HF + 10^{-5} M HCl
3. 0.1 N HF + 10^{-2} M HCl

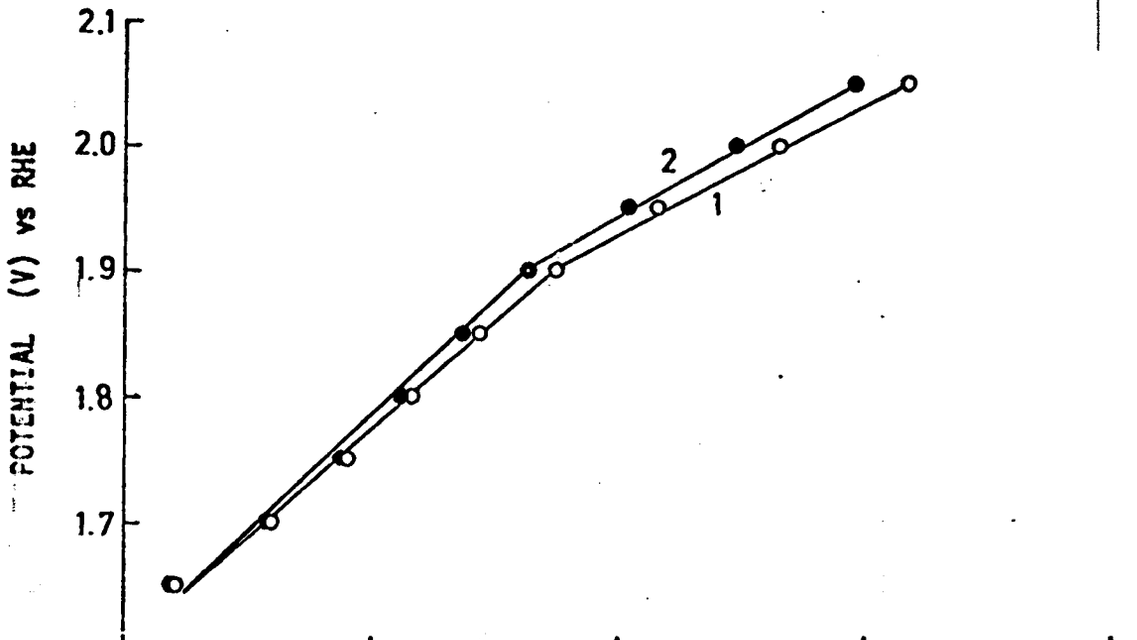

Fig. IV-36. The effect of Cl^- anions on potentiostatic polarization curve of Pt in 0.1 N NaOH.

1. 0.1 N NaOH
2. 0.1 N NaOH + 10^{-3} M NaCl

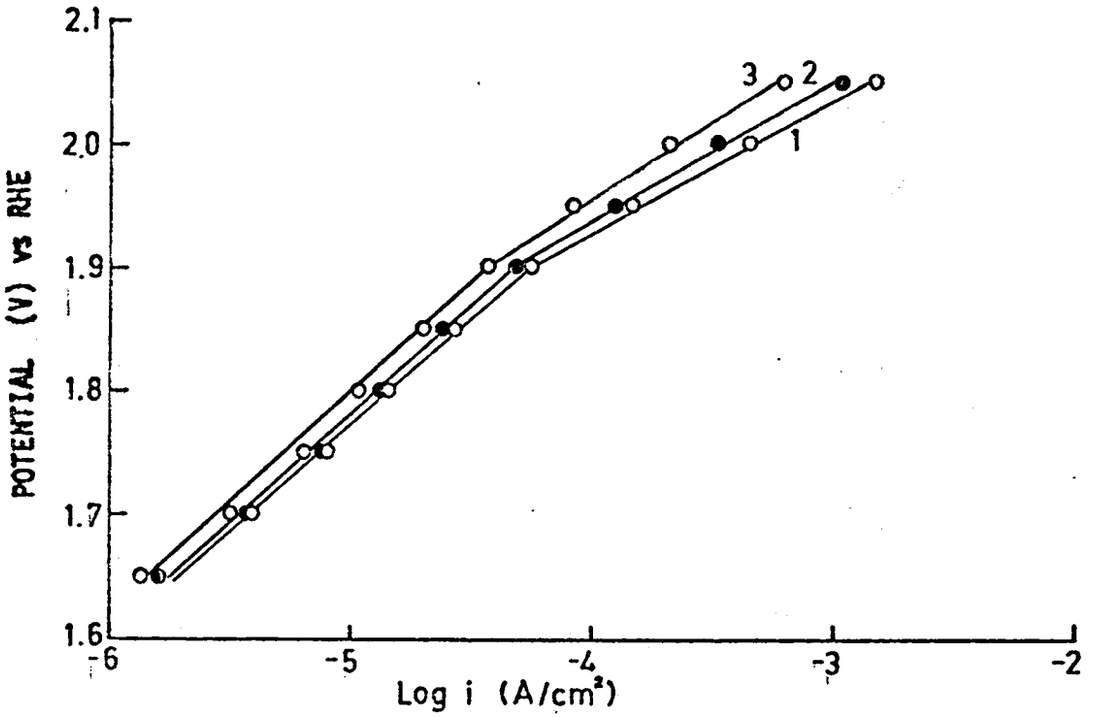

Fig. IV-37. The effect of SiO_3^{2-} anions on potentiostatic polarization curve of Pt in 0.1 N NaOH.

1. 0.1 N NaOH
2. 0.1 N NaOH + 5×10^{-4} M Na_2SiO_3

CHAPTER V

INTERPRETATION AND DISCUSSION

A. Mechanisms For Cation And Anions Effects on Hydrogen Chemisorption on Pt.

Two forms of adsorbed hydrogen have been proposed to explain the principal peaks (I, IV in Fig. IV-1) on Pt in H_2SO_4 solutions; they have been described[107] as weakly and strongly bound hydrogen. The existence of the third peak (III) in the middle of two main peaks in the anodic sweep was recognized later[108]. However, this third kind of hydrogen on Pt is not observed during the cathodic adsorption of hydrogen in H_2SO_4 solutions. Will[108] tentatively suggested that these various peaks could be assigned to hydrogen adsorption on the different crystalline faces. It was shown that on each of the faces studied, all three peaks could be observed with different ratios of peak heights, suggesting that the surface topography did not correspond uniquely to the macrosopic orientation of the single crystals. This explanation, however, did not give a satisfactory answer to the non-existence of the third peak in the cathodic sweep.

Breiter[109] has proposed that the third anodic peak arises from the oxidation of dissolved atomic hydrogen in the platinum crystallite and molecular hydrogen dissolved in the electrolyte, both species being formed during the cathodic sweep. Kinoshita, Lundquist, and Stonehart[110] have criticized this explanation and have shown that the calculated charges due to the oxidation of

dissolved atomic hydrogen and molecular hydrogen are rather small as compared to the experimental charges measured under the third anodic peak. Stonehart[111] has suggested that the third anodic peak having no mirror image, is due to a surface interaction between the weakly and strongly bound hydrogen forms. It is explained that this third species cannot exist until both weak and strong species are present and therefore cannot be observed during hydrogen adsorption. Kinoshita et al.[110] explained the situation by the surface diffusion and reorientation of the strongly bound hydrogen while Angerstein-Kozlowsa et al.[104] explained by the relocation of adsorbed hydrogen.

In the present work, the counterpart of the third anodic peak is evident in the cathodic sweeps in 0.1 N HF and $HClO_4$ (Fig. IV-3,4) although not in 0.1 N H_2SO_4 and H_3PO_4 (Fig. IV-1,2). The non-existence of the third cathodic peak can be due to largely overlapping of this peak with other peaks in the solutions of H_2SO_4 and H_3PO_4. The interpretations in the literature do not appear to be correct.

The existence of four distinct peaks in the anodic sweep was first reported by Angerstein-Kozlowska et al.[104] Two models are favored by these authors. The first model describes the multiple peaks for hydrogen chemisorption as arising from chemically different geometric sites and can be distinguished by their disposition for single or multiple bonding to hydrogen, e.g. hydrogen on top of Pt atoms, between various groups of Pt atoms, etc. The second model is that distinguishable electronic states on the Pt

surface for hydrogen chemisorption arise for a community of adatoms due to collective, long-range electronic effects associated with the properties of the whole surface and adatom system; i.e. the concept of induced heterogeneity.

For a given crystal plane, hydrogen chemisorption and cation-anion effect can be explained by one of the following factors or a combination of these factors.

1. Different Sites

Hydrogen chemisorption may occur at different geometric sites as proposed by Angerstein-Kozlowska et al.[104] The existence of several hydrogen peaks in the voltammogram of Pt is due to the adsorption of hydrogen at different sites for single and multiple bondings. Fig. V-1 illustrates the possible positions of these sites on a Pt [111] surface plane. Site 4 is the possible position for strongly bound hydrogen (peak IV in Fig. IV-1) sitting in the plane of first array of Pt atoms (position 4) or rattling between positions 4' and 4". Site 1 is possible for weakly bound hydrogen (peak I in Fig. IV-1). Similarly, the rest of peaks can be assigned to the adsorption at other sites on 111 or other orientations. Studies of different crystal orientations combining electrochemical and gas-phase surface studies (e.g. LEED) may give some clues about these sites. Unfortunately progress in this field is slow, due to the involvement of highly complicated techniques. The situation is further complicated by the evidence[112,113] that clean Pt 100 surface undergoes crystal reorientation after adsorption of foreign ions.

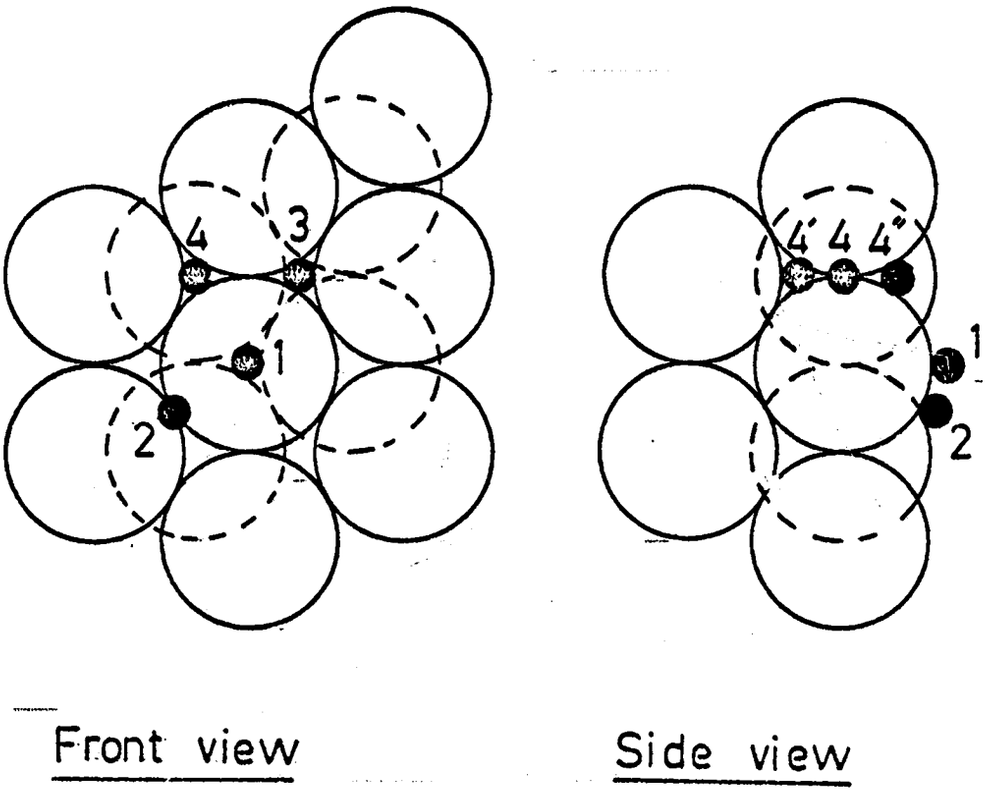

Figure V-1

Different sites for hydrogen chemisorption on a Pt [111] surface plane[104]. Sites 3 and 4 differ by the presence or absence of a Pt atom in the second layer beneath the trigonal hole.

Underpotential deposition of metals such as Ag, Cu, Hg on Pt (104, 114, 115) has been studied in relation to hydrogen chemisorption. A lowering of the hydrogen peaks are clearly shown in these studies, affording the evidence that different adsorption sites are involved for hydrogen chemisorption and are blocked by the deposition of metal cations.

The effect of anions on hydrogen adsorption-desorption can be explained by the cooperative interaction of hydrogen atoms and the anions. The chemisorption of hydrogen on specific site S can be expressed as $H^+ + S + \gamma_H e^- \rightleftarrows S\text{-}H^{(1-\gamma_H)}$ (V-1) while anion adsorption on site S, $X^z + S \rightleftarrows S\text{-}X^{(z + \gamma_x)} + \gamma_x e^-$ (V-2). The displacement of anion by hydrogen on site S in cathodic sweep can be expressed as $H^+ + S\text{-}X^{(z + \gamma_x)} + (\gamma_H + \gamma_x)e^- \rightleftarrows S\text{-}H^{(1-\gamma_H)} + X^z$ (V-3). The process is reversed in the anodic sweep. The interaction between hydrogen and anions results in redistributing the charge under the hydrogen peaks and changes in the peak potentials. Figure V-2 shows the charge under the strongly bound hydrogen peak is changed by the addition of SO_4^{2-} to 0.1 N HF and $HClO_4$. The charge is expressed as a ratio Q_{Hs}/Q_H to the total charge for hydrogen chemisorption. A linear dependence of the charge change on the logarithm of SO_4^{2-} concentration indicates how SO_4^{2-} adsorption influences the adsorption of the strongly bound hydrogen. An attempt to correlate hydrogen and anion adsorptions with Temkin adsorption isotherms was not successful due to a large number of unknown parameters (two parameters for each species and each type of site).

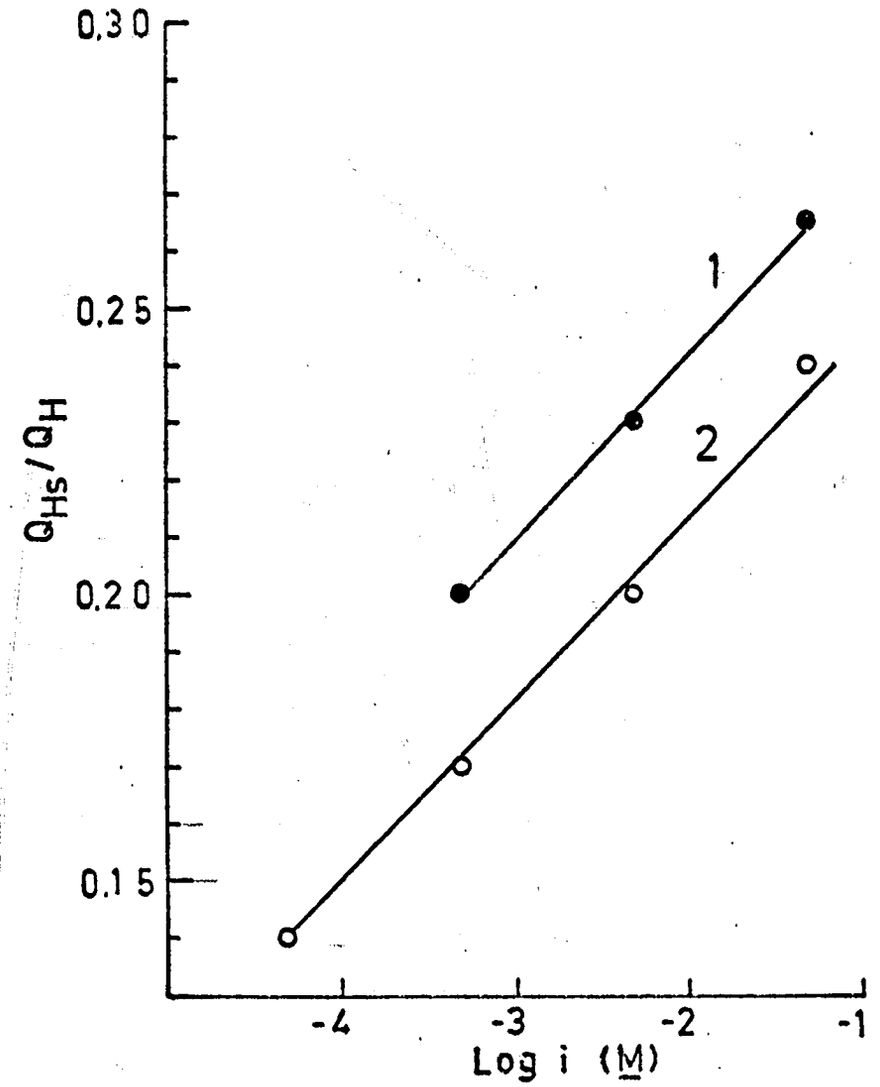

Figure V-2

The plot of the charge under the strongly bound hydrogen peak as a logarithmic function of SO_4^{2-} concentration. The charge is expressed as a ratio Q_{Hs}/Q_H to the total charge for hydrogen chemisorption.

1. SO_4^{2-} in 0.1 N $HClO_4$.
2. SO_4^{2-} in 0.1 N HF.

2. Induced Heterogeneity

Multiple states of hydrogen chemisorption originate from collective long-range electronic effects arising from the electronic interactions between a community of adatoms. A series of distinct energy states at the surface are thus generated for hydrogen adsorption. The concept for hydrogen chemisorption in electrochemical situation was proposed by Angerstein-Kozlowska et al.[104] The interaction is propagated through the metal crystal by means of the delocalized system of electrons. This situation therefore allows a given atom in a surface on which hydrogen is chemisorbed to influence another far away. However, the specific sites that may be involved in the induced heterogeneity effects have not been indicated by the previous authors. The strength of the electronic interactions giving rise to induced heterogeneity should be greatly dependent on site geometry.

This electronic interaction is also dependent on anion adsorption. The electronic surface states available for hydrogen chemisorption can be modified by anion adsorption, causing a variation of hydrogen chemisorption at different energies.

3. Anion or Cation Produced Change in The Potential Distribution Across The Metal-Solution Interface

The effects of anions and cations on hydrogen chemisorption arise from the change of potential distribution across the metal-solution interface. This change results from the change of the dielectric properties of the interface by anion adsorption or the presence of cations in the compact double layer. A change in

potential distribution will then cause a variation on hydrogen adsorption energy.

In acids at the potential region where anions such as Cl^- or SO_4^{2-} are strongly adsorbed, the absorbed hydrogen which is affected is usually the strongly bound hydrogen. At more cathodic potential region where these anions are desorbed, the weakly bound hydrogen adsorption is principally unaffected. This situation is reversed when cations such as Cs^+ are present in H_2SO_4 because the surface excess of Cs^+ has been shown[105] to reach a maximum value in the potential range of the adsorption-desorption of the weakly bound hydrogen.

In alkaline solutions, OH^- is strongly adsorbed on Pt, and only those anions such as I^- or CN^- having stronger adsorbability can displace OH^-. When these two anions are present in alkaline solutions, they are strongly adsorbed in the hydrogen region and influence all hydrogen peaks. When Ba^{2+} and Ca^{2+} are present in alkaline solutions, the positive charge of these cations compensates the negative charge of OH^- in the compact double layer and lowers the adsorption energy of hydrogen.

B. Mechanisms for Anion And Cation Effects on Pt Oxide Film Formation

In the onset of anodic Pt oxide film formation, the most probable reaction in acids is

$$Pt + H_2O \rightarrow PtOH + H^+ + e^- \quad (V-4)$$

and in alkaline solutions

$$Pt + OH^- \rightarrow PtOH + e^- \quad (V-5)$$

Where the PtOH indicates OH adsorbed on the Pt metal. Most workers

4,5,27,28,30 agree on this point. Chemisorption of hydroxyl radical is expected to be influenced by the presence of anions or cations in the solutions.

On the basis of the observation of a shoulder with two peaks in the potential range 0.8-1.1V in 1 N H_2SO_4, Angerstein-Kozlowska et al.[5] have proposed a detailed mechanism for the initial phase of Pt oxide film formation. This mechanism is described in Chapter II. The same fine resolution in the Pt oxide film formation has been observed in this study in 0.1 N H_2SO_4. However, this resolution is only clearly shown in H_2SO_4 solutions, but not in other acids. When SO_4^{2-} is added to other acids such as HF or $HClO_4$, this fine resolution is gradually exhibited. As seen from the results shown in Table IV-2, anion adsorption greatly influences the initial stages of Pt anodic oxide film formation.

The effect of cations in acids is shown to be small with the exception of $(C_2H_5)_4N^+$. The presence of Ba^{2+} and Ca^{2+} in alkaline solutions has a significant effect on oxide film formation.

Those factors assumed to be dominant in the chemisorption of hydroxygen can also be considered in the initial stages of the anodic Pt oxide film formation to afford an explanation for the effect of cations and anions.

Lattice sites are considered by Angerstein-Kozlowska et al.[5] for the initial phase of Pt oxide formation. Anion adsorption may influence OH^- chemisorption on these sites. According to the present work the retardation of Pt oxide formation by Cl^- in acids

and I^- in alkaline solutions reveals that these sites are blocked by the strong adsorption of these anions on Pt. The presence of SO_4^{2-} and PO_4^{3-} in acids may block or strongly influence these sites until their desorption allows oxide film formation to occur. It can be seen that the presence of these two anions in acids shifts the onset of oxide film formation toward more anodic potentials.

The induced heterogeneity from collective long-range electronic effect is also an explanation for the effect of anions. The electronic surface states available for OH^- chemisorption are modified by anion adsorption. The initial stages for oxide film formation are affected with a redistribution of peak potentials and the charge under each peak. Different structure is therefore observed in voltammograms when different anions are present in the solutions.

The effect of cations and anions can also be attributed to a change of potential distribution across the metal-solution interface. However, this modification of potential distribution by most cations in acids is small with the exception of $(C_2H_5)_4N^+$, probably due to its bulk in size. The effect of Ba^{2+} and Ca^{2+} in alkaline solutions is due to the compensation of OH^- charge by these two cations in the compact double layer with a result of retarding OH^- chemisorption.

Anion adsorption will also have a change in potential distribution. However, this effect is not clearly shown in the voltammograms, but is combined with the previous two factors.

Other things equal, it is likely that the delay in the formation of the oxide film caused by strongly bound anions is caused

principally by a combination of blocking and change in potential distribution across the interface.

C. Mechanism For Oxygen Generation And The Effects of Cations And Anions on Oxygen Generation

Under anodic potentials for O_2-generation, the Pt electrode surface is already covered with a film of Pt anodic oxide. The prepolarization of the electrode at 2.05 V for 30 min results in forming a film of ~8 Å thick with a possible structure of bulk metal Pt-O-Pt-O-Pt^z solution.

The main observations made in this study for O_2-generation are:

(1) Tafel slope corresponds to a value of 1/2 for transfer coefficient and is independent of oxide thickness and cation or anion adsorption.

(2) Catalytic activity for O_2-generation appears to be inversely proportional to the thickness of oxide film.

(3) A minor dependence of catalytic activity is observed on coadsorption of anions or cations.

None of conventional electrochemical techniques and classical treatment can clearly unravel the mechanism for O_2-generation. The information obtained above continues to be insufficient to determine the mechanism. However, general observation of a 120 mV/decade Tafel slope with a transfer coefficient of 1/2 suggests that the first charge transfer step is rate controlling. The following mechanism is one of the possibilities for O_2-generation. The first step is an adsorption reaction to form $(PtOH)^{z-1}$ on the electrode

surface:

In acids: $Pt\text{-}O\text{-}Pt\text{-}O\text{-}Pt^{z} + H_2O \rightarrow Pt\text{-}O\text{-}Pt\text{-}O\text{-}(PtOH)^{z-1} + H^{+}$ (V-6)

In alkaline solutions $Pt\text{-}O\text{-}Pt\text{-}O\text{-}Pt^{z} + OH^{-} \rightarrow Pt\text{-}O\text{-}Pt\text{-}O\text{-}(PtOH)^{z-1}$ (V-7)

The PtOH species on the electrode surface is most likely to be non-ionic. It is then highly possible that the charge transfer via electron tunnelling occurs between $(PtOH)^{z-1}$ and bulk metal:

$$Pt\text{-}O\text{-}Pt\text{-}O\text{-}(PtOH)^{z-1} \rightarrow Pt\text{-}O\text{-}Pt\text{-}O\text{-}(PtOH)^{z} + e^{-} \text{ (slow)} \quad \text{(V-8)}$$

This step is then followed by several rapid steps, leading to the final formation of O_2.

Vetter and Schultze[55,106,116] have reported substantial details on charge transfer via electron tunnelling for various reactions including O_2-generation on an oxide covered Pt surface. They also have reached the conclusion that the charge transfer for O_2-generation involves some type of OH^{-} adsorption. Their treatment includes basic electron tunnelling within the traditional framework of the weak interaction charge theory developed by Guney[117] and Gerischer.[118] The following expression has been used by these authors[55] to correlate the tunnelling probability Wt with the oxide thickness d:

$$Wt \sim \exp\left[-\frac{4\pi d}{h}\sqrt{(2Me \cdot \Delta Et)}\right] \quad \text{(V-9)}$$

Where Me is the electron mass, ΔEt is the mean height of the potential barrier. The equation for O_2-generation current is then

derived as:

$$\log i_{O_2} = A - \frac{Ea^\circ - \alpha F\eta}{2.3RT} - \frac{d}{d^\circ} \qquad (V-7)$$

where A, d° are constants, the activation energy Ea° is related to the rearrangement energy λ by

$$Ea = (E-E_F + \lambda)^2/4\lambda \qquad (V-8)$$

and

$$Ea = Ea^\circ - \alpha F\eta \qquad (V-9)$$

The weak interaction theory for charge transfer leads to the prediction of $\alpha \approx 1/2$, essentially in accord with experimental results. The theory further predicts that $\log i_{O_2} \sim d/d^\circ$; this also in accord with experimental observations.

The mechanism proposed above differs from that of Vetter and Schultze[55] with $(PtOH)^{z-1}$ prominently non-ionic. This, however, does not introduce any complication in the interpretation of our results with Vetter and Schultze's model of electron tunnelling through the oxide film.

The potential distribution across the metal-oxide-solution region can be roughly drawn as shown in Figure V-3.

Two assumptions have to make for the proposed mechanism:

(1) For a given electrolyte almost all of the change in potential occurs at the oxide film, i.e. $\phi m - \phi a = \phi m - \phi s$ where ϕa is the surface potential of the oxide covered electrode.

(2) The oxide film Pt-O-Pt-O-Pt^z does not act as an electron bridge for charge transfer in virtual state. The bridge mechanism for charge transfer needs second

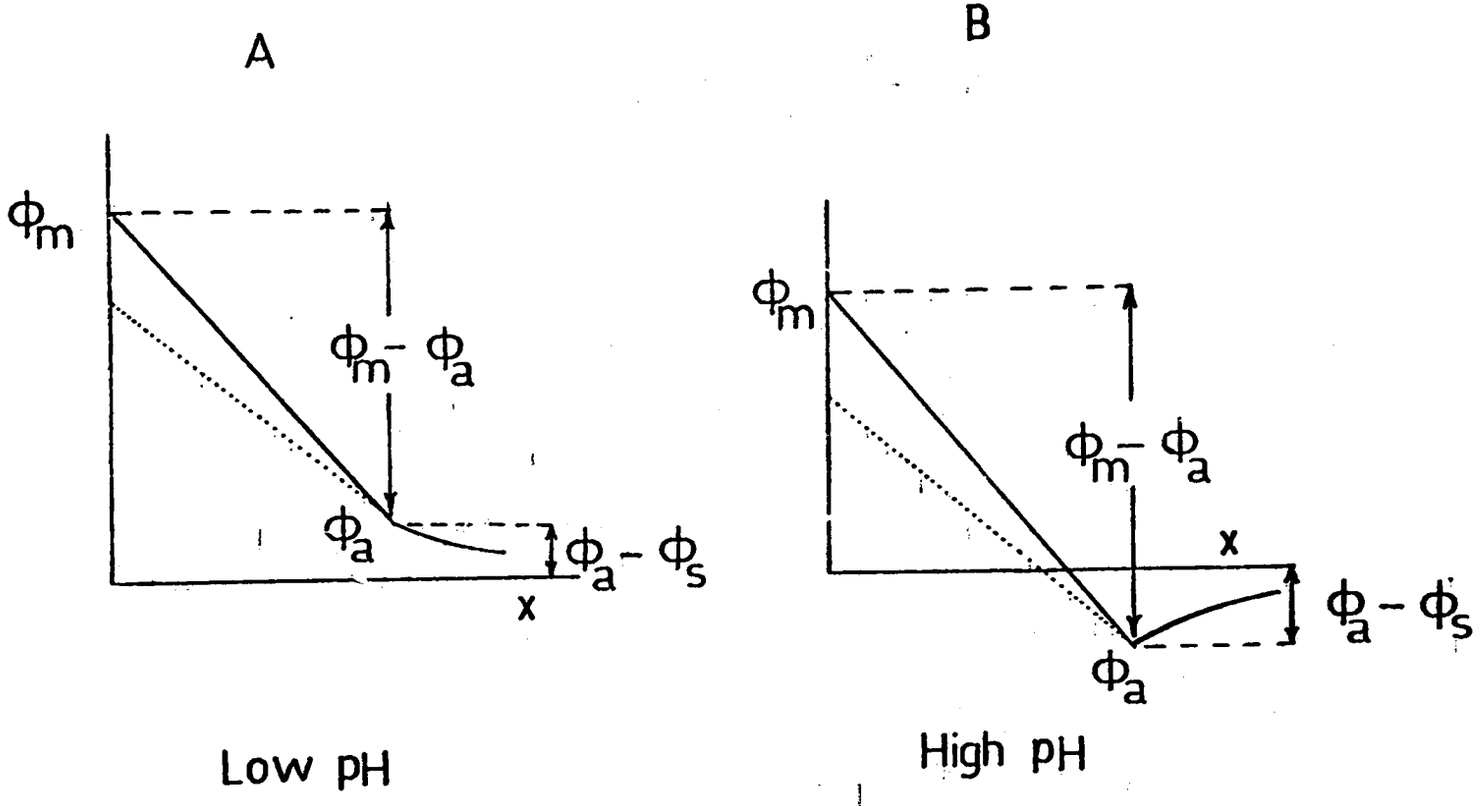

Figure V-3

The potential distribution across the metal-oxide-solution region. A - low pH, B - high pH, Φm - potential of metal, Φa - surface potential of the oxide covered electrode, Φs - potential of bulk solution.

order perturbation theory to calculate the transition probability and could not usually yield $\alpha = 1/2$.

The surface potential ϕa is dependent on pH values over some range of pH, near the pK values of the surface H_2O. The surface charge will change drastically resulting in a large chang in $\phi a - \phi s$. For a given pH, however, most of the change in electrode potential will appear at $\phi m - \phi a$. Vetter and Schultze[106] attempt to consider the pH dependence of O_2-generation on the Pt oxide film arrive at similar conclusion.

The model presented for $(PtOH)^{z-1}$ on the electrode surface does provide some possibility to calculate the reorganization energy in a way analogous to that described by Tench and Yeager.[119] The interaction of Pt in the $(PtOH)^{z-1}$ complex with oxygen in inner coordination sphere can be considered as part of or extension of the solid lattice.

The observed effects of cations and anions are small, indicating a minor influence on $(PtOH)^{z-1}$ species.

The effect of cations and anions on $\phi a - \phi s$ is probably small. The electrode surface can also be partially blocked by adsorbed anions or cations although the fraction is small. The blocked sites can be represented as Pt-O-Pt-O-Pt-Cl, Pt-O-Pt-O-Pt-O-Ba or Pt-O-Pt-O-Pt-O-Si$\begin{matrix} O \\ \diagup \\ \diagdown \\ O \end{matrix}$.

The adsorbed ions may also increase slightly the reorganization energy for the charge transfer by modifying the polarizability of the outer coordination sphere and also introducing further asymmetry in the inner coordination sphere.

D. Suggestions For Future Works

The most pressing need for future works is to obtain more quantitative results sufficient to develop a model for the effect of cations and anions on hydrogen chemisorption, anodic oxide film formation and O_2-generation on Pt. A computer-assisted deconvolution technique is a good approach to deconvolute the peaks in hydrogen chemisorption and anodic oxide film formation regions. Such a technique will be able to show how cations and anions influence each stage of hydrogen chemisorption and anodic oxide film formation.

A combination of non-electrochemical techniques (LEED, AES) with conventional electrochemical techniques would be informative to reveal the adsorption site of hydrogen and oxygen on Pt, and the nature of the Pt anodic oxide film. Other electrochemical techniques such as potential step function could be used to study the kinetics of these processes.

High temperature and high pressure techniques are attractive to provide the information concerning the back reaction of O_2-generation. Using a solution presaturated with Pt species to minimize the dissolution of Pt and combining with high temperature and high pressure techniques, the rate for back reaction may be detected.

REFERENCES

1. S. Gilman, in "Electroanalytical Chemistry", Vol. 2, p. 111, A. J. Bard, Editor, Marcel Dekker, New York (1967)

2. J. P. Hoar, "Electrochemistry of Oxygen", Interscience, New York (1968)

3. A. Damjanovic, in "Modern Aspects of Electrochemistry", No. 5, Chapt. 5, p. 389, J. O'M Bockris and B. E. Conway, Editors, Plenum Press, New York (1969)

4. S. W. Feldberg, C. G. Enke, and C. E. Bricker, J. Electrochem. Soc., 110, 826 (1963)

5. H. Angerstein-Kozlowska, B. E. Conway, and W. B. A. Sharp, J. Electroanal. Chem., 43, 9 (1973)

6. H. A. Laitinen and C. G. Enke, J. Electrochem. Soc., 107, 773 (1960)

7. K. J. Vetter and D. Berndt, Z. Elektrochem., 62, 378 (1958)

8. A. N. Frumkin, E. I. Khrushcheva, M. R. Tarasevich, and N. A. Shumilova, Elektrokhimiya, 1, 17 (1965)

9. D. C. Johnson, D. T. Napp, and S. Bruckenstein, Electrochim. Acta, 15, 1493 (1970)

10. A. Kozawa, J. Electroanal. Chem., 8, 20 (1964)

11. H. Dietz and H. Goehr, Electrochim. Acta, 8, 343 (1963)

12. J. Horkans, B. D. Cahan, and E. Yeager, Surface Sci., 46, 1 (1974)

13. S. Schuldiner and T. B. Warner, J. Electrochem. Soc., 111, 438 (1964)

14. R. Thacker and J. P. Hoare, J. Electroanal. Chem., 30, 1 (1971)

15. F. J. Norton, J. Applied Phys., 29, 1122 (1958)

16. D. A. J. Rand and R. Woods, J. Electroanal. Chem., 35, 209 (1972)

17. M. W. Breiter, Electrochim. Acta, 11, 905 (1966)

REFERENCES (Cont.)

18. S. E. S. El Wakkad and S. H. Emara, J. Chem. Soc., (London), 461 (1952)

19. G. Grube, Z. Elektrochem., 16, 621 (1910)

20. W. M. Latimer, "The Oxidation States of the Elements and Their Potentials in Aqueous Solutions", p. 196, Prentice-Hall, Englewood Cliffs, N. J. (1938)

21. A. Hickling, Trans. Faraday Soc., 41, 333 (1945)

22. J. A. V. Butler and G. Armstrong, Proc. Roy. Soc., 137A, 604 (1932)

23. B. Ershler, Disc. Faraday Soc., 1, 269 (1947)

24. A. D. Obrucheva, Zhur. Fiz. Kim., 26, 1448 (1952)

25. F. C. Anson and J. J. Lingane, J. Am. Chem. Soc., 79, 4901 (1957)

26. M. W. Breiter and J. L. Weininger, J. Electrochem. Soc., 109, 1135 (1962)

27. Boeld and Breiter, Electrochim. Acta, 5, 145 (1961)

28. S. Gilman, Electrochim. Acta, 9, 1025 (1964)

29. D. Gilroy and B. E. Conway, Can. J. Chem., 46, 875 (1968)

30. A. K. V. Reddy, M. Genshaw, and J. O'M Bockris, J. Chem. Phys., 48, 671 (1968)

31. K. J. Vetter and J. W. Schultze, J. Electroanal. Chem., 34, 131, 141 (1972)

32. B. E. Conway and S. Gottesfeld, J. Chem. Soc., Faraday Trans. I, 69, 1090 (1973)

33. B. V. Tilak, B. E. Conway and H. Angerstein-Kozlowska, J. Electroanal. Chem., 48, 1 (1973)

34. R. Greef, J. Chem. Phys., 51, 3148 (1969)

35. R. Parsons and W. H. M. Visscher, J. Electroanal. Chem., 36, 329 (1972)

36. J. D. E. McIntyre and D. M. Kolb, Symp. Faraday Soc., 4, 99 (1970)

REFERENCES (Cont.)

37. K. S. Kim, N. Winograd, R. E. Davis, J. Am. Chem. Soc., 93, 6296 (1971)

38. G. A. Allen, P. M. Tucker, A. Capon, and R. Parsons, J. Electroanal. Chem., 50, 335 (1974)

39. T. Biegler and R. Woods, J. Electroanal. Chem., 20, 73 (1969)

40. W. C. Johnson and L. A. Heldt, J. Electrochem. Soc., 121, 34 (1974)

41. D. J. G. Ives and G. J. Janz, "Reference Electrodes", p. 361, Academic Press, New York (1961)

42. R. Lorenz, Z. Elektrochem., 14, 781 (1908)

43. R. Lorenz, and H. Hauser, Z. Anorg. Allgem. Chem., 51, 81 (1906)

44. H. G. Bain, Trans. Am. Electrochem. Soc., 78, 173 (1940)

45. F. J. Brislee, Trans. Faraday Soc., 1, 65 (1905)

46. G. N. Lewis, J. Am. Chem. Soc., 28, 158 (1906)

47. W. M. Latimer, "Oxidation Potentials", 2nd ed., p. 38-50, Prentice-Hall, Englewood Cliffs, N. J. (1952)

48. E. Yeager, P. Krause, and K. V. Rao, Electrochim. Acta, 9, 1057 (1964)

49. T. P. Hoar, Proc. Roy. Soc., (London) A142, 628 (1933)

50. J. Z. Giner, Z. Elektrochem., 63, 386 (1959)

51. H. Wroblowa, M. L. B. Rao, A. Damjanovic, and J. O'M Bockris, J. Electroanal. Chem., 15, 139 (1967)

52. J. O'M Bockris and A. K. M. S. Huq, Proc. Roy. Soc., (London) A237, 277 (1956)

53. N. Watanabe and M. A. U. Devanathan, J. Electrochem. Soc., 111, 615 (1964)

54. J. P. Hoar, J. Electrochem. Soc., 110, 1019 (1963)

REFERENCES (Cont.)

55. J. W. Schultze and K. J. Vetter, Electrochim. Acta, 18, 889 (1973)

56. W. Nicholson and A. Carlisle, J. Nat. Phil., 4, 179 (1800)

57. K. J. Vetter, "Electrochemical Kinetics", p. 624-632, Academic Press, New York (1967)

58. M. W. Breiter, in "Advances in Electrochemistry and Electrochemical Engineering", Vol. 1, p. 123, P. Delahay, Editor, Interscience, New York (1961)

59. T. Erdey-Gruz, "Kinetics of Electrode Processes", Wiley-Interscience, New York (1972)

60. F. P. Bowden, Proc. Roy Soc., (London) A126, 107 (1929)

61. W. Roiter and R. Yampolskaya, Acta Physiochim. USSR, 7, 247 (1937)

62. E. A. Efimov and H. A. Isgaryshev, Zh. Fiz. Khim., 30, 1606 (1956)

63. T. Erdey-Gruz and I. Shafarik, Soviet Electrochemistry Proc. 4th Conference Electrochemistry, Vol. 2, p. 145, Consultant Bureau, New York (1961)

64. A. Hickling and S. Hill, Trans. Faraday Soc., 46, 550 (1950)

65. J. P. Hoare, J. Electrochem. Soc., 112, 602 (1965)

66. W. Visscher and M. A. V. Devanathan, J. Electroanal. Chem., 8, 127 (1964)

67. A. Damjanovic, A. T. Ward, and M. O'Jea, J. Electrochem. Soc., 121, 1186 (1974)

68. A. Rius, J. Llopis, and P, Grandia, Anales Real. Espan. Fis. Quim., 46B, 225 (1950)

69. T. R. Beck and Moulton, J. Electrochem. Soc., 103, 247 (1956)

70. A. Damjanovic, A. Dey, and J, O'M Bockris, Electrochim. Acta, 11, 791 (1966)

71. A. J. Appleby, J. Electroanal. Chem., 24, 97 (1970)

72. M. Knobel, P. Caplan, and M. Eiseman, Trans. Electrochem. Soc., 43, 51 (1923)

REFERENCES (Cont.)

73. H. Hunt, J. F. Chittum, and H. W. Richey, Trans. Electrochem. Soc., 73, 299 (1938)

74. R. I. Kaganovich and L. M. Lap, Zh. Fiz. Khim., 38, 1656 (1964)

75. R. F. Scarr, J. Electrochem. Soc., 116, 1526 (1969)

76. T. Erdey-Gruz, M. Gallgas, and E. Szetey, Acta Chim. Acad. Sci. Hung., 69, 203 (1971)

77. A. Rius, J. Llopis, and J. Giner, Anales Real. Soc. Espan. Fis. Quim., 49B, 329 (1953)

78. K. I. Rozental and V. I. Veselovskii, Dokl. Akad. Nank USSR, 11, 637 (1956)

79. A. C. Riddiford, Electrochim. Acta, 4, 170 (1961)

80. P. C. Milner, J. Electrochem. Soc., 111, 228 (1964)

81. J. O'M Bockris, J. Chem. Phys., 24, 817 (1956)

82. R. Parsons, Trans. Faraday Soc., 47, 1332 (1951)

83. S. Glasstone and A. Hickling, J. Chem. Soc., Part VI, 1878 (1934)

84. O. J. Walker and J. Weiss, Trans. Faraday Soc., 31, 1011 (1935)

85. H. P. Stout, Disc. Faraday Soc., 1, 246 (1947)

86. Yoneda, Bull. Chem. Soc., Japan, 22, 266 (1949);
Yoneda, J. Electrochem. Soc., Japan, 17, 247 (1949);
Yoneda, J. Chem. Soc., Japan, 71, 216 (1950)

87. A. Slygin, A. Frumkin, and W. Medwedowsky, Acta Physicochim. USSR, 4, 911 (1936)

88. K. Schawabe, Electrochim. Acta, 6, 223 (1962)

89. Y. C. Chiu and M. A. Genshaw, J. Phys. Chem., 73, 3571 (1969)

90. N. A. Balaschova, Electrochim. Acta, 7, 559 (1962)

91. M. W. Breiter, Electrochim. Acta, 8, 925 (1963)

REFERENCES (Cont.)

92. B. I. Podlovchenko, N. A. Epstein, and A. N. Frumkin, J. Electroanal. Chem., 53, 95 (1974)

93. R. F. Lane and A. T. Hubbard, J. Phys. Chem., 79, 808 (1975)

94. M. A. Gerovich, R. I. Kaganovich, V. M. Vegelesov, and L. N. Gorokhov, Dokl. Akad. Nank, USSR, 114, 1049 (1957)

95. E. V. Kasatkin, K. I. Rozental, and V. I. Veselovskii, Elektrokhimiya, 4, 1402 (1968)

96. R. I. Kaganovich, M. A. Gerovich, and E. Kh. Enikeev, Dokl. Akad. Nank USSR, 108, 107 (1956)

97. N. A. Izgaryshev and E. A. Efimov, Zh. Fiz. Khim., 27, 130 (1953); N. A. Izgaryshev and E. A. Efimov, Zh. Fiz. Khim., 31, 1141 (1957)

98. A. Hickling and S. Hill, Trans. Faraday Soc., 46, 550 (1950)

99. A. N. Frumkin, Electrochim. Acta, 5, 265 (1961)

100. R. W. Zurilla and E. Yeager, "Oxygen Electrode Kinetics on Gold", ONR Technical Report No. 23, Contract N 00014-67-C-0389, Project NR 359-277, CWRU, Cleveland, Ohio, May 15 (1969)

101. D. J. G. Ives and G. J. Janz, "Reference Electrodes", p. 111-115, Academic Press, New York (1961)

102. J. P. Hoare, J. Electrochem. Soc., 109, 859 (1962)

103. B. E. Conway, H. Angerstein-Kozlowska, W. B. A. Sharp, and E. E. Criddle, Anal. Chem., 45, 1331 (1973)

104. H. Angerstein-Kozlowska, W. B. A. Sharp and B. E. Conway, in "Proceedings of the Symposium on Electrocatalysis", M. W. Breiter, Editor, Electrochemical Society, Princeton, N. J. (1974)

105. V. E. Kazarinov and Balashova, Dokl. Akad. Nank, USSR, 157, 1174 (1964)

106. K. J. Vetter and J. W. Schultze, Ber. Bunsenges Phys. Chem., 77, 945 (1973)

107. M. W. Breiter, Electrochim. Acta, 7, 25 (1962)

108. F. Will, J. Electrochem. Soc., 112, 451 (1965)